2019

OPTIMIZATION AND CONTROL OF ARRAYS OF WAVE ENERGY CONVERTERS

Jianyang Lyu

OPTIMIZATION AND CONTROL OF ARRAYS OF WAVE ENERGY CONVERTERS

By

Jianyang Lyu

A DISSERTATION

Submitted in partial fulfillment of the requirements for the degree of

DOCTOR OF PHILOSOPHY

In Mechanical Engineering-Engineering Mechanics

MICHIGAN TECHNOLOGICAL UNIVERSITY

2019

This dissertation has been approved in partial fulfillment of the requirements for the Degree of DOCTOR OF PHILOSOPHY in Mechanical Engineering-Engineering Mechanics.

Department of Mechanical Engineering-Engineering Mechanics

Dissertation Co-advisor: *Dr. Ossama Abdelkhalik*

Dissertation Co-advisor: *Dr. Fernando Ponta*

Committee Member: *Dr. Andrew Barnard*

Committee Member: *Dr. Ali Ebnenasir*

Department Chair: *Dr. William Predebon*

Contents

List of Figures

List of Tables

Preface

Chapter 1 presents the introduction of this dissertation, including the renewable energy background, the motivation of this research and the contribution of this thesis. Chapter 2 provides a detailed literature survey of wave energy conversion, including the wave profile, the Wave Energy Converter (WEC) models, the control of wave energy converters, the actuators, and wave energy converter arrays. Chapter 3 introduces the formulation and the result of WEC array optimization using both device dimension and array layout as design variables. Chapter 4 proposes and investigates a hybrid WEC array configuration that has both heaving buoys and OSWCs in the array. The optimization of the hybrid array is also presented in Chapter 4. Chapter 5 presents the formulation and solution of WEC array optimal control problem. The solutions are derived individually using both regular wave and irregular wave as inputs. Chapter 5 also provides the derivation of optimal control solution for a single WEC, using energy loss from a hydraulic PTO unit. The wave-by-wave control reviewed in Chapter 2 is published as references [5]. The material of Chapter 3 is published as references [6].

Acknowledgments

I would like to express my deepest gratitude to all those who have supported me, helped me, and inspired me during my doctoral program at Michigan Technological University. Thanks to everyone, this journey towards PhD is truly wonderful!

I thank my parents for their never-ending love and trust. Your encouragement shined my way forward even in the darkest night.

I would like to thank my advisor, Dr. Ossama Abdelkhalik and all the committee members. Thank you for giving me the opportunity to join your research group and pursue a PhD degree. This work won't be done without your guidance, support, and encouragement. Thanks to Dr. Fernando Ponta, Dr. Andrew Barnard, and Dr. Ali Ebnenasir, without your patience and accommodation I won't be able to finish my PhD so smoothly. Thanks to Dr. Giorgio Bacelli who help me on my very first research project. Thanks to Dr. Umesh Korde, who supported me in 2017 summer and whose notes helped me a lot in understanding the non-linear hydrodynamics. Thanks to Dr. Lucia Gauchia and Dr. Fernando Ponta, who accepted to be my co-advisors and being so nice!

Thanks to my aunt Zhi Hu and uncle John, it warms my heart a lot knowing that there is a place for me to stay, even when I am so far away from home.

I thank my colleges here at Michigan Tech, Shangyan Zou, Jiajun Song and Shadi Darani. Shangyan has answered numerous questions from me, thank you for helping me to understand all those profound concepts! Thanks to Jiajun who taught me how to create Nemoh mesh and everything about numerical simulation.

I thank all my friends at Michigan Tech and in China. Thanks to Mingyang Li, for all the jokes and fun moment we had together! Thanks to Zhihao Zhao, Zhuyong Yang, Haitao Cao, Xuebin Yang, for the time we spend together working on problems! Thanks to Trinoy Dutta, Lopamudra Baruah, Joe Tripp, Mollie Doerner, Lauren Knop, Guilherme Ribeiro, Simone Puel, for the nights of games, movies and beers! Thanks to my friends at CSSA, Houjun Ding, Yanyun Li, Dawei Wu, Yifei Wu, Xiang Zhou and many more, for our band and all those amazing events! Thanks to my friend Yang Lu, Xin Fan, Mitsuha and many more, for all the monster hunting!

Special thanks to all the Michigan Tech staff who helped me in submitting the forms, preparing the meeting rooms, solving my office computer problem, and many other things.

This list can never end since you are all important people to me and I will always cherish these memories. Thank you all again, for making my journey wonderful and full of joys.

List of Abbreviations

BEM	Boundary Element Method
DoF	Degree of Freedom
FFT	Fast Fourier Tranform
JONSWAP	Joint North Sea Wave Observation Project
LMPG	Linear Permanent Magnetic Generator
MDoF	Multi-Degree of Freedom
MPC	Model Predictive Control
OSWC	Oscillating Surge Wave Converter
PD	Proportional Damping Control
PDCCC	Proportional Damping Complex Conjugate Control
PTO	Power-Take-Off
WEC	Wave Energy Converter

Nomenclature

A_{buoy}	Cross Section Surface Area $[m^2]$
A_{ex}	Amplitude of the Excitation Force Coefficient
A_r	Radiation State Space Matrix
B_r	Radiation State Space Matrix
C_r	Radiation State Space Matrix
C_h	Hydro-static Coefficient for OSWC $[Nm/rad]$
D	Draft Height of Buoy $[m]$
f_c	Control Force $[N]$
f_e	Excitation Force $[N]$
f_r	Radiation Force $[N]$
f_s	Hydro-static Force $[N]$
h_r	Kernel of the Radiation Impulse Function
H_s	Significant Wave Height $[m]$
I	Mass Moment of Inertia of the OSWC $[kgm^2]$
K_h	Hydro-static Coefficient for Buoy $[N/m]$
m	Mass $[kg]$
m_a	Added Mass $[kg]$
m_e	Excitation Moment $[Nm]$

m_r	Radiation Moment $[Nm]$
m_s	Hydro-static Moment $[Nm]$
P_{array}	Power Absorbed by WEC Array $[J]$
P_{iso}	Power Absorbed by Isolated WEC $[J]$
q	q-factor
R	Radius of Buoy $[m]$
$S(\omega)$	Wave Spectrum Density m^2s/rad
T_p	Wave Period $[s]$
T_{PTO}	PTO Torque $[Nm]$
x_r	Radiation State
z	Buoy Displacement $[m]$
η	Wave Elevation $[m]$
θ	Rotation Angle of the OSWC $[rad]$
λ	Lagrange Multiplier
ρ	Density $[kg/m^3]$
ϕ_{ex}	Phase of the Excitation Force Coefficient
ϕ_I	Incident Wave Potential $[m^2/s]$
ϕ_D	Diffracted Wave Potential $[m^2/s]$
ϕ_r	Radiated Wave Potential $[m^2/s]$
ϕ_η	Phase of Wave Elevation
ω	Frequency $[rad/s]$

ω_p	Peak Frequency $[rad/s]$

Abstract

Wave Energy Converter Array is a practical approach to harvest ocean wave energy. To leverage the potential of the WEC array in terms of energy extraction, it is essential to have properly designed array configuration and control system. This thesis explores optimal configuration of Wave Energy Converters (WECs) arrays and its optimal control. The optimization of the WEC array allows both dimensions of individual WECs as well as the array layout to vary. In the first optimization problem, cylindrical buoys are assumed in the array where their radii and drafts are optimization parameters. Genetic Algorithms are used for optimization. Three case studies are investigated of different array sizes: 3, 5, and 7 devices in the array. Two types of controls are assumed; the first is the standard impedance matching control while the second is a derivative control. The numerical test cases demonstrate that a higher q-factor is achieved when optimizing the buoys dimensions simultaneously with the array layout. In the conducted test cases, it is shown that optimizing the array layout can increase the q-factor on average by 39.21% when using an optimal control, and increase it on average by a factor of 8.87% when using a derivative control.

Arrays of wave energy converters (WECs) usually have large spacing between members of the array to avoid negative hydrodynamic interaction between members in the array. Errors in estimating the spacing between members may result in a significant

degradation in the performance of the array in terms of the total harvested energy, due to destructive hydrodynamic interaction between members of the array. In this thesis, a hybrid design of wave energy converter arrays, that contains two types of WECs, the heaving buoys and the floating flap-type devices, is investigated and compared against traditional WEC arrays which members are all of the same type. The resulting q-factor is less sensitive to deviations in the spacing from the design layout. This hybrid array, hence, enables more WECs in the same ocean area. The two types of arrays are tested using 40 layouts that has different separation distances ranging from small to large. With the hybrid configuration, the array achieved a variance of the q-factor as low as 0.006. The traditional array has a variance of 0.024 which is four times larger. The optimization is conducted on hybrid array with both layout and dimension as design variables.

The optimal control algorithm for WEC array is developed using the optimality condition. Devices in the array are assumed to be identical heaving buoys. The optimization objective is to maximize the energy extraction at each time step. Both regular and irregular waves are used to excite the array. The unconstrained optimal control problem is solved with a saturation on the control force. The solutions show that good wave estimations and sufficient accuracy of radiation sub-system are the keys to the desired WEC array performance.

Chapter 1

Introduction

In 1956, an early exploration by Hubbert and King [7] finds that the traditional fossil fuel energy has a limit in the global storage. To reduce the risk of fuel energy shortage, alternative energy sources have been developed and studied in many countries. Since the beginning of research of renewable energy, several types of renewable energy have been successfully utilized . In terms of power resources, there are solar, wind-power, hydro-power, bio-power, geothermal-power,ocean-power and bio-electricity [1].

The ocean does not only occupy over 70% of the planet surface but also holds tremendous amount of energy. Follow the energy flow chain of solar-wind-ocean wave [8], we can see that ocean surface wave has the largest power density and thus worth investigation. In the North American Ocean Energy Status report [9], the U.S. wave

energy resource is estimated to be $2100\,TWh/yr$. With realistic consideration and constraints applied, the estimated electricity production is $260\,TWh/yr$, which covers 6.5% of total U.S. electricity supplies. The ocean energy can be categorized into: wave energy, tidal energy, marine current energy, and ocean-thermal energy. In the present research, the study focuses on ocean wave energy.

From the Renewables 2019 Global Status Report, the global ocean energy capacity has been estimated to be 532 MW by the end of year 2018[1]. A more detailed relationship of ocean power, hydro-power and total renewable power is shown on figure 1.1.

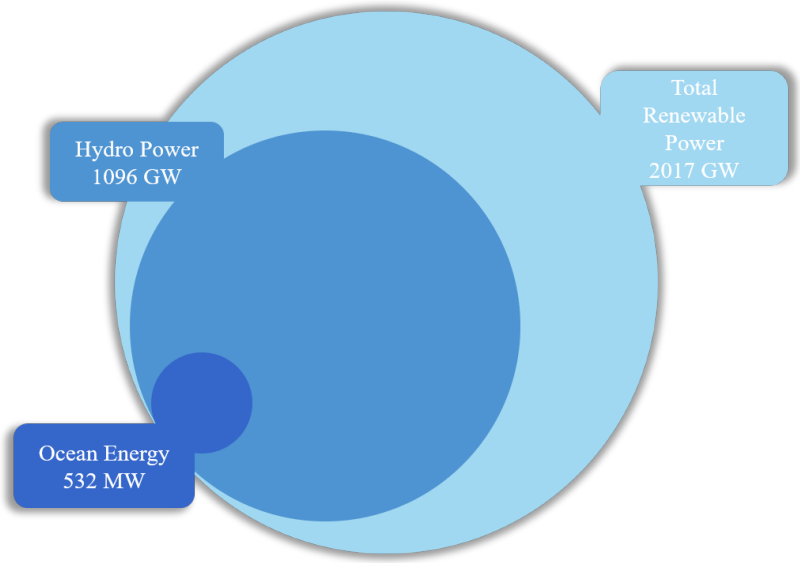

Figure 1.1: Power capacity chart. Data is collected from [1].

The high energy potential in ocean waves motivates the research of more effective design and control techniques for WEC devices and farms.

1.1 Overview of Ocean Wave Energy Conversion

As reviewed and categorized in [8, 10, 11], there are three working principles for wave energy conversion devices: oscillating bodies or systems, oscillating water columns and overtopping devices. All three principles utilize the oscillating nature of the ocean wave, but the conversion happens at different stages. The oscillating body type of devices has submerged or half-submerged structures that oscillate with the ocean surface wave together, and the energy is captured by either a hydraulic or electric conversion system. The implementation includes Archimedes Waveswing, CETO, Pelamis, PowerBuoys, SEAREV, Oyster, etc [12]. The oscillating wave columns are often onshore structures that have a chamber that ocean wave can flow into. Air is compressed or decompressed by the oscillating motion of wave in the chamber and energy is captured through a turbine and the electric system. The overtopping devices are large onshore structures with a reservoir of water on the top, which is designed to be at the mean water level. When the propagating wave hits the WEC, wave above the mean level will flow into the reservoir, and then flow back to the sea. The water turbine at the bottom or the side of the reservoir will be activated by the flowing water, and generates electricity. This thesis explores only the oscillating body system type of WEC device and its array.

The oscillating system type of WECs have been studied since 1980s. Early studies are

conducted by Evans [13], Budal [14], and Falnes [15]. The hydrodynamics, the control techniques and the Power-take-off system of an isolated WEC have drawn considerable amount of attention. Up to today, there are several commercial and open source software packages that can solve for the hydrodynamics of a floating body, such as WAMIT, ANSYS Aqwa, and Nemoh, etc. Analytical/semi-analytical and experimental approaches have also been explored to solve the hydrodynamics of a submerged body [16, 17, 18]. With the hydrodynamics data and other necessary information such as surface elevation and pressure field, proper control algorithms can be developed for a specific WEC model. The target of WEC control problem is often to maximize the power/energy extraction with specified wave input and constraints. Control force is necessary for energy extraction. Complex conjugate control criteria [19] calculates theoretical maximum energy by matching the amplitude and phase of the wave excitation with the velocity of the oscillatory device. Typical control algorithms are model predictive control [20, 21], pseudo-spectral control [22, 23], and optimal singular arc control [24]. More details of the control methods will be introduced in section 2.3. To produce the desired control force/torque and generate energy, hydraulic generators and direct drive generators can be used as energy conversion mechanism. While the hydraulic system is often more robust and maintains against larger loads [25], there are novel designs of the direct drive magnetic generators that also serve the purpose of wave energy conversion [26].

The literature discussed above considers an isolated WEC, where only the WEC

hydrodynamics need to be considered. When it comes to the commercial scale implementation, there are requirements for connecting to the power grid as well as the economical requirements which include the cost of plant and energy storage systems. WEC array is the approach to fulfill both requirements [27]. Practically, WECs should be deployed either in a form of array [28, 29], or grouped with other devices such as a wind turbine [30]. In the array, each device can affect the movement and energy absorption of each other. Thus, the hydrodynamics of the array is more complex when compared with isolated WEC. The hydrodynamic interaction between devices in the array can be either constructive or destructive depending on the array configuration. In designing the WEC array, interaction must be considered such that the array remains productive in terms of energy exaction.

1.2 Motivation

Similar to the design of an isolated WEC, there are large amount of factors that can affect the design of a WEC array such as the layout and the control algorithm. More discussion about each factor and their evaluation will be presented in section 2.5.1. Layout of the array is one of the critical factors in the array design since it directly affects the hydrodynamic interaction between devices. Optimal layout of an array has been studied for many cases and remains a popular topic in array design. Several typical array layouts that have been used in different studies are shown in figure 1.2.

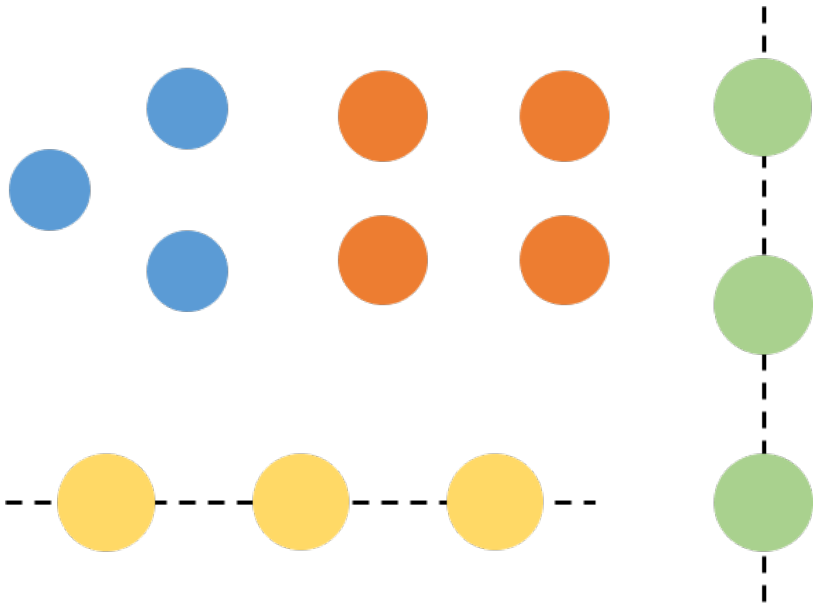

Figure 1.2: Examples of typical array layout used in research.

Separation distance between devices is the simplest way to describe the layout of an array. The effect of separation distance is studied in [31], and the variation in array performance is studied in [3]. Optimal layout under point absorber assumption is found using different optimization algorithms in [2, 32]. In the majority of literature including the above ones, identical devices in the array is assumed in WEC array studies. In doing so, the variables in the array design are significantly reduced. Recently, an expanded multiple scattering method is developed by Goteman [33] which assumes cylindrical devices while allowing the size of each device to change. This study has shown an improved array performance with buoys of different dimensions and great potential in designing large WEC arrays. Further, the shape of a single submerged absorber plate was optimized by Esmaeilzadeh in 2019 using the genetic

algorithm [34]. The contour of the planar was parameterized by Fourier decomposition of a plane geometry. These studies motivates the consideration of the shape and the size of each device to be design parameters when designing the array in order to achieve the optimal performance.

The hypothesis of this research is that optimizing WEC array layout along with buoy dimensions and operation mode of each device will result in better WEC array performance.

Although the theoretical optimal hydrodynamic interaction can be found by optimization, Penalba's study [3] of buoy slenderness indicates that the interaction is mostly destructive and violently fluctuates when the separation distance is relatively small. This finding reveals the difficulty in implementing the optimal array layout, since it is critical to find the exact separation distance and fix the device at the desired location.

While the arrays of one single type of devices have been widely studied, hybrid arrays that contain different types of devices have received little attention. The previous studies [19, 31, 35] indicate that both heave mode and pitch mode can have similar energy potential in wave energy harvesting. The configuration of arrays of flap-type oscillating surge wave converters (OSWC) has also been studied in several references [36, 37, 38]. Similar to the arrays of heaving buoys, optimal separation distance is investigated along with the effect of wave direction. These studies motivate the exploration of a hybrid WEC array that contain both OSWC and heaving buoys,

which may benefit from both types of devices. An example of the hybrid array is shown in figure 1.3.

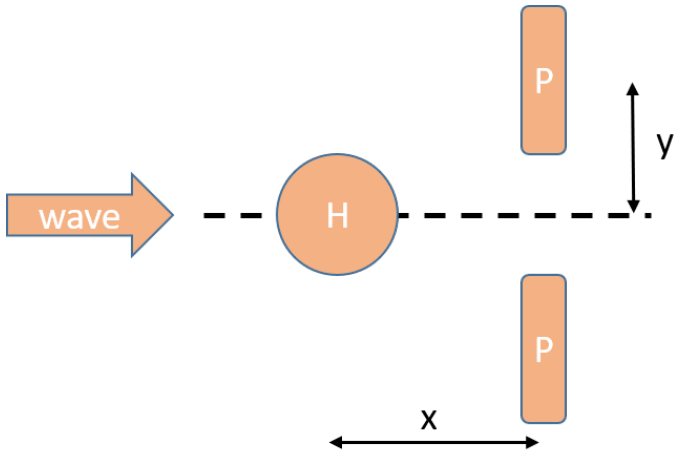

Figure 1.3: An example of the hybrid WEC array.'H' represents a heaving buoy, and 'P' represents an OSWC. Wave indicates the input wave direction.

One major concern of using the hybrid design illustrated in figure 1.3 is the installation of devices. It is well recognized that the flap-type device is more effective in shallow water while the same bottom-hinged mechanism absorbs little energy in deep water due to the fact that the ocean is almost static at its deepest points. On the other hand, heaving buoys are common in deep water applications while the shallow water limits the size and the energy absorption from the device. Recent research [4] reveals a new option for installing OSWC in deep water areas. In reference [4], the OSWC is installed on the platform 'SharpEagle' that is moored in a deep water environment. The 'SharpEagle' test platform has been installed and tested. It proves the hybrid array design to be feasible.

For WEC array, the analytical optimal control solution is uncharted due to the complexity of the problem. It is essential to point out the difference between frequency domain control design and time domain control design.

In frequency domain, assuming linear wave theory, the hydrodynamics of the WEC array can be expressed as an MIMO system. All the linear system control strategies can be applied to the WEC array system such as impedance matching control and simple PD control. The general complex conjugate control formulation for WEC array is developed in [15] and [13] individually.

However, in time domain, radiation states or radiation impulse functions have to be used to model the WEC radiation force which adds difficulty to the control design. More details about the radiation force is explained in section 2.2. Using radiation state matrices, model predictive control has been applied to find the optimal performance of the WEC array in [39]. It is mentioned in [8, 35] that the direct application of Pontryagin's Principle using Lagrange multipliers will result in two-point boundary value problems. Solving the necessary conditions of optimality yields an analytical solution to the optimal control problem. However, the initial guess of the states are critical to the problem and it makes the problem to be case specific and hard to solve.

Alternatively, pseudo-spectral approach can be used to approximate the states of the buoys and the control signal [23]. In [8, 23, 35], the states and control parameter

are approximated using Fourier-Galerkin Direct Transcription. Based on the approximations, the constrained optimal control solution was then derived. Recently, the optimal control problem has been solved by [24] for an isolated WEC. In reference [24], solution is no longer dependent on the initial guess by introducing a 'Bang-Singular-Bang' control law. It is worth expanding the same control strategy and exploring the optimal solution for the WEC array.

This thesis focuses on optimize the performance of WEC arrays. The approaches include optimizing both layout of the array as well as the dimension of each device, utilizing the array that has more than single type of devices in it, and develop an optimal control law for WEC array which maximizes the energy absorption under specific criteria.

1.3 Objectives and Contributions

1.3.1 Research Objectives

To solve the problems mentioned in section 1.2, the objectives of this research are shown as follows:

† Optimize simultaneously both the layout for a WEC array and the dimensions

of each device. The arrays to be used in this research contain only cylindrical heaving buoys. The design parameters are the coordinates, radius, and height of each buoy. The optimization will be done with both regular and irregular wave input to the array.

† Investigate the performance of a hybrid WEC array that has both cylindrical heaving buoys and OSWCs. Both power absorption and its fluctuation will be evaluated for both the hybrid array and the traditional array with only heaving buoys.

† Derive analytical optimal control solution for the WEC array. Investigate if the solution is on a singular arc and compare it with the solution obtained from isolated WEC case. Investigate and compare the switching condition for both a WEC array and an isolated WEC.

1.3.2 Contributions

1. The first contribution of this research is the formulation of the WEC array optimization problem with both array layout and buoy dimensions as design variables. Full hydrodynamic interaction is employed in the formulation of the problem; most of the previous studies employ either point absorber approximation or semi-analytical approximations. The dimension of each WEC can not

be modeled using most of the approximations since they assume each device as a "node". The proposed formulation with both buoy coordinates and dimension as design variables is proved to be effective and can harvest more energy efficiently. In addition, two different control algorithms are applied and the optimal array layout and buoys' sizes are obtained for each of them. This novel formulation made the array design more flexible and more effective in energy conversion.

2. Another contribution of this work is the investigation of the novel hybrid WEC array design. The hybrid array has both heaving buoys and OSWCs in one array. Numerical simulation results indicate a smoother hydrodynamic interaction between devices when a hybrid array is employed. The performance of the hybrid array is less sensitive to deviations in the spacing from the design layout. It is also shown that while a normally distributed random error is applied to the array layout to simulate a real implementation scenarios, the hybrid array has smaller performance fluctuation. The average power per ocean surface area is firstly used as a novel evaluation factor of the array performance.

3. The last contribution of this thesis is the derivation of analytical solution of the WEC array optimal control problem. The solution is derived with both regular wave and irregular wave as input signal to the system. Similar to the solution for an isolated WEC, the solution for an array is also on a singular arc regardless of the type of input ocean wave. The switching condition for the WEC array

takes both diagonal and non-diagonal elements of the hydrodynamic coefficient matrices into consideration. It indicates that the solution is a collective optimal control which uses information from the entire array.

1.4 Organization of The Thesis

This chapter of the thesis introduces the overall research motivations, objectives and contributions. The rest chapters are outlined as follows.

Chapter 2 summarize theory backgrounds of wave energy conversion with necessary reviews of literature. Section 2.1 introduces the modelling techniques and important coefficients of ocean wave profiles. Section 2.2 provides the theory background of the hydrodynamics and the dynamic model for both heaving buoys and bottom hinged OSWCs. Section 2.3 and 2.4 provide the literature review of control techniques and actuators for WEC respectively. Section 2.5 reviews WEC array modeling methods and the array layout optimization study.

The WEC array optimization with both layout and dimension as design variables is provided in chapter 3. Section 3.1 introduces the dynamic model and control algorithms for WEC array optimization. Section 3.2 provides formulation of the optimization problems. Section 3.3 provides the results and discussion.

Hybrid WEC array is investigated in chapter 4. The hydrodynamics and response operator are studied in section 4.1. Hybrid array configuration is presented in section 4.2. Section 4.3 investigates the hydrodynamic coefficients, and provides comparison between the hybrid arrays and the traditional arrays in terms of performance fluctuation. A Gaussian distributed error is introduced to the array layout to simulate the real installation of the WEC array. The problem formulation and the results are shown in section 4.4. The average power per ocean surface area is introduced as a novel evaluation factor in section 4.5. Section 4.6 provides the hybrid array optimization.

Chapter 5 presents the derivation of the analytical optimal control solution for WEC array. Section 5.1 reviews optimal control method and presents the formulation of the problem. Section 5.2 presents the derivation of the solution for WEC array with regular wave input. Section 5.3 presents the derivation of the solution for WEC array with irregular wave. An polynomial approximation for energy loss in a hydraulic PTO unit is proposed in section 5.4. The optimal control solution for WEC array is derived using the energy loss approximation. Numerical results and discussion of the controls are presented in section 5.5.

This research is summarized and concluded in chapter 6. The results are discussed and concluded in section 6.1. The future work is briefly discussed in section 6.2.

Chapter 2

Literature Review: Wave Energy Conversion

To convert ocean wave energy to electric energy, it is essential to have a complete design of the desired wave energy converter or array. This chapter first reviews the background and applications of a general WEC, then provides specific review of the research of WEC arrays. As discussed in the previous chapter, this design process requires several items to be understood thoroughly and derived properly. The first item is the profile of the incoming wave. It serves as the input to the system, and is described in section 2.1. The next item is the hydrodynamics of the target. The target can be an isolated WEC or a WEC array. Once its hydrodynamics information is obtained, the dynamic model of the WEC or its array can be built for next step

controller design and simulation. Both hydrodynamics of the submerged body and the WEC dynamic model are introduced in section 2.2. Based on type of the dynamic model, the control algorithm can be selected and derived. Several essential control techniques are reviewed in section 2.3. To execute the control signal and generate electric energy, a hydraulic system or direct drive system must be installed together with the WEC. The commonly used actuator techniques are reviewed in section 2.4. The WEC array research is reviewed in section 2.5, including the hydrodynamics, the dynamic model, the factors in designing and evaluating the array, the optimization study, and the control techniques.

2.1 Modeling the Ocean Wave

For most of the wave energy converters, ocean surface wave serves as the input to the system. The wave excites motion in the converter and the converter absorbs part of the kinetic energy and converts it to electric energy. However, the ocean environment is complex. The most significant portion of ocean wave are the wind-generated(Ch.6 in [40]). One way to characterize the ocean wave, is to use significant wave height $H_s\,[m]$ and peak period $T_p\,[s]$ which are summarized from wave measurement to build the spectrum that describes the wave behavior [40, 41].

Some of the commonly used wave spectral models are Bretschneider, Pierson-Moskowitz, and JONSWAP spectra. These models are developed for deep water waves and are single-peaked spectrum [40, 42]. Bretschneider firstly used the Rayleigh distribution to relate the empirical data, the average wave height and the wave period and developed the Bretschneider spectrum in 1959. Later Pierson and Moskowitz developed P-M spectrum using empirical data from north Atlantic in 1964. In 1973, the Joint North Sea Wave Project operated by four countries together modified P-M spectrum and developed JONSWAP spectrum [40]. Recent study by Garcia [42] presents a bi-model spectrum which takes information from both wind-sea interaction and swell sea motion. Fusco and Ringwood [43] evaluated five different methods of estimating the wave parameters.

From literature [11, 40], P-M and JONSWAP spectrum has the same frequency band and it is narrower than the band in Bretschneider spectra. In this research, Bretschneider spectrum is chosen to model the ocean wave profile for the same conservative consideration in [11], since a wider band spectrum represents a more general situation for energy extraction than narrow band ones.

The equation of power density using Bretschneider spectrum is shown as follows:

$$S(\omega) = \frac{5\omega_p^4}{16\omega^5} H_s^2 e^{-5\omega_p^4/(4\omega^4)} \tag{2.1}$$

In equation 2.1, S is the power density of the ocean wave, ω_p is the peak frequency which corresponds to the peak period T_p, H_s is the significant wave height, and ω is the frequency in rad/s. With $T_p = 10s$ and $H_s = 1.5m$, an example of the Bretschneider spectrum is shown in figure 2.1.

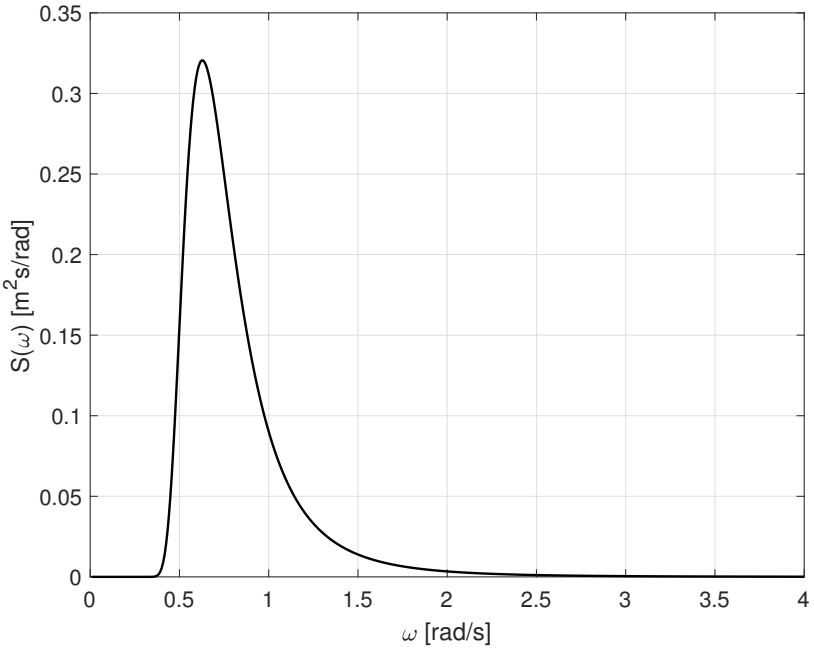

Figure 2.1: Bretschneider spectrum with $T_p = 10s$ and $H_s = 1.5m$.

Based on the definition of power density spectrum, the wave elevation frequency spectrum can be calculated backward from the power spectrum using the following equation. Where in equation 2.2, $\triangle\omega$ is the frequency resolution of the span.

$$\eta(\omega) = \sqrt{2 \triangle \omega S(\omega)} \tag{2.2}$$

2.2 Wave Energy Converter Hydrodynamics

As discussed in chapter 1, this work focuses on oscillating system type of wave energy converters. The hydrodynamics and the modeling of such systems will be discussed in this section. Since the motion of the WEC device is so small in scale when compared with the wave length of the ocean waves, the fluid around the WEC devices is assumed to be in-viscid, in-compressible and irrotational [19, 35, 44, 45]. With the ideal fluid assumption, the Navier-Stokes equation can be simplified to the Bernoulli equation. Then the the linear potential flow theory can be applied to describe the velocity field around the submerged body. This linear assumption is used to derive the dynamic models in the following discussion.

2.2.1 Modeling the WEC Device

The dynamics of a heaving WEC is first provided. The discussion is then expanded to a flap-type OSWC. As shown in figure 2.2, the total velocity potential around a heaving wave energy converter contains three components: incident wave potential, diffracted wave potential and radiated wave potential. With the linear potential flow theory, each of the above potential component has only the first order component and all higher order potential components can be neglected.

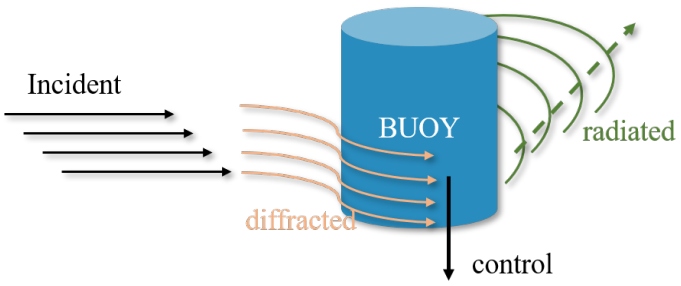

Figure 2.2: The velocity potential around a cylindrical buoy with control force acting on it.

As shown on the free-body-diagram in figure 2.3, the total force from ocean wave acting on each WEC device is expressed as a summation of the wave excitation force, the hydro-static force, the radiation force, and the control force.

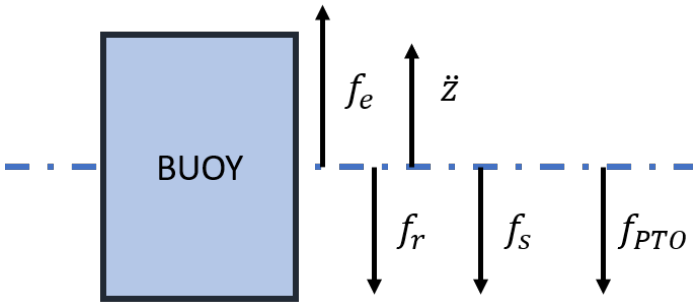

Figure 2.3: The free-body-diagram of a heaving buoy.

For an isolated WEC oscillating in heaving motion in ocean, the equation of motion is written in Eq.2.3.

$$m\ddot{z}(t) = f_e(t) - f_r(t) - f_s(t) - f_v(t) - f_{PTO}(t) \tag{2.3}$$

Where m is the mass of the device, z is the displacement of the device. f_e, f_s, f_r are

wave excitation force, hydro-static force, and radiation force respectively. f_PTO is the control force produced by the Power-Take-Off device.

f_v is the force due to viscous effect. In the research of non-linear optimal control [46] and other studies that involve non-linearity [47], the viscous force is dominant and affects the design of the control algorithms. In this thesis, linear model and control algorithms are employed for every test. In other WEC array studies [2, 48, 49, 50], viscous effect is considered to reduce the expectation of the array performance but won't affect the overall design. For the same reason, the viscous effect is neglected for this research.

2.2.1.1 Excitation Force

Wave excitation force f_e combines the effect from incident wave potential ϕ_I and diffracted wave potential ϕ_D. Assume the buoy is held at the equilibrium point at $z = 0$ as shown in figure 2.3, the excitation force can be expressed as shown in equation 2.4. In equation 2.4, ρ is water density, $\overrightarrow{n}$ is the directional vector that is perpendicular to the WEC surface, S is the wetted surface of the WEC.

$$f_e = i\omega\rho \iint_S (\phi_I + \phi_D)\overrightarrow{n}\, dS \tag{2.4}$$

According to the linear wave theory, both ϕ_I, ϕ_D are linearly proportional to the amplitude of the incoming wave elevation. Then, the excitation force can be interpreted as a response which is excited by the wave elevation [8, 19, 35].

$$f_e = \mathbf{H}(\omega)\eta \tag{2.5}$$

The frequency dependant coefficient $\mathbf{H}(\omega)$ functions as linear impulse response kernel that takes wave elevation as input and outputs excitation force. In time domain, the force can be expressed as shown in equation 2.6.

$$f_e(t) = \int_{-\infty}^{\infty} h_{ex}(t-\tau)\eta(\tau)d\tau \tag{2.6}$$

The kernel in equation 2.6 can be approximated with a series of frequency dependent coefficients. Assuming the excitation force produced by the propagating wave is a real number, the final form of the excitation force is expressed in equation 2.7. Where subscript n denotes the number of frequencies, $A_{ex}(\omega)$ and $\phi_{ex}(\omega)$ are frequency dependent excitation force coefficients, and $\eta(\omega)$ and $\phi_\eta(\omega)$ are frequency decomposed wave elevation coefficients. $A_{ex}(\omega)$ and $\phi_{ex}(\omega)$, together with the radiation coefficients introduced in the next part are called hydrodynamic coefficients. The calculation method of these coefficients is provided in section 2.2.1.4

$$f_e(t) = \sum_{n=1}^{N} \Re(A_{ex}(\omega_n)\eta(\omega_n)e^{i(\omega t+\phi_{ex}(\omega_n)+\phi_\eta(\omega_n))}) \tag{2.7}$$

The excitation force can also be expressed as the integration of all pressure around the submerged WEC device. This particular formulation is useful when pressure sensor is employed to obtain measurements. More discussion on this topic can be found in [51]. In this research, equation 2.7 and its frequency domain counterpart are used to calculate excitation force.

2.2.1.2 Hydro-static force

Hydro-static force is the restoring force that is described by the the static pressure component in the Bernoulli equation. This force acts like a spring force and can be calculated by the difference between gravity and buoyancy. Again, assume the buoy is half submerged, and held at the equilibrium point at $z = 0$ as shown in figure 2.3. The hydro-static force for a heaving buoy is written as equation 2.8.

$$f_s(t) = \rho_{water} g A_{buoy} z(t) \tag{2.8}$$

where ρ_{water} is the water density, g is the gravitational acceleration, A_{buoy} is the cross section surface area of the buoy.

The hydro-static coefficient for a heaving WEC is defined as:

$$K_h = \rho_{water} g A_{buoy} \tag{2.9}$$

Once the geometry of the WEC is defined, the hydro-static coefficient can be calculated with equation 2.9.

2.2.1.3 Radiation force

As shown in figure 2.2, the radiation force is the result of the radiation potential acting on the WEC. Assuming the WEC is forced to move with no wave excitation, the water around the WEC is excited by the motion of the WEC and a wave is radiated. Similar to the incident wave case, the radiation force can be expressed as a linear system with the velocity of the buoy as input and the resulting radiation force as output. As the radiation is a result of the body velocity, an frequency dependent impedance can be used to describe the radiation process [19] as shown in equation 2.10.

$$F_r(\omega) = Z(\omega)V(\omega) = (i\omega m_a(\omega) + b_r(\omega))V(\omega) \tag{2.10}$$

Where $F_r(\omega)$ and $V(\omega)$ are the radiation force and the WEC velocity in frequency domain. $Z(\omega)$ is the radiation impedance of the WEC with $m_a(\omega)$ as the added-mass and $b_r(\omega)$ as the radiation damping. When the input wave is a regular wave which has one frequency component, equation 2.10 can be used for both time domain and frequency domain analysis. With irregular wave inputs, it is valid only in frequency domain, since the memory effect of radiation interaction is not present in equation 2.10. In 1962, Cummins [52] first derived the time domain representation of the radiation force, and it is called the Cummins Equation. In equation 2.11, $m_a(\infty)$ is the added-mass at infinite frequency and $h_r(\tau)$ is called radiation kernel.

$$f_r(t) = m_a(\infty)\ddot{z} + \int_0^t h_r(\tau)\dot{z}(t-\tau)d\tau \tag{2.11}$$

Since the convolution term in equation 2.11 is computationally expensive to solve when running time domain simulation, an alternative model could be built. Firstly, both linear systems in equation 2.10 or equation 2.11 can be used to approximate the coefficients of the transfer function for the radiation force.

$$H_r(s) = \frac{p_n s^n + p_{n-1}s^{n-1} + ... + p_1 s + p_0}{q_m s^m + q_{m-1}s^{m-1} + ... + q_1 s + q_0} \tag{2.12}$$

Where in equation 2.12, p and q are the transfer function coefficients, and $n < m$.

This transfer function can then be used to construct the radiation state matrices A_r, B_r, and C_r shown in equation 2.13. This radiation state space model is easy to accommodate with the WEC dynamic model and is widely used in simulations.

$$\begin{aligned} \dot{z}_r &= A_r z_r + B_r \dot{z} \\ f_r &= m_a(\infty)\ddot{z} + C_r z_r \end{aligned} \tag{2.13}$$

2.2.1.4 Hydrodynamic Coefficients

To simulate the response of a WEC with respect to a given input wave profile, the coefficients mentioned in section 2.2.1.1 – 2.2.1.3 must be solved to build the dynamic model for any specific heaving WEC.

In early studies [13, 14, 15] where computational power was limited and recent researches that do not focus on the model itself such as [2, 32], the point absorber approximation is used to approximate the extracted power. This analytical approximation was first addressed by Budal in [14], and assumes axis-symmetric heaving WEC with uni-directional regular input waves. With proper setup, this approximation can efficiently calculate the absorbed power. However, since it does not use any hydrodynamics parameters, the design ability is highly limited.

Semi-analytical approach has been studied in [16, 53, 54, 55, 56] and many other papers. Most of the semi-analytical methods use either direct matrix method or multiple-scattering method to model the wave-body interaction and the hydrodynamic interaction between WECs. These semi-analytical approaches all have different assumptions. Although the application can be limited, they provides relatively fast and accurate calculation for the WEC hydrodynamic parameters.

The Boundary Element Method, known as the BEM solvers have proven to be the most powerful modeling techniques under the linear wave theory [57]. There are both commercial solvers such as WAMIT, Aquaplus, ANSYS Aqwa, and open source solvers such as WECsim and Nemoh. These solvers provide accurate calculation of all the hydrodynamic coefficients. One concern with these methods is that they are relatively computationally expensive. Another problem is that most solvers assume uniform water depth on the design domain.

In this research, one major objective is to obtain an accurate model for the WEC array so that changes made on the WEC dimension and mode of motion can be accurately reflected on the power extraction. Considering the requirements of accuracy and design flexibility, BEM solver is the most suitable choice. Open source BEM solver Nemoh [58] is employed over other choices for the following reasons:

1. The ability to be embedded in MATLAB or Python code

2. The ability to solve hydrodynamic coefficients for both isolated WEC and WEC array

Other than the approaches introduced above, there are other methods to model the hydrodynamic interaction of the WEC device. In [59], machine learning method is implemented to calculate power absorption from a WEC cluster. An experimental method was developed by Nader [60] to model the hydrodynamic interaction of a WEC array. A surrogate model is proposed in [11] to replace the full hydrodynamic interaction of the WEC array.

2.2.1.5 Modeling the Flap-type Device

A typical flap-type OSWC is shown in figure 2.4. This bottom hinged device can rotate with respect to the bottom shaft, and has one degree of freedom. Similar to a heaving buoy, when the incoming wave hits the wall of the OSWC, the same types of velocity potential will be generated and they will result in the same types of force/torque.

The equation of motion for a bottom hinged OSWC is written in equation 2.14. I is the moment of inertial of the OSWC, and θ is the angular displacement. Similar to the heaving buoy dynamics, m_e, m_s, and m_r are the excitation moment, hydro-static restoring moment, and radiation moment respectively. T_{PTO} is the control torque

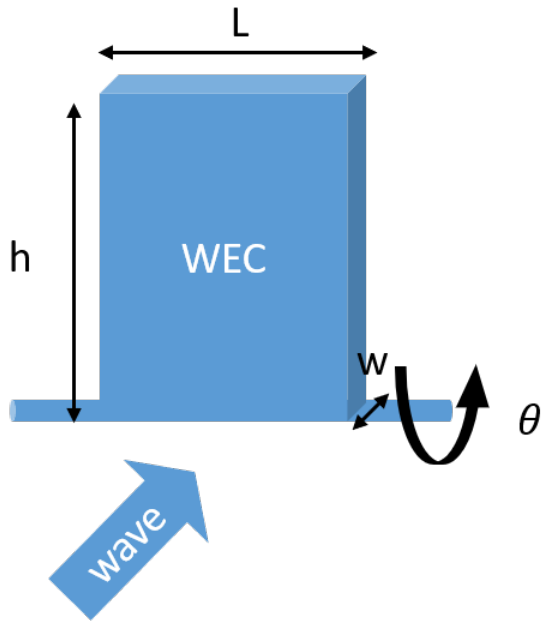

Figure 2.4: A flap-type oscillating surge wave converter.

applied on OSWC. For the same reason that has been discussed for the heaving buoy, viscous effect is neglected from the equation of motion.

$$I\ddot{\theta} = m_e(t) - m_r(t) - m_s(t) - T_{PTO} \tag{2.14}$$

The hydrodynamic moments m_e and m_r are modeled with the same method introduced in section 2.2.1.1 and section 2.2.1.3, and can be computed using hydrodynamic coefficients which are solved from Nemoh.

When the wave excites the motion of a submerged OSWC, as shown in figure 2.5, The location of buoyancy center and gravity center will change. The hydro-static moment

acting on an OSWC is trying to resist this change and restore to the previous location.

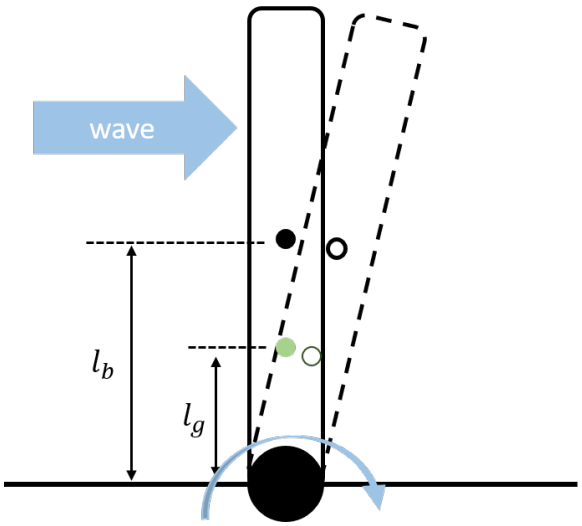

Figure 2.5: Motion of an OSWC. l_g is the distance between gravity center and the hinged ground. l_b is the distance between buoyancy center and the hinged ground.

Based on the geometry information, the equation of the hydro-static moment is written as:

$$m_s(t) = (\rho_{water} - \rho_{flap}) v_{flap} g \theta(t) \tag{2.15}$$

Where ρ_{water} and ρ_{flap} are the density of water and OSWC respectively, g is the gravitational acceleration, v_{flap} is the submerged volume of the OSWC. The hydro-static coefficient for an OSWC is defined as:

$$C_h = (\rho_{water} - \rho_{flap}) v_{flap} g \tag{2.16}$$

Besides the heaving buoy and the bottom hinged OSWC that are introduced in this research, there are other WEC designs such as SEAREV [61, 62], Pelamis [63], Salter Duck [64], etc. Babarit [65] reviewed different WEC devices with different operation principles.

Although it is not in the scope of this research, it is worth noting that when the WEC operates beyond the normal conditions and the motion is large enough to be considered as severe condition, non-linearity must be considered in all aspects of the WEC design process. More discussion of the non-linear WEC model can be found in [66, 67, 68]. Another source of non-linearity comes from the irregular shape of the device. When the vertical cross section of the buoy has different shape or size, a nonlinear Fourde-Krylov model must be applied [69, 70].

2.2.2 Modeling the Hydrodynamic Interaction For WEC Array

The analysis of the WEC array hydrodynamics is often considered to be complex and difficult. The difficulty comes from two sources, which are the wave diffraction

problem and the array radiation problem. Each device in the WEC array interacts not only with the ocean wave but also with other devices in the array.

The hydrodynamic interaction among WECs has been studied extensively in the literature. Most of the early studies employ the point absorber approximation to calculate the power extraction by the WEC array [14]. Although this approach is developed due to the limitation of computational power, the assumption is proved to be accurate under certain conditions and is useful in WEC array layout study [2, 32, 48]. Semi-analytical approaches such as direct matrix method and the multiple-scattering method are also powerful tools in the WEC array analysis. In [71] two semi-analytical approaches are compared in the modeling of a OSWC array. Boussinesq Wave approach is found to be better at modeling the near field interactions and Spectral Wave is found to be better at modeling the far field interactions. As a continuation of the original finite-depth interaction theory [16], the two hydrodynamic operators are implemented in BEM solver Nemoh, and a comparison with multiple-scattering method in [72] is made by Flavia [73]. In [36, 37, 50], both semi-analytical approach and full BEM modeling are discussed and implemented for flap-type WEC arrays. Similar to the modeling of a single WEC, BEM tools are considered to be the most powerful and accurate method [57].

On the other hand, due to the complexity of the WEC array hydrodynamic interaction problem, people have borrowed ideas from other research areas and developed several

novel approaches to solve for the hydrodynamic interaction between WECs. In [74], based on the power extraction from an isolated WEC, a stochastic model is developed to predict the power extraction from a WEC array. An experimental approach is taken by Nader [60] to understand the hydrodynamic interaction of the array. In [75], the wave-WEC interaction for the WEC array is modelled numerically by solving the wave scattering boundary conditions. A fast approach that couples both BEM and plane wave approximation is investigated by Singh [76]. A surrogate model that approximates the hydrodynamic interaction between devices by a mass-spring-damper system is proposed and investigated by Abdelkhalik [77].

Meanwhile, there are new WEC designs that deviate from the traditional shape of WECs. In [78], an articulated raft wave energy converter is modelled analytically. A WEC array that connects with a runway on the top is proposed and evaluated by [79]. As an expansion of the current WEC array modelling techniques, non-linearity in the WEC array model is studied by [3, 80]. In [81], rapid phase oscillation is removed and a modeling method for large arrays is investigated.

2.2.2.1 WEC Array Dynamic Model

The derivation of the WEC array equation of motion follows the same logic as the derivation for single WEC dynamics. The analysis is first done on frequency domain as it is easier to interpret the WEC array hydrodynamic interaction in frequency

domain. The analysis is then expanded to the time domain and a state space model with full radiation interaction is presented.

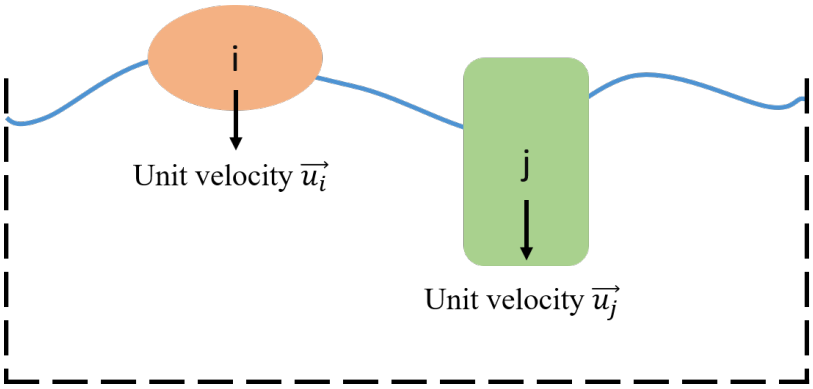

Figure 2.6: Two oscillating bodies excited by the ocean wave. i and j represents the two bodies, the arrows represent unit velocities on each body

An example of the radiation problem is shown in figure 2.6. Assume each body in figure 2.6 is moving with a unit velocity u, the radiation each body experienced will have two parts: the radiation excited by itself and the radiation excited by the other body. While the radiation excited by itself is well explained in section 2.2.1.3, the radiation excited by the anther body can be similarly expressed with a radiation impedance term shown in equation 2.17.

$$Z_{ij} = i\omega m_{a_{ij}}(\omega) + b_{r_{ij}}(\omega) \tag{2.17}$$

The total radiation force acting on body i is then the combination of the two force components shown in equation 2.18. Where the first half is the independent radiation force, and the later half is the force that represents the radiation between devices.

$$f_{r_i}(\omega) = (i\omega m_{a_{ii}}(\omega) + b_{r_{ii}}(\omega))u_i(\omega) + (i\omega m_{a_{ij}}(\omega) + b_{r_{ij}}(\omega))u_j(\omega) \tag{2.18}$$

The full equation of motion for an WEC array is written in compact matrix form in equation 2.19. Since the radiation forces acting on each WEC in the array is modeled as frequency dependent radiation impedance, the same discussion for equation 2.10 applies. Considering regular wave as the input to the system, the WEC array dynamics expressed by equation 2.19 can be used for both time domain and frequency domain analysis. When the incoming wave becomes irregular, frequency is introduced as an additional dimension to all the hydrodynamic coefficient matrices. Thus, only frequency domain analysis is valid with irregular wave input using equation 2.19.

$$-\omega^2(\mathbf{M} + \mathbf{M_a}(\omega))\overrightarrow{\mathbb{Z}} + j\omega(\mathbf{B_v} + \mathbf{B_r}(\omega))\overrightarrow{\mathbb{Z}} + \mathbf{K_h}\overrightarrow{\mathbb{Z}} = \overrightarrow{\mathbb{F}_{ex}} + \overrightarrow{\mathbb{F}_c} \tag{2.19}$$

In equation 2.19, $\mathbf{M}$ and $\mathbf{M_a}(\omega)$ are the mass and added mass matrices of the array, $\mathbf{B_v}$ and $\mathbf{B_r}(\omega)$ are the viscous and radiation damping matrices, and $\mathbf{K_h}$ is the hydrostatic coefficient matrix of the array. $\mathbf{M}$, $\mathbf{B_v}$ and $\mathbf{K_h}$ are the static force coefficient matrices and contain only diagonal elements. In the radiation coefficient matrices $\mathbf{M_a}(\omega)$ and $\mathbf{B_r}(\omega)$, the hydrodynamic interaction is shown by off-diagonal elements. Vector $\mathbb{Z}$ is the displacement vector of array. $\mathbb{F}_{ex}$ and $\mathbb{F}_c$ are the excitation force and

control force vectors respectively. The term $\mathbf{B_v}$ is dropped in latter analysis since the viscous effect is neglected from this research.

$$M_{a_{array}}(\omega) = \begin{bmatrix} m_{a_{11}}(\omega) & m_{a_{12}}(\omega) & \dots & \dots & m_{a_{1n}}(\omega) \\ m_{a_{21}}(\omega) & m_{a_{22}}(\omega) & m_{a_{23}}(\omega) & \dots & m_{a_{2n}}(\omega) \\ \vdots & \vdots & \vdots & \ddots & \vdots \\ m_{a_{n1}}(\omega) & \dots & \dots & \dots & m_{a_{nn}}(\omega) \end{bmatrix}$$
$$B_{r_{array}}(\omega) = \begin{bmatrix} b_{r_{11}}(\omega) & b_{r_{12}}(\omega) & \dots & \dots & b_{r_{1n}}(\omega) \\ b_{r_{21}}(\omega) & b_{r_{22}}(\omega) & b_{r_{23}}(\omega) & \dots & b_{r_{2n}}(\omega) \\ \vdots & \vdots & \vdots & \ddots & \vdots \\ b_{r_{n1}}(\omega) & \dots & \dots & \dots & b_{r_{nn}}(\omega) \end{bmatrix} \tag{2.20}$$

The radiation matrices are presented in equation 2.20, where the hydrodynamic interaction is clearly shown. The diagonal elements are the independent radiation terms and the off-diagonal elements represent the radiation interaction between devices. According to the discussion for equation 2.17, the radiation impedance for device i is the same as the radiation impedance for device j. Thus, in equation 2.20, $m_{a_{ij}}(\omega) = m_{a_{ji}}(\omega)$ and $b_{r_{ij}}(\omega) = b_{r_{ji}}(\omega)$.

In this thesis, for the reasons stated in section 2.2.1.4, the BEM solver Nemoh is

employed to solve for the WEC array hydrodynamic coefficients.

To expand the analysis of WEC array to time domain, the radiation interaction must be properly modeled. Similar to the single WEC case, the derivation starts from the Cummins equation 2.11. For the WEC array, each device will interact with the others through radiated wave, and the Cummins equation must be rewritten to resemble the radiation interaction between devices.

The radiation force for each WEC in the array can be written as:

$$f_{r_i}(t) = m_{a_i}(\infty)\ddot{z}_i(t) + \sum_{j=1}^{N} \int_{-\infty}^{t} h_{r_{ij}}(\tau)\dot{z}_j(t-\tau)d\tau \tag{2.21}$$

Equation 2.21 can be separated into two parts to construct radiation matrices.

$$\begin{aligned} f_{r_i}(t) &= f_{r_{ii}} + \sum f_{r_{ij}}, \quad where\, i \neq j \\ f_{r_{ii}}(t) &= m_{a_i}(\infty)\ddot{z}_i(t) + \int_{-\infty}^{t} h_{r_i}(\tau)\dot{z}_i(t-\tau)d\tau \\ f_{r_{ij}}(t) &= \int_{-\infty}^{t} h_{r_{ij}}(\tau)\dot{z}_j(t-\tau)d\tau, \quad where\, i \neq j \end{aligned} \tag{2.22}$$

The radiation state matrices for each WEC are then generated with the two parts shown in equation 2.23.

$$\begin{aligned}
\begin{Bmatrix} \dot{z_{r_{ii}}} \\ f_{r_{ii}} \end{Bmatrix} &= \begin{bmatrix} A_{r_{ii}} \\ C_{r_{ii}} \end{bmatrix} z_{r_{ii}} + \begin{bmatrix} B_{r_{ii}} \\ \mathbf{0} \end{bmatrix} \dot{z}_i + \begin{bmatrix} \mathbf{0} \\ m_{a_i}(\infty) \end{bmatrix} \ddot{z}_i \\
\begin{Bmatrix} \dot{z_{r_{ij}}} \\ f_{r_{ij}} \end{Bmatrix} &= \begin{bmatrix} A_{r_{ij}} \\ C_{r_{ij}} \end{bmatrix} z_{r_{ij}} + \begin{bmatrix} B_{r_{ij}} \\ \mathbf{0} \end{bmatrix} \dot{z}_j
\end{aligned} \tag{2.23}$$

Combining the two parts in equation 2.23, the total radiation force acting on each WEC in the array is written in equation 2.24.

$$f_{r_i}(t) = \begin{bmatrix} C_{r_{i1}}, C_{r_{i2}}, \ldots, C_{r_{in}} \end{bmatrix} \begin{Bmatrix} z_{r_{i1}} \\ z_{r_{i2}} \\ \vdots \\ z_{r_{in}} \end{Bmatrix} + m_{a_i}(\infty)\ddot{z}_i \tag{2.24}$$

2.3 Review of Control Strategies in Ocean Wave Energy Conversion

Since the beginning of wave energy conversion research, control is an essential part of the study. The energy can only be harvested if a control force is applied to the WEC.

The control law varies from the simplest resistive control with a damping mechanism to complex optimal control algorithms.

2.3.1 Optimal Control of an Isolated WEC

In the early development of WEC control, phase matching was first studied by Budal and Falnes [82]. This control method is called latching control, and it remains useful even today due to easy implementation using a hydraulic PTO system. When both the amplitude and the phase of the incoming wave are matched, the control law is called impedance matching.

Impedance matching optimal control, as it can produce the theoretical maximum amount of energy, has been studied and implemented in many cases [19]. This controller takes the form of a PD controller and tunes the impedance of the WEC so that it resonates in the frequency of the ocean wave. With the optimal tuning, the optimal velocity in [19] is shown in equation 2.25.

$$v_{opt}(\omega) = \frac{F_{ex}(\omega)}{2b_r(\omega)} \tag{2.25}$$

The optimum power for array is then found to be:

$$P_{max}(\omega) = \frac{F_{ex}(\omega)^2}{8b_r(\omega)} \tag{2.26}$$

This optimum power extraction represents the theoretical limit of an isolated WEC device and functions well as an performance indication or comparison against other controllers. In [83], the impedance matching control is implemented with a FFT based observer. Taking the concept of impedance matching, a constrained sub-optimal wave-by-wave control was developed by Korde [5, 84]. Another sub-optimal controller was investigated under different wave climates By Folley [85].

A constrained 'Bang-Bang' control with several variations was evaluated in [86]. A 'Bang-Singular-Bang' controller was developed by Zou [24]. The optimal control is found to be on a singular arc and it yields the same trajectory with the impedance matching control when there are no saturation on the control force. Using the same method of deriving the analytical optimal solution, a simple-model-control was developed by Abdelkhalik and Zou [87]. Numerical optimal control was done on single WEC device using a pseudo-spectral approach by Zou [22], where the system was approximated using Fourier Series.

Model predictive control (MPC) is another powerful controller that has been studied in [20, 21, 88, 89]. MPC is also proved to reach the theoretical maximum power extraction with perfect knowledge of the input wave.

With unconstrained optimal controller, the WEC device often moves with an unrealistic amplitude of motion. Since the linear wave theory is valid only when the motion of the body is small, non-linearity rises as another problem during the design of WEC controllers.

In [90], an optimal feedback controller is designed with non-linear buoyancy force. Another study that also considers the change in buoyancy force is the shape-based control by Abdelkhalik [91].

2.3.2 WEC Array Optimal Control

The control methods for single WEC can be applied to WEC array with proper modification on the dynamic model. However, as stated before, the hydrodynamic interaction adds complexity and difficulty to the WEC array problems including the control design. Thus, two approaches are taken by the majority of the WEC array research. One is to design the layout and other aspects of the WEC array that directly affects the hydrodynamic properties of the WEC array using simple controllers such as resistive control and latching control. This is discussed in detail in section 2.5. The other approach is to focus on the control itself with a fixed and relatively simple WEC array design.

As pointed out in [23, 92], the performance of a WEC array depends on the hydrodynamic interaction between devices. Thus, the purpose of the WEC array control is to enhance the positive hydrodynamic interaction in the target array. The complex conjugate control formulation for WEC array is developed in [15] and [13] individually. This complex conjugate control is an extension of the isolated WEC complex conjugate control and considers the radiation interaction between devices. More recently, a collective proportional-damping collective controller is developed in [11]. These controllers that considers the hydrodynamic interaction between buoys are called global control in [35] and [92]. Sub-optimal cases where each device in the array is controlled with only the information collected from itself are also studied in[85].The comparison between the global array control and the independent array control is made in [35][92] and [23]. A model-predictive controller neglecting the cross device interaction is developed by [93]. The WEC array MPC with complete hydrodynamic interaction is developed in [39] where the optimization problem is solved using quadratic programming.

2.4 Review of Actuators Used in Ocean Wave Energy Conversion

To provide control force and perform energy extraction, the power-take-off unit is necessary for all types of WEC device. Two types of PTO are introduced in this section, which are hydraulic actuator system and direct drive system accordingly. In depth review of different PTO units and the corresponding devices and control techniques are given in [65, 94, 95, 96].

2.4.1 Hydraulic PTO Unit

A typical hydraulic PTO system is shown in figure 2.7. The PTO system is connected with the heaving WEC with a rigid link. The WEC motion is directly converted to the volume and pressure change in chambers of the hydraulic piston. Two accumulators are used as energy storage and stabilize the output of the hydraulic motor. The fluid flow from the high pressure accumulator to the motor and then goes into the low pressure accumulator. A rectifying system is used to rectify the flow from piston chambers to the accumulators.

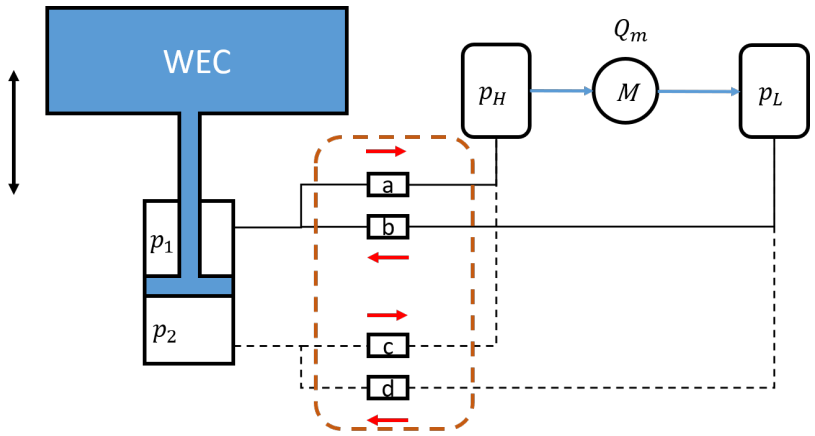

Figure 2.7: A hydraulic system connected with a heaving buoy. p_1 and p_2 are the pressure in the two chambers. p_H and p_l are the pressure in the high/low pressure accumulators respectively. M is the hydraulic motor which will be connected with the generator. Q_m is the flow rate through the motor. a to d are the four rectifying valves.

The hydraulic PTO dynamic equations are derived in [97] and different control methods are applied and tested. The additional control accumulators are found to produce more energy from the WEC, while the efficiency is reduced since more components are introduced to the hydraulic circuit. A parameter based control was developed by Falcao [98], in which the control was derived using the relationship between motor flow rate and the pressure difference between the pressure accumulators. A mathematical model was developed by Eidsmoen [99] for slack-moored WEC with full dynamics of the hydraulic system. Other than the heaving type WECs, a numerical model was developed by Josset, Babarit and Clement [61] for the second generation SEAREV WEC with hydraulic PTO circuit.

For realistic considerations, energy efficiency of the hydraulic PTO circuit is studied by many researchers. A comparison of WEC energy extraction with and without

considering the energy loss is performed by Plummer [25]. Losses in hydro-static pumps and motors are modelled and investigated in [100]. Pipe pressure drop, torque loss, and friction loss are modelled and analyzed in [11, 96].

Hydraulic PTOs often operate in low frequency range, which matches the frequency range of the WEC and ocean wave. Another advantage of hydraulic PTOs is the high force amplitude they support, as the control force required by WEC is often large. Other advantages are the system robustness, energy storage and smoothing effect provided by hydraulic accumulators.

2.4.2 Direct Drive PTO Unit

A typical direct drive PTO system is shown in figure 2.8. The translator of the generator is connected with the WEC with a rigid link. The relative motion between the stator and translator converts part of the kinematic energy to magnet-electric energy. Comprehensive reviews of the direct drive technology are provided in [26, 101, 102].

The optimum control and resistive control for WEC arrays using direct drive generator is evaluated in [103]. Similar to the implementation on single WEC, the optimal control requires accurate wave prediction and produces theoretical maximum amount of energy extraction. The resistive control is easy to implement and the performance

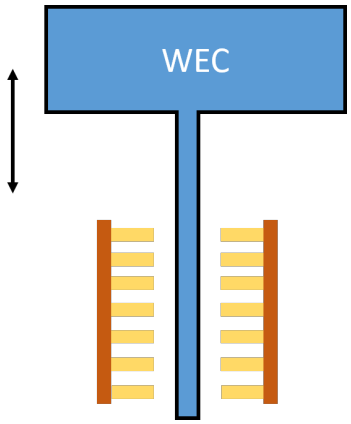

Figure 2.8: A direct drive system connected with a heaving buoy. The connection between WEC and the translator is rigid.

is inferior. An emulation based resistive control for direct drive WECs is developed in [104], where the regular wave responses from the WEC are taken to emulate the irregular wave responses. A sub-optimal current control is employed in [105]. In [106], a direct drive surge converter with high capture width ratio is modeled and evaluated. An emulator was developed by Nie [107] to produce the characteristics of a direct drive linear WEC. In [108], three variations of the magnet-electric generators were developed and tested. Considering the economic aspects, the latching controls are investigated and compared against the resistive control for direct drive WECs by [109]. The efficiency of using direct drive generators is studied in [110, 111].

Compared with hydraulic PTO unit with full non-linear dynamics, the direct drive approach has less intermediate processes and the PTO unit is less complex. The direct drive PTO unit is more efficient in energy conversion and easier to connect to the power grid. However, the linear permanent magnet generators tend to operate under high frequencies and often have relatively smaller force output. These aspects

require the LMPG unit to be large enough to support the design requirement of a WEC device. The cost of the unit and the maintenance process are also items that have to be considered.

2.5 Review of the WEC Array Layout Study

Hydrodynamic interaction between devices in the array plays the most essential role in the WEC array analysis. The study of WEC array design is actually the research of factors that enhance positive hydrodynamic interaction. To evaluate the performance of a WEC array, Budal [14] first developed the q-factor as an evaluation parameter. The q-factor is the total power absorbed by a WEC array divided by the summation of the power absorbed by isolated WEC devices as shown in equation 2.27.

$$q = \frac{P_{array}}{NP_i} \tag{2.27}$$

The summation of power from isolated WECs are calculated as NP_i since the array is assumed to be constructed with identical devices. The power extracted from the array is more than the summation of power from isolated WECs when the q-factor is greater than one, and the array is less efficient when the q-factor is smaller than one. The q-factor indicate whether the hydrodynamic interaction between devices in

a WEC array is constructive or destructive.

An alternative way to evaluate the array performance is to use the modified q-factor (q-mod) developed by Babarit [31]. The q-mod is defined as the difference between the power absorbed by a WEC in the array and the power absorbed by the WEC isolated, divided by the maximum power extracted from the isolated WEC, and is shown in equation 2.28. The sign of the q-mod represents the effect of hydrodynamic interaction and also compares the performance of the array with the maximum possible power from isolated devices when a proper control is applied.

$$q_{mod} = \frac{P_i - P_{iso}}{max_T P_{iso}(T)} \tag{2.28}$$

The q-factor is used to evaluate the WEC array performance and serves as the optimization objective in chapter 3 and chapter 4.

2.5.1 Factors Affect The WEC Array Design

Global layout and size of array, shape and dimension of each device, along with wave profile including wave direction and sea states, all have great impact on the array performance [32, 54, 112]. Babarit [31] studied the wave park effect and the energy

flux after a WEC device. The energy flux is found to recover after 500 meter separation between the two devices, thus the hydrodynamic interaction can be neglected. The interaction between buoys in the array with an arbitrary layout was studied in [73, 113, 114]. Penalba [3] studied arrays with different buoy slenderness and the hydrodynamic interaction is found to be mostly destructive and fluctuates violently when the separation distance is relatively small. This finding reveals the difficulty in implementing the optimal array layout, since it is critical to find the exact separation distance and fix the device at the desired location.

Besides the separation distance, size and shape of WEC are also significant factors in designing arrays. Earlier study of the compact array has found that the center buoy always has a higher response compared to the other buoys in the array [114]. The impact from varying separation distance of each device in the array was studied by Korde and Ringwood[35] with arrays containing 2,3 and 4 buoys with four arbitrary geometries of the layout. A 40% higher q-factor was found when control and separation distance were selected properly. Recently, an expanded multiple scattering method was developed by Goteman[33] which assumes cylindrical device while allowing the size of each device to change. This study showed an improved array performance with buoys of different dimensions and great potential in designing large WEC arrays.

The effect of input wave direction was studied in [32, 38, 48, 49, 115]. In [32], The

integration of q-factor calculated from all directions around the array is found to be a constant number of one. The wave direction β is found to have great significance in the sense of q-factor fluctuation [31, 115]. Reference [115] points out that the q-factor does not fluctuate too much when the incident wave direction is perpendicular to the array direction. However, the overall hydrodynamic interaction becomes small or even destructive.

Another critical factor that affects the design of a WEC array is the ocean environment. In reference [35], different types of WEC are discussed and each of them has unique advantages in certain environments such as a specific water depth and wave profile. OWSC type devices are superior in shallow water [116][117] while cylindrical heave-mode WEC can be deployed in deep water areas with some other functions installed. Due to the complex nature of the ocean environment, there are always times where different types of device can not be evaluated clearly. Thus, the type of device should also be considered when finding the optimal configuration of an array.

2.5.2 WEC Array Layout Optimization

Layout optimization has been done for both regular and irregular waves to achieve the optimal performance of an WEC array. Due to the complex nature of hydrodynamic interaction [2], global optimization is required to find the optimal layout

that provides constructive interaction. Similar to Fitzgerald's study [32], Child [48] modified the layout optimization problem and formulated a local optimization. The parabolic intersection method Child developed is more efficient but less accurate than traditional GA. Moarefdoost [2] borrowed the idea and further increased calculation speed by using point absorber approximation from Budal [14] rather than using exact hydrodynamics. Meanwhile, layout optimization was conducted by McGuinness with the constrains of device motion [118]. In 2017, Tay and Venugopal studied the optimal spacing of an oscillating wave surge converter (OSWC) array using a modified genetic algorithm [38]. The scatter parameter was found to affect the optimal spacing significantly. The optimal layout for an OSWC array was found to have to let the wave propagate through the array with little reflection. Time domain simulations of heaving WEC arrays were conducted by Bozzi [119]. The three-phase electric power model was employed to calculate the power take-off force. Different array layouts and wave directions were considered in their work.

Optimization has been employed by many researches ([32, 38]) to find the WEC array configuration that enhances the hydrodynamic interaction. Relatively sparse array layouts with a separation distance of 100m or more were found to be optimal, for both regular and irregular waves, in several numerical investigations that use Boundary Element Methods (BEM) for hydrodynamic calculations [2, 32, 49]. On the other hand, some studies that employ semi-analytical approaches, under certain assumptions, find that the relatively compact arrays are more competitive in irregular

waves [112, 120].

The configuration of arrays of flap-type oscillating surge wave converter (OSWC) has also been studied in several references [36, 37, 38]. Similar to the arrays of heaving buoys, optimal separation distance was investigated along with the effect of wave direction.

Chapter 3

Optimization of Both Layout of the Array and Dimension of Each Device

In [2, 32, 48] and many other studies, the optimal layout of an array of heaving buoys is found using the point absorber approximation. Since the shape and the size of devices have significant impact on the performance of an array of heaving buoys as shown in [33, 35]. One objective of this thesis is to investigate if the WEC array performance can be further enhanced for an array with optimal layout if the dimension of each device is optimized.

This chapter explores the optimal configuration of both dimension and layout of arrays of heaving buoys with full interaction and exact hydrodynamics from the numerical BEM solver Nemoh. The dimension of each buoy is optimized with full hydrodynamics calculated using Nemoh. The WEC array with identical buoys and optimal layout found by [2, 32] is used as a comparison as shown in figure 3.1.

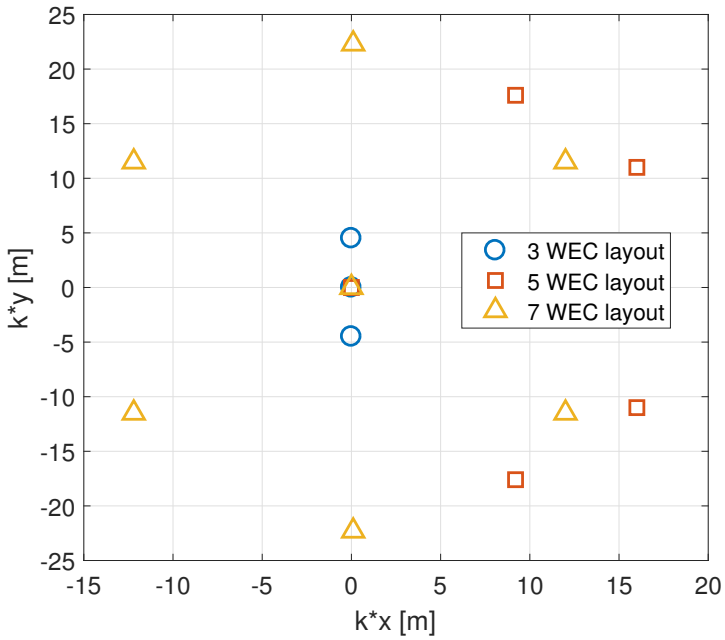

Figure 3.1: Optimal layout for array of 3 WEC, 5 WEC and 7 WEC [2]

3.1 Dynamic Model and Control for The WEC Array

The WEC array dynamics has been discussed in section 2.2.2.1. Two cases will be evaluated in this work. One case optimizes the array layout and buoy dimensions with regular wave as input. The other case optimizes the array layout and buoy dimensions with irregular wave as input. To optimize the WEC array configuration with full hydrodynamics using reasonable computational cost, frequency domain analysis is employed with the WEC array dynamic equation 2.19. The hydrodynamic coefficient matrices of the WEC array are solved using BEM solver Nemoh.

Note that in equation 2.19, $\overrightarrow{\mathbb{F}_{ex}}$ is the hydrodynamic excitation force coefficient calculated from the BEM solver assuming a unity wave input. Physically both $\mathbf{M_a}(\omega)$ and $\mathbf{B_r}(\omega)$ are symmetric since the radiation impedance between any two bodies are the same with the unit velocity. It implies that $m_{a_{ij}}(\omega) = m_{a_{ji}}(\omega)$ and $b_{r_{ij}}(\omega) = b_{r_{ji}}(\omega)$ where i and j are the index for WECs in the array. A power calculated from Eq.3.2 is always real. But with the BEM solver such as Nemoh, there is a numerical error between $m_{a_{ij}}(\omega)$ and $m_{a_{ji}}(\omega)$ when WECs in the array are no longer identical. In the later simulation, only half of the hydrodynamic matrix is carried into calculation as a correction to this problem. With the impedance matching control, this power can

be considered as theoretical maximum absorbed power from the array.

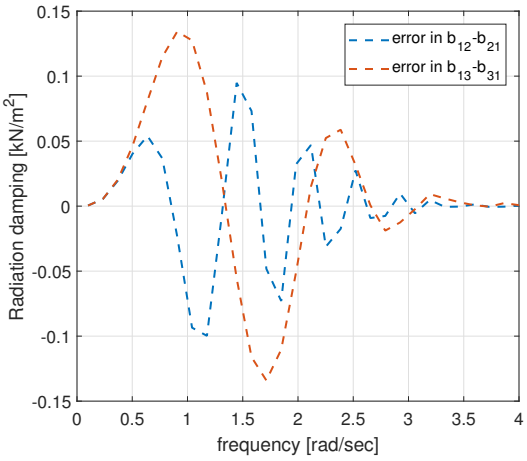

Figure 3.2: Numerical error from BEM solver. The difference is calculated between symmetric off diagonal elements $b_{12} - b_{21}$ and $b_{13} - b_{31}$ when the 3 devices in the array are not identical

As the control algorithm is find to affect the WEC array performance significantly, two different control strategies are employed. The unconstrained impedance matching control reveals the theoretical optimum power absorption. The WEC array configurations optimized using impedance matching control are compared with the optimal WEC array layout using identical buoys presented in [2]. The passive derivative control is employed to investigate the WEC array performance with realistic consideration of control implementation.

the impedance matching solution is given by Falnes [19]. In the absence of constraints, the collective optimal velocity is given by equation 3.1.

$$\overrightarrow{\mathbf{u}_c}(\omega) = \frac{1}{2}\mathbf{B_r}(\omega)^{-1}\overrightarrow{\mathbb{F}_{ex}}(\omega) \tag{3.1}$$

The optimum power for the WEC array is then found to be:

$$P_{max}(\omega) = \frac{1}{8}\overrightarrow{\mathbb{F}_{ex}}(\omega)^{*} v \mathbf{B_r}(\omega)^{-1}\overrightarrow{\mathbb{F}_{ex}}(\omega) \tag{3.2}$$

The second control implemented in this work is passive control. The control force defined to be proportional to the array velocity as shown in equation 3.3.

$$\overrightarrow{\mathbb{F}_c}(\omega) = j\omega \mathbf{K_d}\,\overrightarrow{\mathbb{Z}}(\omega) \tag{3.3}$$

The coefficient matrix $\mathbf{K_d}$ has only the diagonal elements of $\mathbf{B_r}(\omega)$, and the power from array is written as Eq.3.4. The independent control force needs only the information from each buoy itself, and there is no communication in the array. The extracted power at each frequency is shown in equation 3.4.

$$
\begin{aligned}
P_{passive}(\omega) &= -j\omega \sum_{i=1}^{i=N} f_{c_i}(\omega) z_i(\omega) \\
&= \omega^2 \sum_{i=1}^{i=N} k_{d_i}(\omega) |\bar{z}_i(\omega)|^2
\end{aligned}
\tag{3.4}
$$

With the extracted power defined, the performance of the array can be evaluated using the q-factor. However, since the buoys in the array are no longer identical in this study, equation 2.27 needs to be modified. The q-factor being used in this chapter is formulated as shown in equation 3.5. Where P_i is the power for each isolated WEC.

$$
q = \frac{P_{array}}{\sum P_i} \tag{3.5}
$$

3.2 Formulation of The WEC Array Optimization Problem

3.2.1 Optimization of the dimensions of each buoy in the WEC array with Genetic Algorithm

In this section, the q-factor of the array is optimized with the design parameters selected as the radius of each buoy in the array. The layout of the array is optimized separately with the equation of q-factor simplified with the point absorber approximation [2]. With the wave direction of 0°, the optimized layouts for arrays that contain three, five and seven WECs are solved in the literature [2] and the result is shown in figure 3.1

Once the optimal layout is obtained, it will be used for optimization of the dimension of each buoy in the array. The variables that define the dimension of the cylindrical buoys are:

1. radius of each buoy $R_1, R_2, ...R_n$

2. draft height of each buoy $D_1, D_2, ...D_n$

Here we constrained the design variables by fixing the mass of each device. This leads to a constant submerged volume of each buoy. The constraint can be written as:

$$V_i = \pi R_i^2 D_i = constant \tag{3.6}$$

Without using constrained optimization, the designed variables can be rearranged using the constraint to simplify the problem formulation. The design variables are defined as the radius of each buoy $R_1, R_2, ...R_n$ with the draft height of each buoy defined as $D_i = \frac{V_i}{\pi R_i^2}$.

The initial volume of each buoy is selected as $1\,m^3$. The formulation of the optimization is written as:

$$\begin{aligned} &\underset{dimension,layout}{max} \quad q = \frac{P_{array}}{\sum P_i} \\ &s.t. \qquad D_i = \frac{1}{\pi R_i^2} \quad \forall \quad i = 1, 2, 3, ... \\ &R_i \subset [0.5, 2]m \quad \forall \quad i = 1, 2, 3, ... \end{aligned} \tag{3.7}$$

3.2.2 Optimization of both dimension and layout of WEC array

The mathematical formulation of the novel dimension-layout optimization for a WEC array is presented in this section. Similar to the optimization in section 3.2.1, the objective is to maximize the q-factor of an WEC array. The design parameters are selected as both the layout of the array and the dimension of each WEC device. Since the optimal layout of a WEC array is symmetric under the point absorber approximation [32], another constraint on the location of each WEC needs to be considered. In this study, only impedance matching control is applied to calculate the power from the array. This optimization is done only on the array of three WECs.

The design variables are the radius of each buoy R_1, R_2, R_3, and the location of each buoy $[x_1, y_1], [x_2, y_2], [x_3, y_3]$ in Cartesian coordinate. Applying the constraint of symmetric layout, the location of the first buoy is fixed at the origin, the location of the second buoy is on the upper half plain and the location of the third buoy is on the lower half plain. The formulation of this optimization is written as:

$$
\begin{aligned}
&\underset{dimension,layout}{max} \quad q = \frac{P_{array}}{\sum P_i} \\
&s.t. \qquad D_i = \frac{1}{\pi R_i^2} \quad \forall \quad i = 1,2,3 \\
&R_i \subset [0.5,2]m \quad \forall \quad i = 1,2,3 \\
&x_1 = y_1 = 0m \\
&x_2, x_3 \subset [-10,10]m \\
&y_2 \subset [4.5/k - 50, 4.5k + 50]m \quad \& \quad y_3 \subset [-4.5/k - 50, -4.5k + 50]m
\end{aligned}
\tag{3.8}
$$

Where k is the wave number and $[0, \pm 4.5k]m$ is the optimal location for the second and the third buoy solved with point absorber approximation.

Since the WEC array optimization is a global optimization problem, the Genetic Algorithm built in MATLAB ® is employed to solve the parameter optimization problems with the settings shown in table 3.1.

Items	**Value**
Max generation	100
Max population	10*nWEC
Mutation Function	zero mean Gaussian
Crossover Option	Scattered
Increment in searching R_i	0.15m

Table 3.1
Settings of Genetic Algorithm built in MATLAB ®

At each generation a random binary vector that has the same length as design variable

vector will be created. The genes of the crossover child will be taken from the first parent if the corresponding element in the crossover vector is 1. The genes will be taken from the second parent if the corresponding element is 0. A random number, selected using zero mean Gaussian distribution with respect to each element in the parent vector, will be added to the parent vector to create mutation in the children.

3.3 Numerical Results

3.3.1 Simulation setup

All simulations are conducted on Michigan Tech's shared high-performance computing cluster. The cluster has 32 CPU cores (Intel Xeon E5-2683 2.10 GHz) and 256 GB RAM. The initial WEC array layout is shown in figure 3.1. The initial dimension for all WECs are selected as $R = 1m$, $D = 1m$. The wave number used for comparison is $k = 0.2$. The wave direction is set to $\beta = 0°$ for all simulation. Hydrodynamics BEM solver Nemoh is employed to compute the exact hydrodynamics for all simulation.

Reference [2] presents a case study of an array of 3 WECs that will be investigated further in this paper. Reference [2] uses a point absorber approximation, assuming all buoys have identical dimensions, and show that the q factor remains unchanged if the product of kR is constant. Here we firstly use a numerical boundary element

method (Nemoh) to validate this conclusion. Table 3.2 shows a comparison between the results presented in [2], and the results obtained using Nemoh for the same array, assuming identical buoys dimensions. The product $kR = 0.2$ was kept the same in all the cases; the resulting q-factor did not change significantly. The following sections will highlight the impact of allowing different buoys in the array to have different dimensions on the q factor.

tests	q	k	R	D	kR	nWEC	hydrodynamics
Reference [2]	1.9848	0.04	5m	20m	0.2	3	approx.
test 1	1.9846	0.2	1m	1m	0.2	3	Nemoh
test 2	1.9822	0.04	5m	20m	0.2	3	Nemoh

Table 3.2
Compare the literature result with the Nemoh results

3.3.2 Optimization of dimension of each buoy in the WEC array

With the layout shown in figure 3.1, and the mathematical formulation in section 3.1, optimization of the dimension of each WEC in the arrays of three, five and seven buoys are done with both the impedance matching control and the passive control. Optimization results using the impedance matching control are shown in figure 3.3, and results using the derivative are shown in figure 3.4. For the array of three WECs, buoy 1,2,3 refer to the buoy on the center, the buoy on the top and the buoy on the bottom. For the array of five WECs, buoy 1 to 5 are the buoy on the center, the

upper buoy on the 2nd column, the lower buoy on the 2nd column, the upper buoy on the 3rd column, and the lower buoy on the 3rd column respectively. For the array of seven WECs, buoy 1 is on the center, buoy 2,4,6 are the upper buoys on column 1,2,3, and buoy 3,5,7 are the lower buoys on each column.

All simulations are conducted on Michigan Tech's shared high-performance computing cluster. The cluster has 32 CPU cores (Intel Xeon E5-2683 2.10 GHz) and 256 GB RAM. The computational costs for arrays of 3,5 and 7 WECs using impedance matching control are 3.05 hours, 23.42 hours and 82.59 hours respectively. The costs for the same arrays using passive damping control are 2.95 hours, 24.11 hours, and 92.21 hours respectively. The growth of the array size will produce a quadratic growth in the calculation of radiation matrices. The growth of computational cost shows a similar trend.

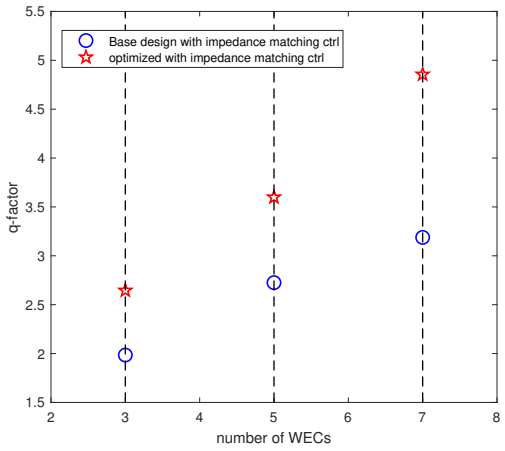

Figure 3.3: The q-factors optimized using impedance matching control. The circles represent the results with initial set up, and pentagrams represent the results with optimized dimensions

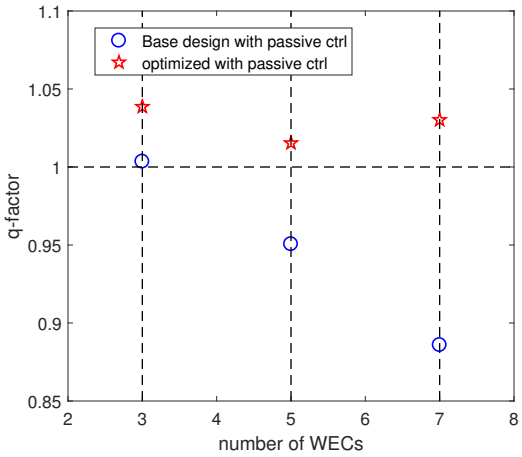

Figure 3.4: The q-factors optimized using passive control. The circles represent the results with initial set up, and pentagrams represent the results with optimized dimensions

As the results in figure 3.3 and figure 3.4 indicate, higher q-factors are achieved by optimizing the dimension of buoys. The average optimized q-factor is 39.21% higher using the impedance matching control and it is 8.87% higher using the derivative control. The q-factors increase differently in the two presented categories of tests. The first batch of tests are ones that use impedance matching control (complex conjugate control.) This control method is known for providing the maximum possible energy without considering constraints. As a result, the resulting q-factors shown on figure 3.3 are significantly higher while the buoys oscillate with unrealistic displacement which can be seen from table 3.3. In table 3.3, z_3,z_5, and z_7 exceed 2 meters using impedance matching control, which are higher than the wave amplitude of one meter. The harvested mean power is also higher for each of the tests. These tests are good for showing the maximum possible potential of the array, but are not good for realistic considerations. The second batch of tests use damping control which also increase

the q-factors. These tests are good for realistic considerations while there exist room for the improvement of the control design. The q-factor results shown in figure 3.3 indicate that the q-factor increases along with the array size. This is the same finding as presented in [2, 32].

	q_3	$p_3[kW]$	$z_3[m]$	q_5	$p_5[kW]$	$z_5[m]$	q_7	$p_7[kW]$	$z_7[m]$
initial	1.98	1565.6	1.03	2.72	5972.1	1.00	3.18	13693	0.97
optimal	2.64	1780.1	2.52	3.59	6878.5	2.26	4.85	17424	2.42

Table 3.3
the q-factors, absorbed power and displacements from the optimized arrays using the impedance matching control. The test group "initial" refers to the tests using fixed size buoys. The test group "optimal" refers to the tests using optimal sized buoys. The footnotes "3,5,7" refer to the number of WECs in the array. z_3, z_5, z_7 are the averaged displacements of the three tested arrays.

With the initial setup, arrays using the derivative control do not perform as well as arrays using the impedance matching control. This is because the selected layout is optimized with the point absorber approximation which assumes the impedance matching control. But with optimization of the dimension, the q-factors for all three arrays are above one. It indicates a constructive coupling effect between each buoy in the array, which is shown on figure 3.4.

On figure 3.5, the red circles are optimized radius of each buoy and the black circles are the initial radius of each buoy. For the tests with the impedance matching control, we can see that the center buoys in all three arrays have the largest possible radius, and almost all other buoys have the smallest possible radius. For the tests with the derivative control, the center buoys have the largest radius, and the buoys on the

third column have the 2nd largest radius.

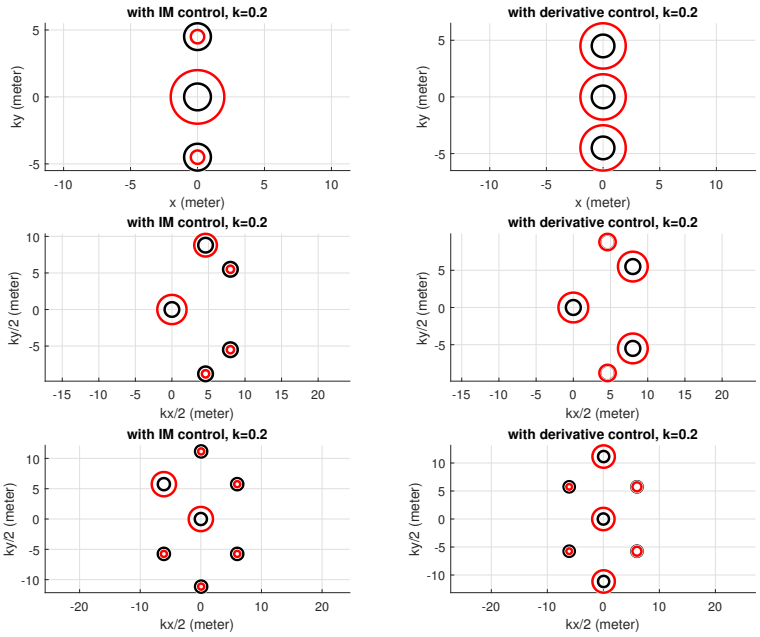

Figure 3.5: Optimized dimensions for each WEC in the array. Figures on the left are optimized dimensions using the impedance matching control. IM stands for impedance matching. Figures on the right are results using derivative control. The red circles represent the sizes after optimization, the black circles represent the sizes before optimization (identical radius and height.)

To further understand the results, detailed dimensions and hydrodynamics have been examined. The buoys initial and optimized dimensions are shown in figure 3.5, and the excitation force coefficients are shown on figure 3.6. In the test with impedance matching control, the center buoy in all 3 arrays have larger dimensions than the other buoys in array, and all buoys on the side are small, and thus only experience small excitation force except for top left buoys on figure 3.5. On the left part of figure 3.6, buoy 2 has a larger radius than 3 in both array of 5 and 7 WECs, which

experiences a higher excitation force, as shown as blue triangles.

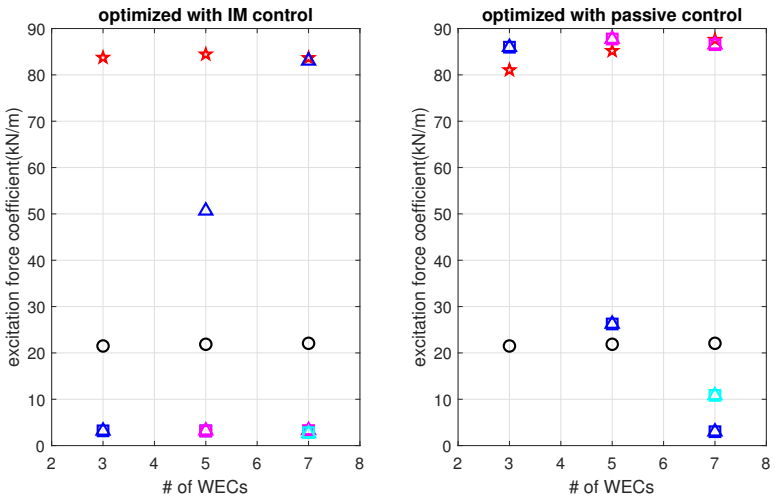

Figure 3.6: excitation force coefficients from optimization. Black circles are from initial set up. Red stars are coefficients for center buoy.

test index	control	group 1	group 2	group 3
1	impedance matching	buoy1	2nd largest buoy	small buoys
2	passive control array of 3 WEC	buoy1,2,3		
3	passive control array of 5 WEC	buoy1,4,5	buoy2,3	
4	passive control array of 7 WEC	buoy1,4,5	buoy4,5	buoy2,3

Table 3.4
different groups of buoys defined by their optimized radius

Based on observation above, we can separate buoys in the arrays into different groups by their radius, then further investigate the effect of hydrodynamic coefficients for each group. Buoys in group1 in all tests have radius of $2m$ and buoys in group 3 have radius of $0.5m$. Buoys in group 2 have radius between $1m$ and $1.5m$.

Since radiation impedance is affected by dimension and relative distance between

each buoy, it is useful to observe the radiation impedance of each group and coupled impedance between each group. Radiation impedance of each group is defined to be Z_{g_i} and coupled impedance is defined to be $Z_{g_{ij}}$, where i and j denotes group number. Discussion will be focused on radiation damping Br_{g_i} and $Br_{g_{ij}}$ which is the real part of the impedance.

From optimization results with impedance matching control, on figure 3.7 it is shown that center buoys are optimized to have larger radiation damping on themselves and buoys around them are all optimized to have small radiation damping on themselves. We can see that the radiation damping coefficients are grouped together for buoys of the same dimensions on figure 3.7. All the optimal arrays using the complex conjugate control have one larger buoy at the center with larger radiation impedance, and smaller buoys on the side with smaller radiation impedance. When optimized using the passive control, buoys in the middle group have the same larger size and buoys in other groups have smaller sizes. The groups are shown in table 3.4.

Besides the radiation acting on each buoys themselves, the coupling terms in radiation damping matrices are also presented in table 3.5

From results in table 3.5, optimization with derivative control results in larger radiation damping coefficients for entire radiation impedance matrix. While results with impedance matching control focus most on the center buoy in array and diminishes the effect from other buoys.

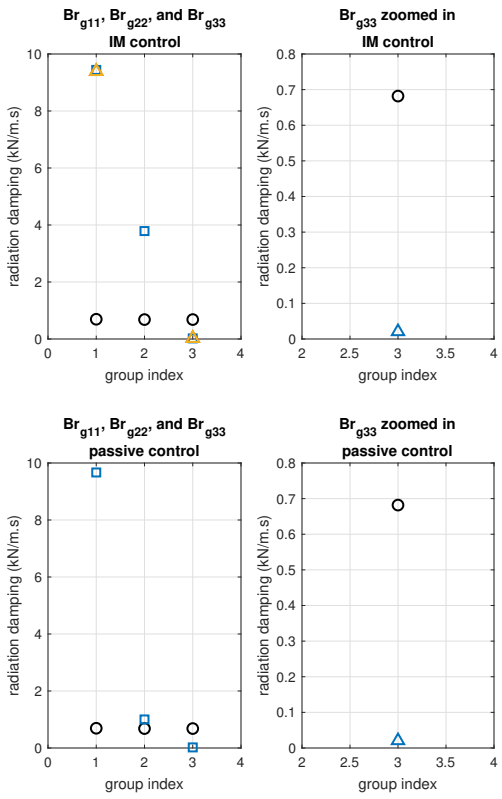

Figure 3.7: radiation damping coefficients computed for case with impedance matching control are shown on this figure. black circles present radiation damping for initial set up. the plot on the right is zoomed in part of $B_{r_{g33}}$. Top 2 plots are results with optimal, bottom 2 tops are from derivative control

3.3.3 Optimization of both layout and dimension of WECs in the array

Point absorber approximation is used to calculate and to optimize the layout of array in literature [2]. When impedance matching control is applied, the power calculated with exact hydrodynamics is the same as solution from point absorber approximation.

$B_r(Ns^2/m)$	b12	b23	b13	b35	b16	b67
initial	-233.1	-43.5	122.5	-118.7	-134.1	-133.6
impedance matching	-190.2	-1.4	64.4	-3.9	-68.6	-3.4
derivative control	-356.9	44.5	555.7	-491.4	-287.4	-42.3

Table 3.5
b12 and b23 are coupled radiation damping terms from array of 3 WECs, b13 and b35 are radiation damping terms from array of 5 WECs, b16 and b67 are terms from array of 7 WECs

Then it is possible to optimize of both layout and dimension together. And when impedance matching control is employed, the solution of layout and dimension should be the same as the solution from section 3.3.2.

To optimize both layout of array and dimension of buoys, additional constraints need to be considered. From the results of previous optimization, when impedance matching control is employed, the buoy in the center of array has the most significant contribute to the total power extraction. So center buoy will be fixed at origin of the domain. Then with symmetry of layout considered, the side buoys are constrained to move only in half of the domain in y direction. The new layout constraint for array of 3 WECs is shown on figure 3.8.

The location constraint shown on figure 3.8 is set to be 10 meters. This optimization result is shown in table 3.6. In table 3.6, cases 1 to 3 are comparisons against the result from reference [2]. Case 4 is a comparison with case 3 to show that the solution is optimal, even when a larger search range is given. Items WEC2 and WEC3 in table 3.6 refer to the coordinates for the second and the third WEC in the array

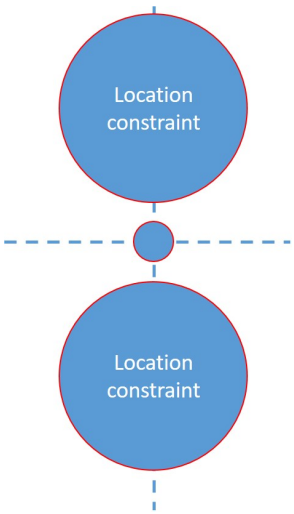

Figure 3.8: Location constraint for array of 3 WECs. Center buoy is fixed at origin

respectively.

With different wave numbers, the optimal solution remains $[0, 4.5/k]$ for all the cases. From case 1 to case 3, the coordinates for WEC2 and WEC3 remain symmetric, and the values of y coordinates are all equal to $4.5/k$ for different wave numbers. q-factor from this optimization is smaller than q-factors in table 3.2, because the search step for GA is set to be 1 meter to reduce computation time. When calculating q-factors with each of the coordinates set to the exact value of $[0, 4.5k]$, the q-factors are the same as results in table 3.2. The last column in table 3.6 is the constraint on x coordinate of both the second and the third WEC. Case 1 to case 3 are optimized with a small searching range of the x coordinate. Case 4 is given a larger search range, and it serves as a comparison to case 3, to show that the solution is globally optimal.

test	q	k	WEC2 (m)	WEC3 (m)	x constraint(m)
Ref[2]	1.98	0.04	[0,4.5/k]	[0,-4.5/k]	[-10,10]
case1	2.10	0.2	[0,22]	[0,-22]	[-10,10]
case2	2.08	0.3	[0,15]	[0,-15]	[-10,10]
case3	2.07	0.04	[0,109]	[0,-109]	[-10,10]
case4	2.07	0.04	[0,109]	[0,-109]	[-100,100]

Table 3.6
Compare optimization of both array layout and size with different wave number. Locations for WEC2 and WEC3 are shown. Constraint is the location limit in x direction

3.3.4 Optimization with irregular waves

When the input ocean wave is irregular, which contains more than one frequency, the optimization with GA is computational expansive if exact hydrodynamics is employed. Due to this limitation, only 7 population is used for optimization under irregular wave. Irregular wave employed bretschneider spectrum with $1.158m$ significant wave height and 8 sec as peak period. Results for array of 3 WECs is shown on figure 3.9. q-factor calculated from this setup is 1.77

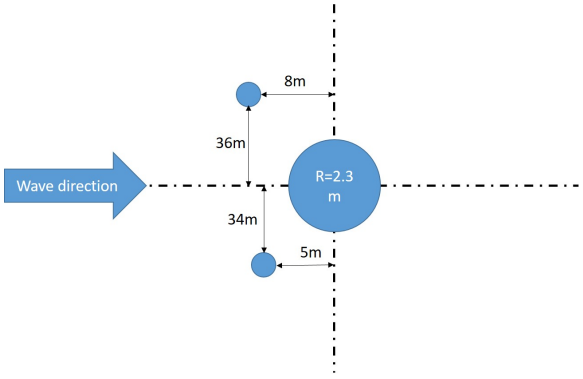

Figure 3.9: Optimized layout and dimension for array of 3 WECs under irregular wave

This layout is not symmetric but we can see that the center buoy was optimized to be more important over the buoys on the side. This is the same behavior that has been observed for tests with regular wave.

Chapter 4

Hybrid Wave Energy Converter Array Analysis

In this chapter, a novel hybrid WEC array design is investigated. The key items motivates this hybrid configuration. Firstly, the performance of the heaving WEC array fluctuates severely around the optimal layout [3]. However, during the realistic installation, the fixed WEC location is hard to achieve. Since it is well recognized that the radiation excited from one degree-of-freedom is hard to interact with the radiation from another degree-of-freedom, a novel design of hybrid WEC array that contains both heaving buoys and OSWCs is proposed.

4.1 Single WEC hydrodynamics and response

Isolated WEC dynamics for both heaving buoy and OSWC is studied in this section. Since this study employs the passive damping control for the sake of implementation, the size of each type of the device must be tuned carefully so that the device resonates with the incoming wave. The size of each type of the buoy is listed in table 4.1.

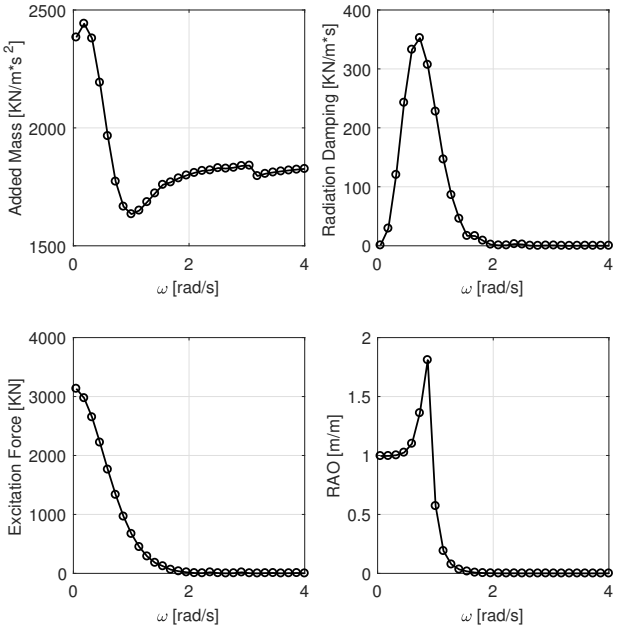

Figure 4.1: Hydrodynamic coefficients and the response amplitude operator (RAO) for a cylindrical heaving buoy with the radius of $10\,m$ and the draft height of $8\,m$

The hydrodynamic coefficients for an isolated heaving buoy and an OSWC are calculated using BEM solver NEMOH and they are shown on figure 4.1 and figure 4.2. The response amplitude operators are plotted on the same figures. The shapes are

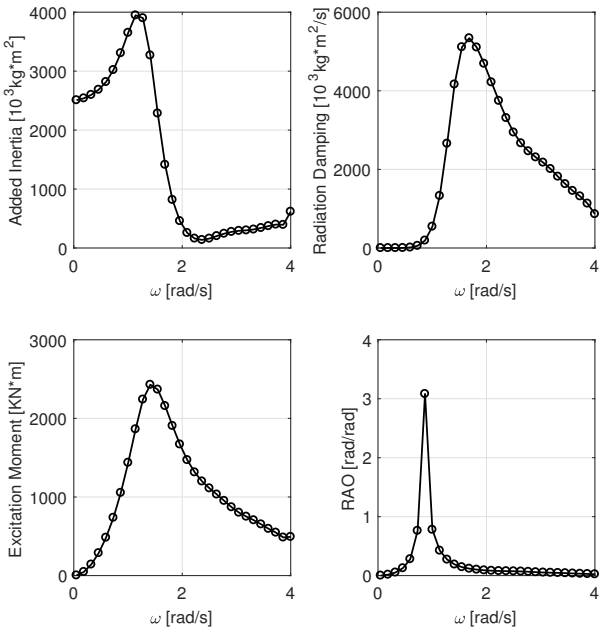

Figure 4.2: Hydrodynamic coefficients and RAO for a OSWC with the width of $10\,m$, height of $5\,m$ and the thickness of $4\,m$

chosen to resonate with the peak frequency of the wave spectrum at $0.7854\,rad/s$.

4.2 Hybrid array configuration

An array with five identical cylindrical heaving buoys is firstly examined and the q-factor is calculated at varying separation distances. Then the q-factor is calculated with a hybrid array that has the center buoy as an OSWC at same separation distances. The proposed configuration is shown on figure 4.3.

Table 4.1
SIMULATION OPTIONS

Item	Value
H_s	$1.158\,m$
T_p	$8\,s$
R	$10\,m$
D	$8\,m$
L_x	$4\,m$
L_y	$10\,m$
L_z	$5\,m$
h	$60\,m$
ω	$[0.05 - 4]\,rad/s$
d	$[4R - 80R]\,m$

Parameters used in simulation. R and D are radius and draft height of cylindrical buoys, h is the water depth and d is the separation distance shown on Fig 4.3.

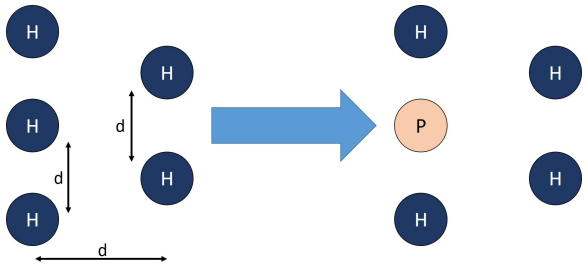

Figure 4.3: Hybrid array that changes the center buoy from a heaving cylinder to an floating OSWC. The left array layout is from reference [3]. The center buoy in the right array is labeled P, which indicates that it moves in pitch mode.

The Bretschneider spectrum is employed to construct the irregular wave. The significant wave height and peak period is shown in table 4.1 from section 4.1. The wave spectrum is shown on figure 4.4.

Since the 'Sharp Eagle' design from [4] proved that it is possible to design surface

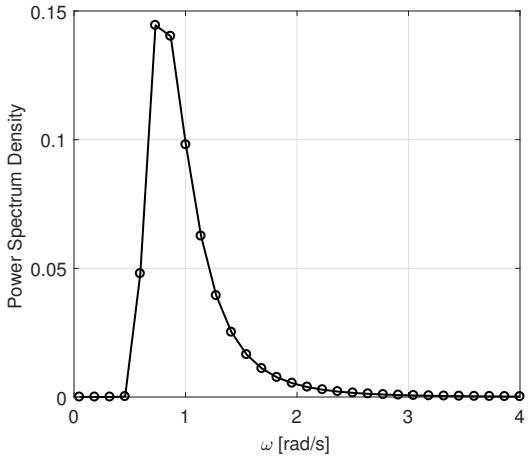

Figure 4.4: Irregular wave spectrum used in simulations

OSWC in deep water region, the array we propose will be placed at deep water and the installation of each type of the device is shown on figure 4.5. The entire array will be place at deep water area where the water depth $h > 60m$. The array design is shown on figure 4.3, where the hybrid array has one OSWC on the center to smooth the fluctuation of hydrodynamic interaction.

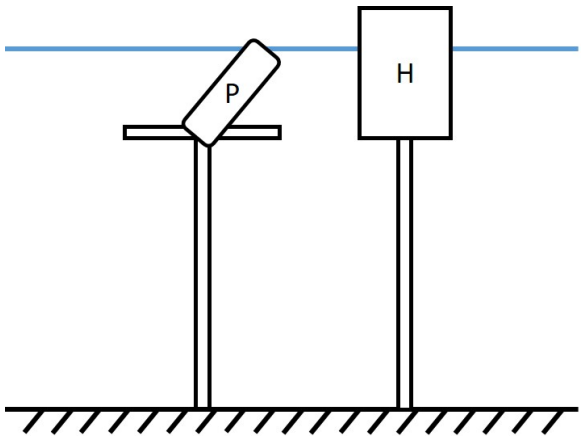

Figure 4.5: The sample installation of each type of the WEC device. The floating OSWC platform is verified in reference [4]

4.3 Compare Hybrid Array with Traditional Array

This simulation employs an uni-directional irregular Bretschneider wave (figure 4.4) and two types of arrays (figure 4.3). The numerical parameters used in this simulation are shown in table 4.1.

The WEC array hydrodynamics are calculated at each separation distance d for both the traditional array and the hybrid array. The q-factor is then evaluated and compared at each separation distance. Statistical analysis is employed to further understand the hybrid array configuration.

4.3.1 WEC array hydrodynamics and response

At separation distance of $100\,m$, the hydrodynamic coefficients are shown on figure 4.6 and figure 4.7. When plotting on the same figure it is more obvious that the OSWC has different radiation impedance behavior from the heaving buoys. Also, we can see that the radiation damping of a OSWC with the given size is one order of magnitude larger than that of the heaving buoy. Still, the RAO of the two devices have similar response amplitude which is previously shown on figure 4.1 and figure

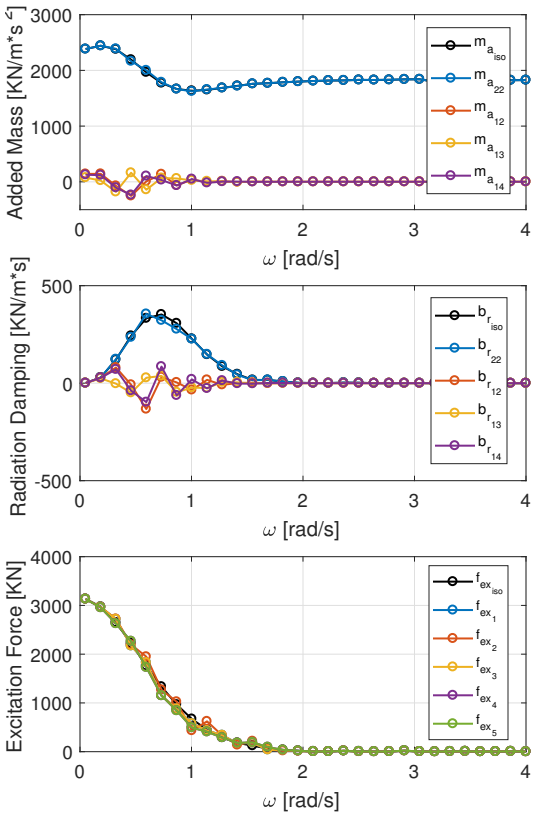

Figure 4.6: Hydrodynamic coefficients for a traditional array with separation distance of 100 m. The black circles are the data from an isolated heaving buoy.

The interaction between devices of different type is smaller than the interaction between the same type of devices. Since the layout on figure 4.3 is symmetric, the symmetric off-diagonal elements in radiation impedance matrices are the same, which can be seen on figure 4.8. On figure 4.8 we can also see that all the coupled radiation impedance terms from the hybrid array are smaller than the ones from the traditional array except for the symmetric elements $b_{r_{24}}$ and $b_{r_{25}}$. However, the system resonates

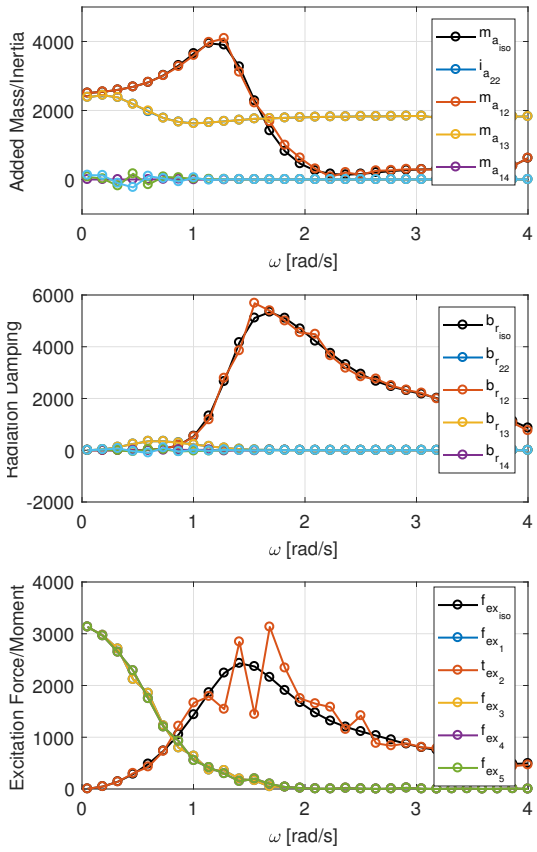

Figure 4.7: Hydrodynamic coefficients for a hybrid array with separation distance of $100m$. The units for each of the coefficients are the same as the units on figure 4.1 and figure 4.2. The black circles are the data from an isolated OSWC.

at the frequency $\omega = 0.78\,rad/s$ which is shown on the RAO. And for the element $b_{r_{24}}$ from the hybrid array (blue stars), at the resonance frequency, the amplitude of the radiation impedance is still smaller than that from the traditional array (purple circles.) This behavior is more significant on radiation damping.

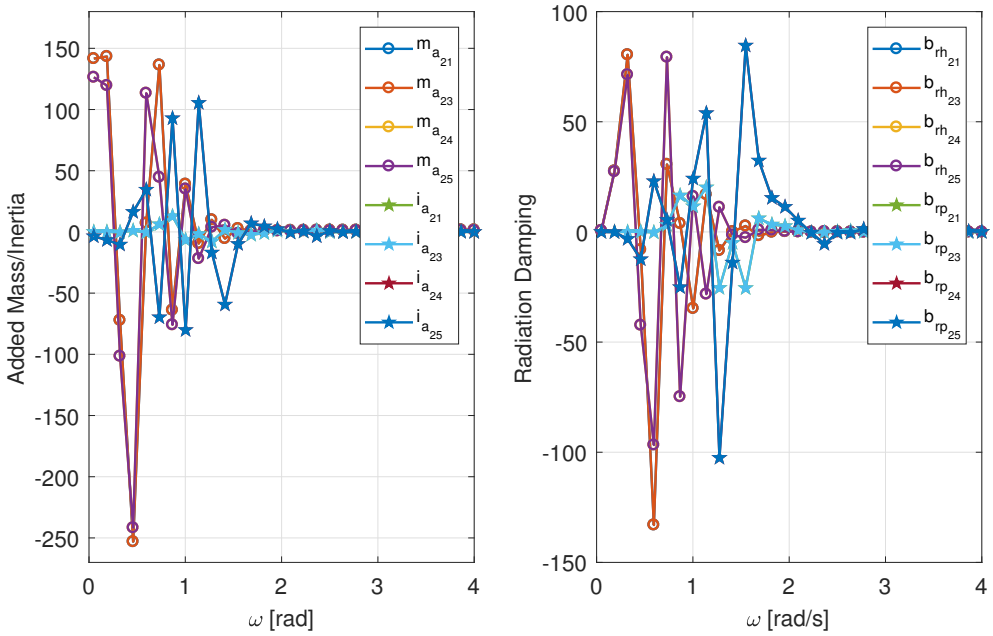

Figure 4.8: Off-diagonal elements in radiation impedance matrices for a hybrid array with separation distance of 100 m. The units for each of the coefficients are the same as the units on figure 4.1 and figure 4.2. Circles are the coefficients calculated from a traditional array. Stars are the coefficients calculated from a hybrid array

4.3.2 The q-factor comparison

Using the hydrodynamic coefficients obtained from section 4.3.1, the q-factor is calculated for both the traditional array and the hybrid array. The result is shown on figure 4.9, where it can be observed that the q-factor fluctuation using the hybrid array is smaller than when using the traditional array. Meanwhile, the mean value of the q-factors from the two arrays are almost identical. The mean q-factor from the traditional array is 1.0166 and the mean q-factor from the hybrid array is 1.0041.

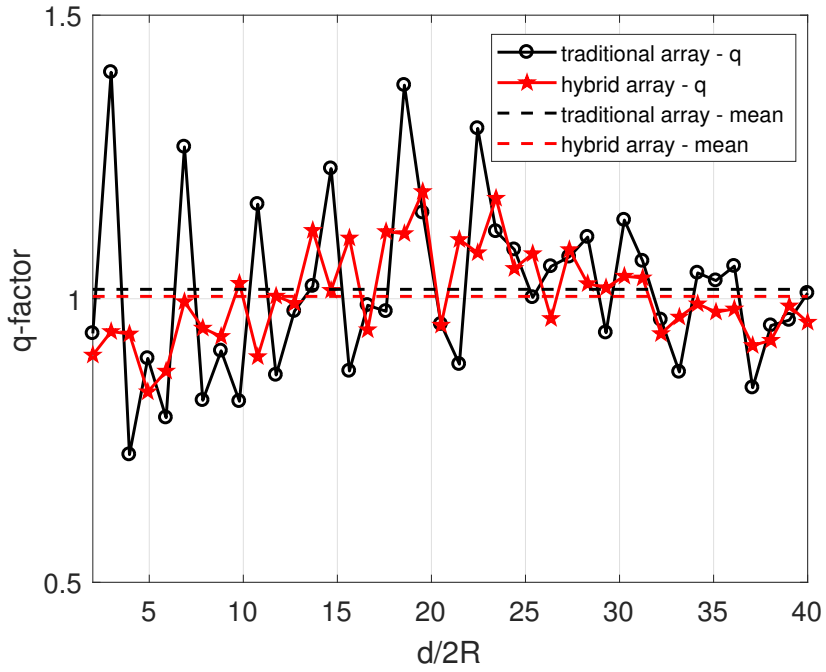

Figure 4.9: Comparison of the q-factor calculated from a traditional array and that from a hybrid array. d refers to the separation distance and R is buoy radius.

It is worth noting that, although the q-factor across the entire range of separation distance remains the same, the q-factor level in short separation distance using hybrid array is smaller than the q-factor level using traditional array at the same distance range.

4.3.3 The fluctuation of the hydrodynamic interaction

Before the further analysis on the data obtained, we firstly define the following terms:

† short separation distance: $[20 - 200]\, m$

† medium separation distance: $[200 - 500]\, m$

† large separation distance: $[500 - 800]\, m$

† q_{max} : maximum value of the q-factor calculated from an array

† q_{min} : minimum value of the q-factor calculated from an array

† interaction: $(q - 1) * 100\%$

† var_{short} : variance of the q-factor at short separation distance

† var_{medium} : variance of the q-factor at medium separation distance

† var_{large} : variance of the q-factor at large separation distance

Table 4.2
THE Q-FACTOR AND STATISTICS OF THE SEPARATION DISTANCE

Array	q_{max}	q_{min}	var_{short}	var_{medium}	var_{long}	var_{total}
T	1.39	0.72	0.05	0.023	0.006	0.024
H	1.18	0.83	0.003	0.007	0.002	0.006

Statistical comparison of the two arrays. 'T' represents the traditional array and 'H' represents the hybrid array.

On table 4.2, the variance of q-factor is calculated at each separation distance range for each array configuration. And we can see the variance of the q-factor using the hybrid array is significantly smaller than the variance of the q-factor using the traditional array. To further visualize the trend of the q-factor variance the variance is also plotted against the separation distance on figure 4.10.

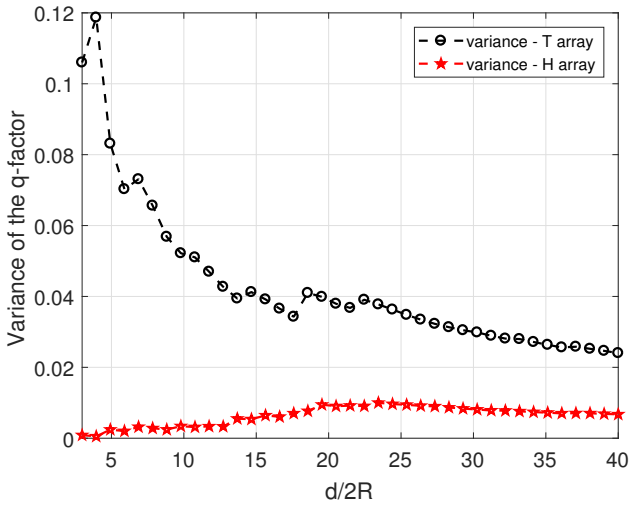

Figure 4.10: Comparison of the q-factor variance from a traditional array and that from a hybrid array.

It is obvious from figure 4.10 that the fluctuation of the hybrid array is more stable and consistent across the entire separation distance range.

Considering the more practical situation when deploying the WEC array on ocean environment, it is often hard to fix the exact location of each device at its designed location due to the rapidly changing ocean conditions. The hybrid array design thus proved itself to be a more consistent design when the separation distance between each device is hard to hold still.

4.4 Sensitivity of the q-factor with respect to the error in layout

As discussed previously, during installation of the WEC array, each WEC in the array is possibly floating around the designed target location. A set of normally distributed random error of location is applied to the layout to simulate the location error. Three layouts with different separation distances are selected from figure 4.9, and the same set of error is applied to each layout to observe the behavior of the q-factor.

The three cases are:

† separation distance $d = 50m$

† separation distance $d = 150m$

† separation distance $d = 200m$

50 sets of normally distributed random error are then applied to the three layout. The layout with separation distance of 50 meters is shown on figure 4.11. At $d = 50m$, $q_T > q_H$, where q_T is the q-factor calculated from the traditional array and q_H is the q-factor calculated from the hybrid array. At $d = 150m$, $q_T = q_H$, at $d = 200m$, $q_T < q_H$. There is no direct correlation between q-factor value and the separation

distance, and there are layouts where separation distance is small and $q_T < q_H$. The three layouts are selected to show the variation of the q-factor under uncertainty of the layout.

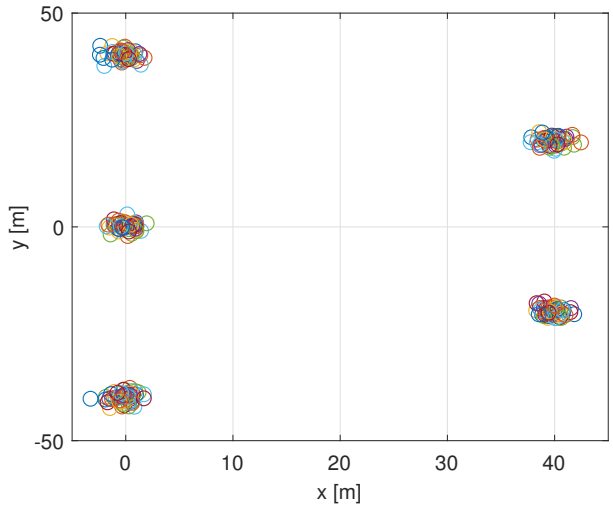

Figure 4.11: Array layout with separation distance of 50 m. 50 sets of random error are applied to the location of each WEC

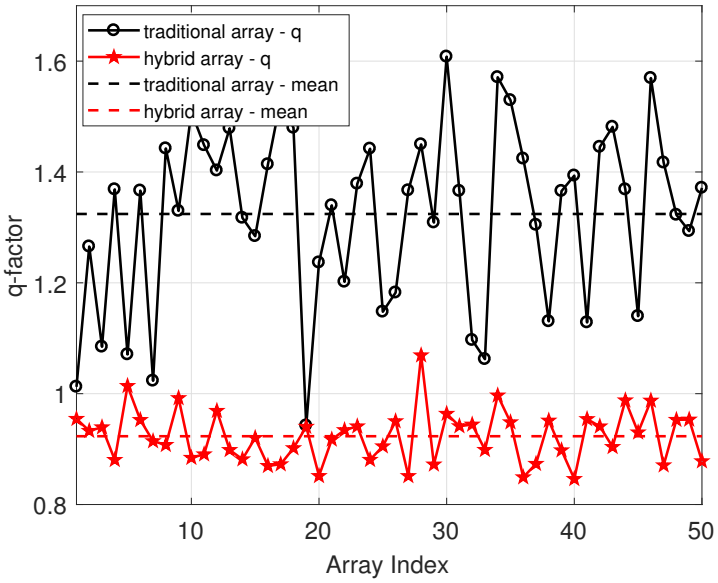

Figure 4.12: Array with separation distance of 50 m and normally distributed location random error. Initial $q_t > q_h$.

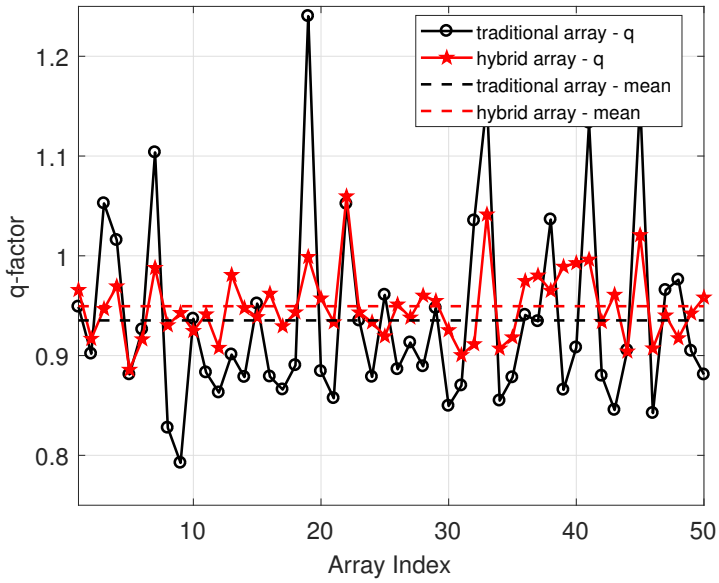

Figure 4.13: Array with separation distance of 150 m and normally distributed location random error. Initial $q_t = q_h$.

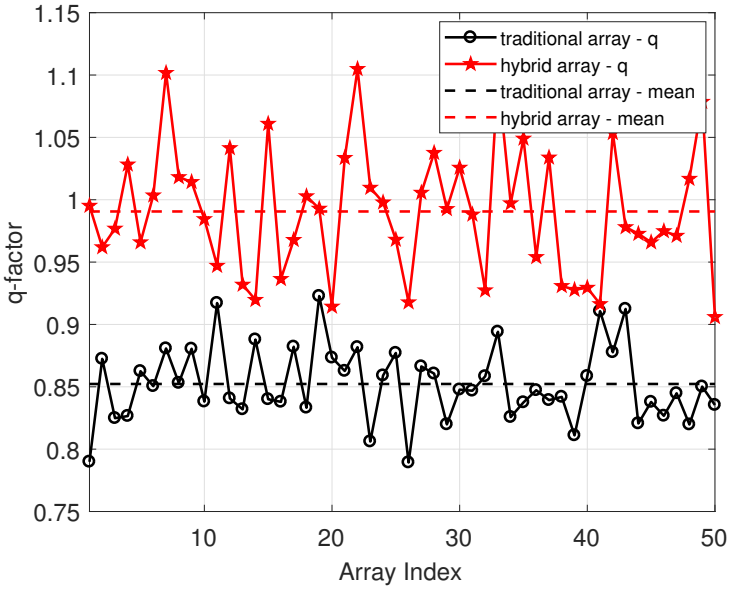

Figure 4.14: Array layout with separation distance of 200 m and normally distributed location random error. Initial $q_t < q_h$.

The resulting q-factors for all three cases are shown on figure 4.12 - 4.14. From the results, the hybrid array has smaller q-factor variance than the traditional array. Thus, the power output from the array is more stable with uncertainty in the WEC location.

Table 4.3
THE Q-FACTOR STATISTICS OF ARRAYS WITH RANDOM ERROR

Array	q_{max}	q_{min}	var
1_T	1.60	0.94	0.026
1_H	1.06	0.84	0.002
2_T	1.24	0.79	0.009
2_H	1.06	0.88	0.001
3_T	0.92	0.78	0.001
3_H	1.10	0.90	0.002

'T' represents the traditional array and 'H' represents the hybrid array. While the case 1 to 3 refer to $d = 50m$, $d = 150m$ and $d = 200m$ respectively. Where d denotes the separation distance.

From table 4.3, the only case that the variance of the hybrid array is slightly larger than that of the traditional array is when $q_T < q_H$. The separation distance for case 3 is 200 meters, and the variance for traditional and hybrid array are 0.001 and 0.002 respectively which both are considered to be small. Another fact we can observe from table 4.3 is that the array with larger average q-factor always has larger variance and thus it is harder to predict the power output when location error is being considered.

4.5 Mean power per ocean surface area

When installing a WEC array on the ocean, it is also important to consider the area taken by the WEC farm. Even if the theoretical design finds the optimal layout for an array under given conditions, it would not be practical for installation if a small farm takes extremely large space. Thus we also need to consider the power absorption per ocean surface area of an WEC array.

To quantify the characteristics of power absorption per ocean surface area of a given array, we define the power per ocean surface area ratio as:

$$r_p = \frac{q - factor}{farm\ area/smallest\ possible\ farm\ area} \tag{4.1}$$

Based on our definition, r_p is the q-factor from an array scaled by the WEC farm surface area. The consideration of power over a given surface area leads to more compact design of the farm. Here for preliminary study we arbitrarily add more devices to the farm shown on figure 4.15.

As the devices are closer to each other we expect the q-factor for the two new designs to be smaller than the previous ones. Also, the variance of the q-factor is larger for the new designs. The calculated power per area ratio for all four arrays are shown on

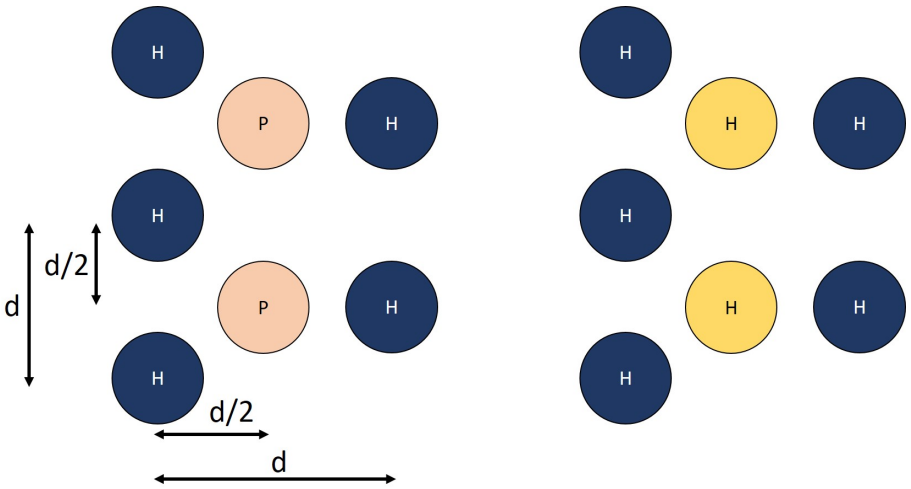

Figure 4.15: Insert devices in between the buoys in the traditional array

figure 4.16.

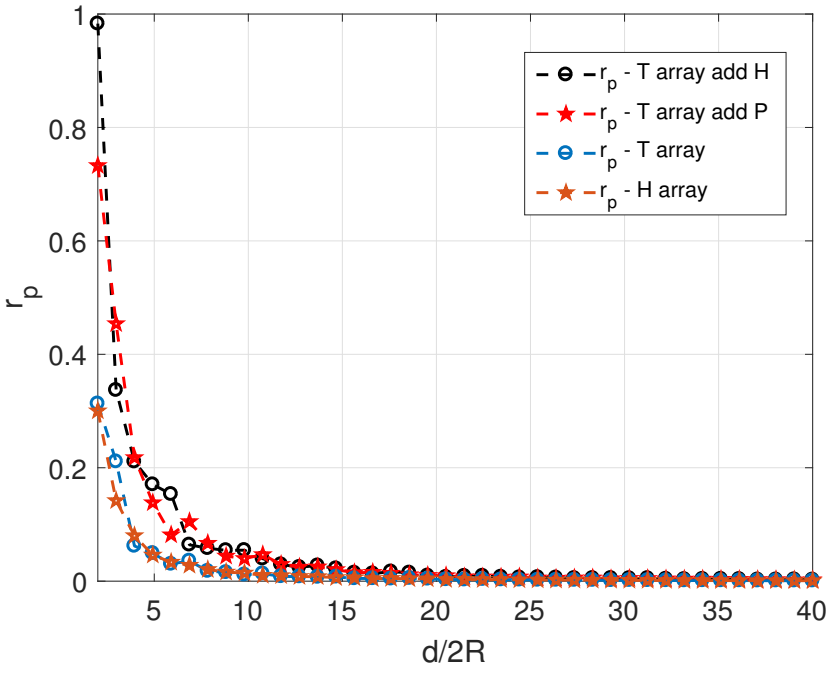

Figure 4.16: Power per area ratio of the arrays.

From the results we can see that the two new designs produce more power per surface area since r_p is higher, and the mean q-factor is smaller than the old designs. With

more devices in the array, we draw the same conclusion as reference [3] that the larger array results in destructive interaction when the separation distance is small, and each device produces overall less power than it is isolated. However, the area power ratio is significantly higher under the same conditions. Also, r_p decreases exponentially when the area of the farm increases. This should be taken into consideration when designing actual WEC farms since the power production per ocean surface area also affects the cost of the associated energy storage system and the wires on the sea bed.

4.6 Optimization of the Hybrid Array

As shown on figure 4.17, two hybrid arrays with arbitrary triangular configurations are optimized in this section. The HPP array has one heave-mode buoy in the front column and 2 pitch-mode devices in the back column. The PHH array has one pitch-mode device in the front column and 2 heave-mode buoys in the back column. Water depth is chosen as $5\,m$ for all hybrid array optimization. Regular wave of frequency $\omega = 0.7854\,rad/s$ is chosen as the input to all arrays. Again, the impedance matching control is employed in this work to ensure the system has the maximum possible response at its natural frequency.

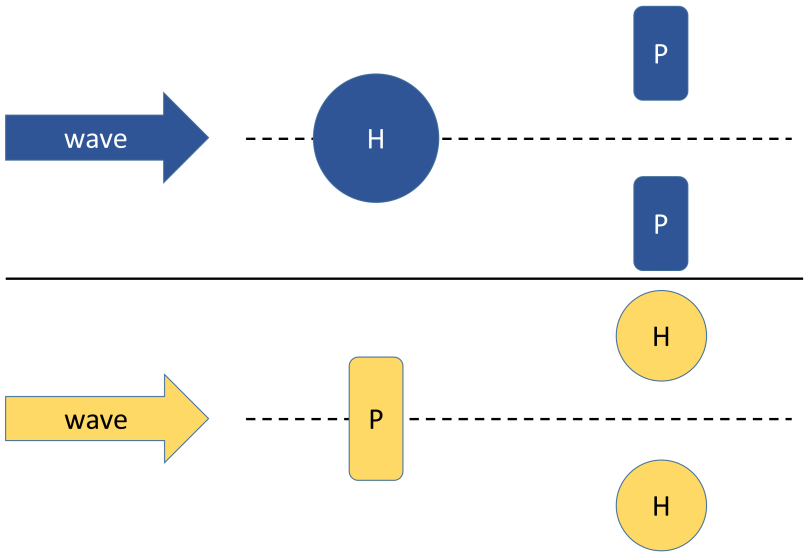

Figure 4.17: Wave refers to the wave direction. H represents the heave-mode WEC and P represents the pitch-mode WEC

4.6.1 Hybrid Array Optimization Formulation

4.6.1.1 Hybrid Array Layout Optimization

To optimize only the layout of the two hybrid arrays, the formulation of the regular array layout optimization is written as 4.2:

$$
\begin{aligned}
\underset{x_i,y_i}{min} \quad & J = -q \\
s.t. \qquad & x_i \subset [10, 250]m \quad \forall \quad i = 2, 3, ... \\
& y_2 \subset [10, 250]m \\
& y_3 \subset [-250, -10]m
\end{aligned}
\tag{4.2}
$$

Similar to the optimization in chapter 3, the front buoy is fixed at the domain origin. The lower boundary of the separation distance is $10\,m$ to avoid the clash of devices, and the upper boundary is $250\,m$ to keep enough hydrodynamic interaction between devices [31].

4.6.1.2 Hybrid Array Optimization With Both Layout and Dimension as Design Variable

In this section, dimension of each type of the device is optimized with the layout together. Each type of the device will have the same size. The optimization is used to find the optimal size for the given buoy type. The design variables that define the heave-mode buoy size are the radius R and the draft D. The design variables that define the pitch-mode buoy size are the width L_y and the height L_z.

$$
\begin{aligned}
&\min_{x_i, y_i, R, D, L_y, L_z} \quad J = -q \\
&s.t. \qquad x_i \subset [10, 250]m \quad \forall \quad i = 2, 3, ... \\
&\qquad\quad y_2 \subset [10, 250]m \\
&\qquad\quad y_3 \subset [-250, -10]m \\
&\qquad\quad R \subset [1, 5]m \\
&\qquad\quad D \subset [1, 3]m \\
&\qquad\quad L_y \subset [1, 5]m \\
&\qquad\quad L_z \subset [1, 3]m
\end{aligned}
\tag{4.3}
$$

An initial configuration is used as the baseline design for the two hybrid arrays. It has $10\,m$ as the separation distance is both x and y direction. Heave-mode buoys have radii as $2\,m$ and draft as $2\,m$. Pitch-mode buoys have width as $2\,m$ and height as $2\,m$. Pitch-mode devices are all hinged on sea bed with water depth as $5\,m$.

For the hybrid array optimization, the minimum separation distance in y direction is $10\,m$, which prevents the column layout to be selected by the algorithm. The reason for doing so is that column layout is the known best layout for any arrays since the energy flux does not decay and each WEC can absorb the maximum possible amount of energy from the plane ocean wave [112]. The energy carried by the wave will recover after certain separation distance [31]. And as shown on Fig 4.18, the optimization

algorithm has selected the desired layout for such target. It is worth noting that the optimal configuration for the hybrid array does not have as much improvement on array performance as the optimal configuration for regular arrays. This phenomenon is discussed in next section.

4.6.2 Hybrid Array Optimization Results

The optimal layout of the hybrid array is shown on figure 4.18, the blue asterisks and red circles lay on the top of each other which indicates that the optimal layout are the same with or without dimension as design variable. The optimal dimension for hybrid arrays is shown in table 4.4. Similar to the the result for regular arrays, the size of each type of device is optimized to have a natural frequency that close to the regular wave frequency with taken the hydrodynamic interaction into consideration.

Table 4.4
optimal dimension for hybrid arrays

Array	R	D	L_y	L_z
HPP	$5\,m$	$1\,m$	$4\,m$	$2\,m$
PHH	$5\,m$	$1\,m$	$4\,m$	$2\,m$
initial	$2\,m$	$2\,m$	$2\,m$	$2\,m$

Optimal q-factors of hybrid arrays are shown on figure 4.19. The q-factors are below 1 with initial arbitrarily selected layout and dimension of devices, and are all above 1 after both the optimization of layout and the optimization of layout with dimension

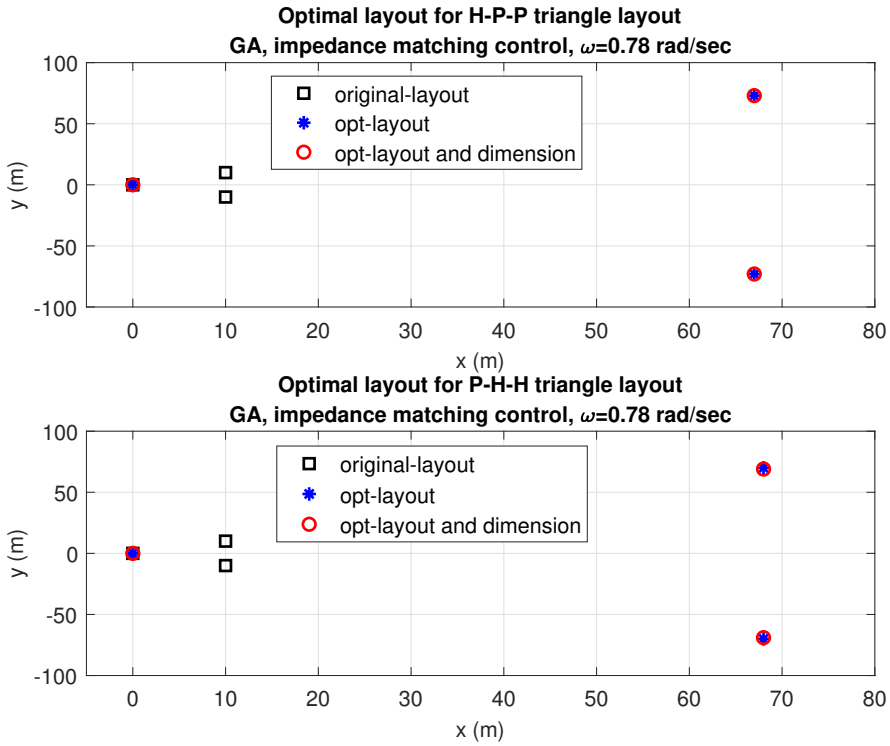

Figure 4.18: Optimal layout of the hybrid WEC array. Original layout refers to the initial set up with $10\,m$ as the separation distance for both directions.

together. Similar to the regular array optimization results, the optimization algorithm is able to select the array configuration such that the hydrodynamic interaction is constructive. However, the improvement of introducing dimension optimization if not obvious for the hybrid arrays. The q-factors of the hybrid arrays only increased slightly after optimizing the dimension with layout together.

From the comparison shown in Table 4.5, including dimension in the q-factor optimization improves the performance of the array for all test cases. The improvement is significant for the regular array optimization results obtained from chapter 3. The

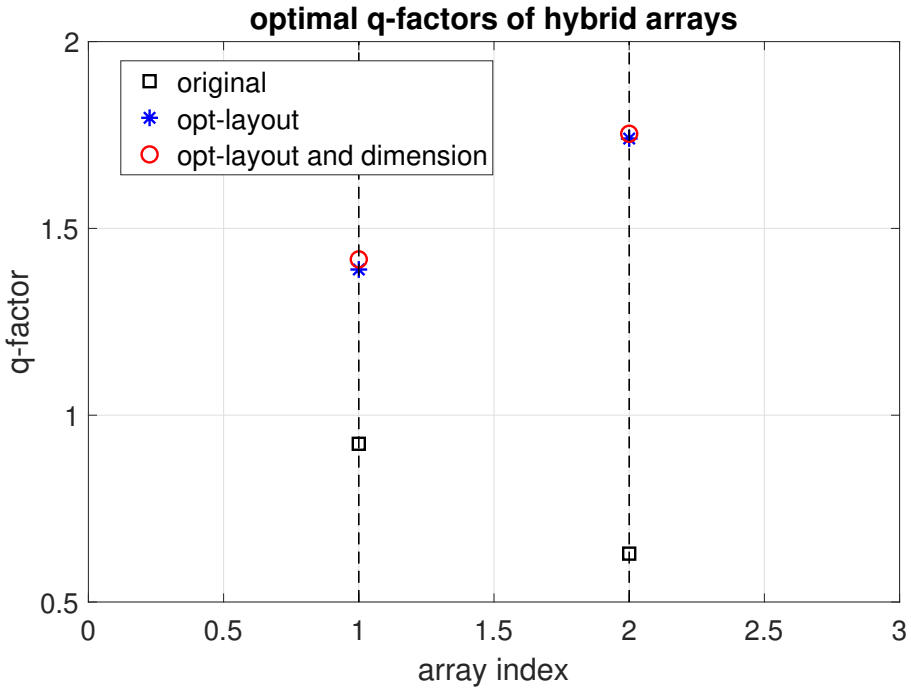

Figure 4.19: index=1 refers to the H-P-P triangular array and index=2 refers to the P-H-H triangular array. Black squares are q-factors calculated with the original arbitrary layout and dimensions, blue asterisks are q-factors calculated with the optimal layouts and the original arbitrary dimensions, and red circles are q-factors calculated with the optimal layout and the optimal dimensions.

Table 4.5
COMPARISON OF Q-FACTORS

	Opt-Layout	Opt-Layout&Dimension
3H	1.98	2.64
5H	2.72	3.59
7H	3.18	4.85
HPP	1.39	1.41
PHH	1.74	1.75

"Opt-Layout" refers to the optimization of only the layout of an array. "Opt-Layout&Dimension" refers to the optimization of both layout of an array and dimension of devices. Item $3H$, $5H$, and $7H$ refer to the optimization results obtained from chapter 3

q-factor increased 33.33%, 31.98%, and 52.15% for 3H, 5H and 7H arrays respectively. However, the improvement of introducing dimension as design variable is not so obvious for hybrid arrays. The q-factor increased 1.95% and 0.73% for HPP and PHH arrays respectively.

From table 4.5, the regular arrays have distinguishable higher q-factors than the hybrid arrays. And it indicates that the hydrodynamic interaction between buoys of the same type is higher than the hydrodynamic interaction between buoys of different types.

Considering the hybrid array that has only two devices in it, we can define b_1 and b_2 to be the independent radiation damping terms, and b_{12} to be the off-diagonal elements which represents the interaction between the first and the second device.

When the hybrid array contains one heave-mode buoy and one pitch-mode buoy. For the heave-mode buoy, the term b_{12} represents the radiation damping in heave excited by unit angular velocity in pitch. Thus, this radiated energy from pitch is not effective on driving the motion in heave. Same analysis can be done for the pitch-mode buoy.

Chapter 5

Optimal Control of Wave Energy Converter Array

In this chapter, the analytical time domain optimal control solutions are derived and investigated for different WEC arrays. A continuous dynamic system is illustrated in figure 5.1. The optimal control problem for such systems has been developed in the context of variational calculus. The optimal control theory introduces a scalar function called the *Hamiltonian* [121]. The Hamiltonian is constructed using the performance index, the Lagrangian multiplier, and the constraint equations. In the WEC array optimal control problem in this chapter, the performance index is the harvested energy, and the constraints are the WEC array dynamic equations. The structure of the Hamiltonian is shown in equation 5.1, where L is the performance

index and f is the same system dynamics in figure 5.1.

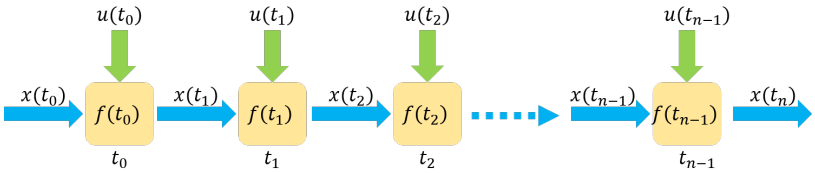

Figure 5.1: Flow chart of a continuous dynamic system. x is the system state, f is the system dynamics, u is the controller

$$H(x(t), u(t), t) = L[x(t), u(t), t)] + \lambda^T(t) f[x(t), u(t), t] \tag{5.1}$$

After the Hamiltonian is formulated, a set of equations known as the Euler-Lagrange equations must be satisfied to solve for the optimal control parameter u. The Euler-Lagrange equations are shown in equation 5.2.

$$\begin{aligned} \dot{\lambda}^T &= -\frac{\partial H}{\partial x} \\ \dot{x} &= f(x, u, t) \\ \frac{\partial H}{\partial u} &= 0 \end{aligned} \tag{5.2}$$

The control parameter is determined by solving $\frac{\partial H}{\partial u} = 0$, with the states and co-states solved from the two-point boundary-value problems shown as the first two dynamic equations in 5.2. In this work, optimal control for the arrays of heaving

buoys is studied. The analytical optimal control solution will be derived using both regular wave and irregular wave as input. The two types of input are chosen as such since regular wave is a sinusoidal input to the WEC array system which enables a simplified dynamic model, where the irregular wave requires full radiation states representation for time domain simulation. The development of the presented optimal control follows the optimal control theory using Pontryagin's Principle and Lagrange multipliers which are introduced above.

5.1 WEC Array Optimal Control Problem Formulation

The absorbed energy by the WEC array is chosen as the optimization objective. Assuming a control force is provided by the PTO unit, the free-body-diagram of the buoy is shown in figure 5.2.

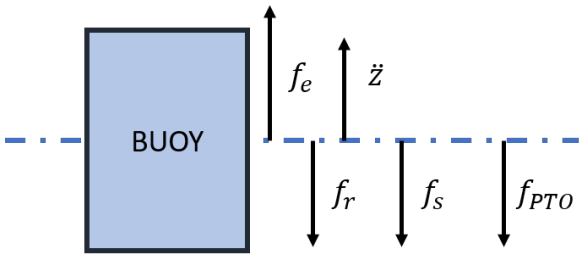

Figure 5.2: Free-body-diagram of a WEC device

The energy for a single heaving WEC is defined in equation 5.3, where u is the control

force and $\dot{z}$ is the buoy's velocity.

$$E_i = \int_0^T \big\{u(t)\dot{z}(t)\big\}dt \tag{5.3}$$

The energy extracted from the entire array is defined in equation 5.4

$$E_{array} = \sum_{n=1}^{N} \int_0^T \big\{u_n(t)\dot{z}_n(t)\big\}dt \tag{5.4}$$

The optimization objective is to maximize the energy extracted from the array. Equivalently, the objective function is defined in equation 5.5 to minimize the negative value of the energy.

$$\begin{aligned} &\underset{\mathbf{u(t)}}{min} \quad J(\dot{z}_n(t), u_n(t)) = -\sum_{n=1}^{N} \int_0^T \big\{u_n(t)\dot{z}_n(t)\big\}dt, \quad where\, n = 1, 2, 3, \ldots \\ &s.t. \qquad system\, dynamic\, equations \end{aligned} \tag{5.5}$$

Since time as a variable affects the system dynamics and cannot be controlled, the WEC array dynamic system presented in chapter 2 is considered as non-autonomous. For such dynamic system, the state vector is defined as:

$$
\begin{aligned}
\mathbf{x} &= [\mathbf{x_1}, \mathbf{x_2}, x_3]^T, \\
\mathbf{x_1} &= [z_1, z_2, z_3, \ldots, z_n]^T, \\
\mathbf{x_2} &= [\dot{z}_1, \dot{z}_2, \dot{z}_3, \ldots, \dot{z}_n]^T, \\
x_3 &= t
\end{aligned}
\tag{5.6}
$$

Where $\mathbf{x_1}$ is the displacement vector of the array and $\mathbf{x_2}$ is the array velocity vector. The control force vector is defined respectively as:

$$
\mathbf{u} = [u_1, u_2, u_3, ...u_n]^T \tag{5.7}
$$

Where each element in $\mathbf{u}$ corresponds to the control force acting on the nth buoy. With the state vector and control vector, the WEC array optimization performance index is written as a compact matrix form, shown in equation 5.8.

$$
J(\dot{z}_n(t), u_n(t)) = -\sum_{n=1}^{N} \int_0^T \left\{ u_n(t)\dot{z}_n(t) \right\} dt = \int_0^T (-\mathbf{u}^T \mathbf{x_2}) dt \tag{5.8}
$$

The Hamiltonian is written as shown in equation 5.9, where $\mathbf{F}$ represents the the WEC array dynamic equations $\dot{\mathbf{x}} = \mathbf{F}(\mathbf{x}, \mathbf{u}, t)$.

$$H = -\mathbf{u}^T\mathbf{x_2} + \boldsymbol{\lambda}^T\mathbf{F}(\mathbf{x}, \mathbf{u}, t) \tag{5.9}$$

The optimal control solution depends on the shape of $\mathbf{F}$. For the regular wave case, the WEC devices will be excited at only one frequency. Thus, the radiation impedance can be directly transformed to the time domain.

$$F_r(\omega) = -\omega^2 m_a(\omega)Z(\omega) + i\omega b_r(\omega)Z(\omega) \iff f_r(t) = m_a(\omega)\ddot{z}(t) + b_r(\omega)\dot{z}(t) \tag{5.10}$$

For the irregular wave case, radiation states must be approximated, and expressed as shown in equation 5.11, which is copied from equation 2.13.

$$\begin{aligned} \dot{z}_r &= A_r z_r + B_r \dot{z} \\ f_r &= C_r z_r \end{aligned} \tag{5.11}$$

With the two representations of radiation force shown in equation 5.10 and 5.11, we can formulate two different state space systems with respect to each of them. The WEC array optimal control problem is then solved using each of the systems.

5.2 WEC Array Optimal Control With Regular Wave Input

As discussed in [24], the partial derivative of the Hamiltonian with respect to the control force is linear to the control for an isolated WEC. This means the partial derivative of the Hamiltonian does not have control parameter u in it. A singular arc problem needs to be formulated and solved. For the WEC array problem, the Hamiltonian will be constructed with respect to two input waves to the array. Then the optimality condition will be solved to find the solution of u.

5.2.1 Optimal Control Solution

Under regular wave excitation, the dynamic model of the WEC is a multi-degree-of-freedom mass-spring-damper system. Each DoF represents the heaving motion of each WEC respectively. Assuming the WEC array has n devices and the fluid is in-viscid, using equation 5.10 and the state vectors defined in equation 5.6, the state-space model for the WEC array is written in equation 5.12. It is worth noting that the excitation force vector $\mathbf{f_e}$ is a function of the state x_3.

$$\begin{Bmatrix} \dot{\mathbf{x_1}} \\ \dot{\mathbf{x_2}} \\ \dot{x_3} \end{Bmatrix} = \mathbf{A} \begin{Bmatrix} \mathbf{x_1} \\ \mathbf{x_2} \\ x_3 \end{Bmatrix} - \mathbf{Bu} + \mathbf{Bf_e}(x_3) + \begin{bmatrix} \mathbf{0}_{2n*1} \\ 1 \end{bmatrix} 1$$

$$\mathbf{A} = \begin{bmatrix} \mathbf{0}_{n*n} & \mathbf{I}_{n*n} & \mathbf{0}_{n*1} \\ [-[\mathbf{M}+\mathbf{M_a}(\omega)]^{-1}\mathbf{K_h}]_{n*n} & [-[\mathbf{M}+\mathbf{M_a}(\omega)]^{-1}\mathbf{B_r}(\omega)]_{n*n} & \mathbf{0}_{n*1} \\ \mathbf{0}_{1*n} & \mathbf{0}_{1*n} & \mathbf{0}_{1*1} \end{bmatrix} \tag{5.12}$$

$$\mathbf{B} = \begin{bmatrix} \mathbf{0}_{n*n} \\ [\mathbf{M}+\mathbf{M_a}(\omega)]^{-1}_{n*n} \\ \mathbf{0}_{1*n} \end{bmatrix}$$

In equation 5.12, $\mathbf{M_a}(\omega)$ and $\mathbf{B_r}(\omega)$ are frequency dependent radiation coefficient matrices which has been previously shown in equation 2.20. $\mathbf{K_h}$ is the hydro-static coefficient matrix. Using equation 5.12, the constraint equations and the Lagrange multiplier vector (co-state vector) in the Hamiltonian are written as:

$$\mathbf{F} = \mathbf{Ax} - \mathbf{Bu} + \mathbf{Bf_e}(x_3) + \begin{bmatrix} \mathbf{0}_{2n*1} \\ 1 \end{bmatrix} 1 \tag{5.13}$$

$$\boldsymbol{\lambda}^T = [\boldsymbol{\lambda_{1n}}, \boldsymbol{\lambda_{2n}}, \lambda_3]^T$$

Where the length of the co-states vector is $2n+1$, which is the same as the number of the constraint equations . In equation 5.13, the elements in the co-state vector $\boldsymbol{\lambda_{1n}}$ refer to the co-states that correspond to the displacements of each device, and the elements in vector $\boldsymbol{\lambda_{2n}}$ refer to the co-states that correspond to the velocities of each device. Using equation 5.9, 5.13 and 5.2, the dynamic equations for the co-state are written as:

$$\begin{aligned}
\dot{\boldsymbol{\lambda}} &= -\frac{\partial H}{\partial \mathbf{x}} \\
\dot{\boldsymbol{\lambda}}_{\mathbf{1n}}{}^{T} &= -\frac{\partial H}{\partial \mathbf{x_1}} = \boldsymbol{\lambda_{2n}}{}^{T}[\mathbf{M} + \mathbf{M_a}(\omega)]^{-1}\mathbf{K_h} \\
\dot{\boldsymbol{\lambda}}_{\mathbf{2n}}{}^{T} &= -\frac{\partial H}{\partial \mathbf{x_2}} = -\boldsymbol{\lambda_{1n}}{}^{T} + \boldsymbol{\lambda_{2n}}{}^{T}[\mathbf{M} + \mathbf{M_a}(\omega)]^{-1}\mathbf{B_r}(\omega) + \mathbf{u}^{T} \\
\dot{\lambda_3} &= -\frac{\partial H}{\partial x_3} = -\boldsymbol{\lambda_{2n}}{}^{T}[\mathbf{M} + \mathbf{M_a}(\omega)]^{-1}\frac{\partial \mathbf{f_e}(x_3)}{\partial x_3}
\end{aligned} \tag{5.14}$$

The optimality condition $\frac{\partial H}{\partial \mathbf{u}} = 0$ is shown as:

$$H_u = \frac{\partial H}{\partial \mathbf{u}} = -\mathbf{x_2}{}^{T} - \boldsymbol{\lambda_{2n}}{}^{T}[\mathbf{M} + \mathbf{M_a}(\omega)]^{-1} \tag{5.15}$$

From equation 5.15, the optimality condition is linear to the control $\mathbf{u}$. Thus, the WEC array optimal control problem with regular wave input is a singular arc problem when the optimality condition $\frac{\partial H}{\partial \mathbf{u}} = 0$ is met. The method introduced in reference

[24] can solve the singular arc problem without solving the two-point boundary value problem directly. Thus, the same treatment is employed to find the optimal solution for WEC array control problem.

From equation 5.15, we can write:

$$\mathbf{x_2}^T = -\boldsymbol{\lambda_{2n}}^T[\mathbf{M} + \mathbf{M_a}(\omega)]^{-1} \tag{5.16}$$

Differentiate both sides of equation 5.16 with respect to time yields:

$$\dot{\mathbf{x}}_\mathbf{2}^T = -\dot{\boldsymbol{\lambda}}_{\boldsymbol{2n}}{}^T[\mathbf{M} + \mathbf{M_a}(\omega)]^{-1} \tag{5.17}$$

Substituting equation 5.16 into the equation of $\dot{\boldsymbol{\lambda}}_{\boldsymbol{1n}}$ we can obtain:

$$\dot{\boldsymbol{\lambda}}_{\boldsymbol{1n}}{}^T = -\mathbf{x_2}^T[\mathbf{M} + \mathbf{M_a}(\omega)][\mathbf{M} + \mathbf{M_a}(\omega)]^{-1}\mathbf{K_h} = -\dot{\mathbf{x}}_\mathbf{1}^T\mathbf{K_h} \tag{5.18}$$

By integrating equation5.18, $\boldsymbol{\lambda}_{\boldsymbol{1n}}$ is solved as:

$$\boldsymbol{\lambda_{1n}}^T = -\mathbf{x_1}^T\mathbf{K_h} + \mathbb{C} \tag{5.19}$$

Substituting equation 5.19 into the equation of $\dot{\boldsymbol{\lambda}}_{\mathbf{2n}}$ from 5.14 yields:

$$\dot{\boldsymbol{\lambda}}_{\mathbf{2n}}{}^{T} = \mathbf{x_1}^{T}\mathbf{K_h} - \mathbb{C} + \boldsymbol{\lambda}_{\mathbf{2n}}{}^{T}[\mathbf{M} + \mathbf{M_a}(\omega)]^{-1}\mathbf{B_r}(\omega) + \mathbf{u}^{T} \tag{5.20}$$

Substituting the control $\mathbf{u}$ from equation 5.12, $\boldsymbol{\lambda}_{\mathbf{2n}}$ from equation 5.16 and $\dot{\boldsymbol{\lambda}}_{\mathbf{2n}}$ from equation 5.17 to equation 5.20 yields the switching condition shown as equation 5.21.

$$\mathbb{C} = 2\mathbf{B_r}(\omega)\mathbf{x_2}(x_3) - \mathbf{f_e}(x_3) \tag{5.21}$$

When the switching condition in equation 5.21 is met, the solution is on the singular arc, and the solution of the control $\mathbf{u}(t)$ is derived by differentiating both sides of the equation 5.21.

$$\begin{aligned} \mathbf{0} &= 2\mathbf{B_r}(\omega)\dot{\mathbf{x}}_{\mathbf{2}} - \frac{\partial \mathbf{f_e}(x_3)}{\partial x_3} \\ \mathbf{0} &= 2\mathbf{B_r}(\omega)[\mathbf{M} + \mathbf{M_a}(\omega)]^{-1}\Big[\mathbf{f_e}(x_3) - \mathbf{u} - \mathbf{K_h}\mathbf{x_1} - \mathbf{B_r}(\omega)\mathbf{x_2}\Big] - \frac{\partial \mathbf{f_e}(x_3)}{\partial x_3} \end{aligned} \tag{5.22}$$

By solving equation 5.22, the expression of the control $\mathbf{u}$ is shown as:

$$\mathbf{u}(x_3) = \mathbf{f_e}(x_3) - \mathbf{K}\mathbf{x_1}(x_3) - \mathbf{B_r}(\omega)\mathbf{x_2}(x_3) - [2\mathbf{B_r}(\omega)(\mathbf{M} + \mathbf{M_a}(\omega))^{-1}]^{-1}\frac{\partial \mathbf{f_e}(x_3)}{\partial x_3} \quad (5.23)$$

Similar to the controller developed in [86], reference [24] uses a Bang-Bang control outside the region defined by the optimality condition. In this work, the saturation of the control force is introduced. Using the Pontryagin's Minimum Principle, the 'Bang-Singular-Bang' control law is expressed as follows:

$$\mathbf{u_r} = \begin{cases} \gamma & \mathbb{C} > 0 \\ \mathbf{u_{sa}} & \mathbb{C} = 0 \\ -\gamma & \mathbb{C} < 0 \end{cases} \quad (5.24)$$

Where γ is the control force limit and $\mathbf{u_{sa}}$ is the singular arc solution shown in equation 5.23.

5.2.2 Discussion

The singular arc solution is derived in the context of optimal control theory. Another general optimal controller which has been widely used is the impedance matching

control. With regular wave input at a given frequency ω, the impedance control is written as:

$$\mathbf{u_{im}} = \Big[\omega^2[\mathbf{M} + \mathbf{M_a}(\omega)] - \mathbf{K}\Big]\mathbf{x_1} + \mathbf{B_r}(\omega)\mathbf{x_2} \tag{5.25}$$

The optimality condition $H_u = 0$ yields a relationship of $2\mathbf{B_r}(\omega)\mathbf{x_2}(x_3) = \mathbf{f_e}(x_3)$. If we apply this relationship to the solution u_{sa}, the optimal control solution u_{sa} from equation 5.23 can be arranged as:

$$\begin{aligned}
\mathbf{u_{sa}} &= 2\mathbf{B_r}(\omega)\mathbf{x_2} - \mathbf{K}\mathbf{x_1} - \mathbf{B_r}(\omega)\mathbf{x_2} - [2\mathbf{B_r}(\omega)(\mathbf{M} + \mathbf{M_a}(\omega))^{-1}]^{-1}\frac{\partial(2\mathbf{B_r}(\omega)\mathbf{x_2})}{\partial t} \\
&= \mathbf{B_r}(\omega)\mathbf{x_2} - \mathbf{K}\mathbf{x_1} - [2\mathbf{B_r}(\omega)(\mathbf{M} + \mathbf{M_a}(\omega))^{-1}]^{-1}\frac{\partial\big[2\mathbf{B_r}(\omega)\mathbf{x_2}\big]}{\partial t} \\
&= \mathbf{B_r}(\omega)\mathbf{x_2} - \mathbf{K}\mathbf{x_1} - (\mathbf{M} + \mathbf{M_a}(\omega))\frac{\partial \mathbf{x_2}}{\partial t}
\end{aligned} \tag{5.26}$$

The term $\frac{\partial \mathbf{x_2}}{\partial t}$ yields the acceleration vector of the WEC array. At the given frequency ω, it can be re-written with the displacement vector as $\frac{\partial \mathbf{x_2}}{\partial t} = -\omega^2\mathbf{x_1}$. Then, at the singular arc, the optimal control solution:

$$
\begin{aligned}
\mathbf{u_{sa}} &= \mathbf{B_r}(\omega)\mathbf{x_2} - \mathbf{K}\mathbf{x_1} - (\mathbf{M} + \mathbf{M_a}(\omega))\big(-\omega^2\mathbf{x_1}\big) \\
&= \mathbf{B_r}(\omega)\mathbf{x_2} + \Big[\omega^2[\mathbf{M} + \mathbf{M_a}(\omega)] - \mathbf{K}\Big]\mathbf{x_1} \\
&= \mathbf{u_{im}}
\end{aligned}
\tag{5.27}
$$

As can be seen from equation 5.27, the singular arc control results in the same controller expression as the impedance matching control under optimality condition.

5.3 WEC Array Optimal Control With Irregular Wave Input

Time domain analysis on WEC array with irregular waves relies on proper interpretation of the radiation force. As shown in section 2.2.2.1, equation 2.23 and equation 2.24 provide the expression of radiation force for WEC array using additional radiation states. With radiation state-space system, the state vector of the WEC array dynamic model is written as:

$$
\begin{aligned}
\mathbf{x} &= [\mathbf{x_1}, \mathbf{x_2}, \mathbf{x_r}, x_3]^T, \\
\mathbf{x_1} &= [z_1, z_2, z_3, \ldots, z_n]^T, \\
\mathbf{x_2} &= [\dot{z}_1, \dot{z}_2, \dot{z}_3, \ldots, \dot{z}_n]^T, \\
\mathbf{x_r} &= [\mathbf{x_{r11}}, \mathbf{x_{r12}}, \ldots, \mathbf{x_{r1n}}, \ldots, \mathbf{x_{rn1}}, \mathbf{x_{rn2}}, \ldots, \mathbf{x_{rnn}}]^T, \\
x_3 &= t
\end{aligned}
\tag{5.28}
$$

In equation 5.28, each radiation vector $\mathbf{x_{r_{ij}}}$ represents the subsystem that outputs the corresponding radiation force $f_{r_{ij}}$. The radiation systems that describes the hydrodynamic interaction between two devices are the same. For example, $A_{r_{ij}} = A_{r_{ji}}$, since the radiation impedance $Z_{ij}(\omega) = Z_{ji}(\omega)$. However, the propagation of the radiation states depends on the velocity of each device as shown in equation 2.23. This indicates that $x_{r_{ij}} \neq x_{r_{ji}}$ and $f_{r_{ij}} \neq f_{r_{ji}}$.

5.3.1 Optimal Control Solution

Again, the viscous effect is neglected from this research. From simulation, the number of states for each radiation sub-system is determined to be four. With each radiation vector $\mathbf{x_{r_{ij}}}$ to be a $4 * 1$ vector, the WEC array dynamic model with full radiation states is shown as equation 5.29.

$$\begin{Bmatrix} \dot{\mathbf{x_1}} \\ \dot{\mathbf{x_2}} \\ \dot{\mathbf{x_r}} \\ \dot{x_3} \end{Bmatrix} = \mathbf{A} \begin{Bmatrix} \mathbf{x_1} \\ \mathbf{x_2} \\ \mathbf{x_r} \\ x_3 \end{Bmatrix} - \mathbf{Bu} + \mathbf{Bf_e}(x_3) + \begin{bmatrix} \mathbf{0}_{(2n+4n^2)*1} \\ 1 \end{bmatrix} 1$$

$$\mathbf{A} = \begin{bmatrix} \mathbf{0}_{n*n} & \mathbf{I}_{n*n} & \mathbf{0}_{n*4n^2} & \mathbf{0}_{n*1} \\ [-[\mathbf{M}+\mathbf{M_a}(\infty)]^{-1}\mathbf{K_h}]_{n*n} & \mathbf{0}_{n*n} & -[\mathbf{M}+\mathbf{M_a}(\infty)]^{-1}_{n*n}[\mathbf{C_r}]_{n*4n^2} & \mathbf{0}_{n*1} \\ \mathbf{0}_{4n^2*n} & \mathbf{B_r}_{4n^2*n} & \mathbf{A_r}_{4n^2*4n^2} & \mathbf{0}_{4n^2*1} \\ \mathbf{0}_{1*n} & \mathbf{0}_{1*n} & \mathbf{0}_{1*4n^2} & \mathbf{0}_{1*1} \end{bmatrix}$$

$$\mathbf{B} = \begin{bmatrix} \mathbf{0}_{n*n} \\ [\mathbf{M}+\mathbf{M_a}(\omega)]^{-1}_{n*n} \\ \mathbf{0}_{4n^2*n} \\ \mathbf{0}_{1*n} \end{bmatrix} \tag{5.29}$$

$\mathbf{A_r}$ is a diagonal matrix. The structure of $\mathbf{A_r}$ $\mathbf{B_r}$and $\mathbf{C_r}$ are shown as follows:

$$
\mathbf{A}_{\mathbf{r}4n^2*4n^2} = \begin{bmatrix} \mathbf{A}_{\mathbf{r_{11}}} & \mathbf{0} & \dots & \dots & \mathbf{0} \\ \mathbf{0} & \ddots & \mathbf{0} & \dots & \vdots \\ \vdots & \mathbf{0} & \mathbf{A}_{\mathbf{r_{ij}}} & \dots & \vdots \\ \vdots & \vdots & \vdots & \ddots & \mathbf{0} \\ \mathbf{0} & \dots & \dots & \mathbf{0} & \mathbf{A}_{\mathbf{r_{nn}}} \end{bmatrix}
$$

$$
\mathbf{B}_{\mathbf{r}4n^2*n} = \begin{bmatrix} \mathbf{B}_{\mathbf{r_{11}}} & \dots & \mathbf{0} \\ \vdots & \ddots & \vdots \\ \mathbf{0} & \dots & \mathbf{B}_{\mathbf{r_{1n}}} \\ \mathbf{B}_{\mathbf{r_{21}}} & \dots & \mathbf{0} \\ \vdots & \ddots & \vdots \\ \mathbf{0} & \dots & \mathbf{B}_{\mathbf{r_{2n}}} \\ \vdots & \vdots & \vdots \\ \mathbf{B}_{\mathbf{r_{n1}}} & \dots & \mathbf{0} \\ \vdots & \ddots & \vdots \\ \mathbf{0} & \dots & \mathbf{B}_{\mathbf{r_{nn}}} \end{bmatrix} \tag{5.30}
$$

$$
\mathbf{C}_{\mathbf{r}n*4n^2} = \begin{bmatrix} \mathbf{C}_{\mathbf{r_{11}}} & \dots & \mathbf{C}_{\mathbf{r_{n1}}} & \mathbf{0} \\ \vdots & \vdots & \vdots & \vdots \\ \mathbf{0} & \mathbf{C}_{\mathbf{r_{n1}}} & \dots & \mathbf{C}_{\mathbf{r_{nn}}} \end{bmatrix}
$$

Each $A_{r_{ij}}$ is a $4*4$ matrix, while $B_{r_{ij}}$ is a $4*1$ matrix and $C_{r_{ij}}$ is a $1*4$ matrix. Since

additional radiation states are introduced to the dynamic system, the Lagrangian multipliers need to be added respectively. The constraint equations and the Lagrange multiplier vector (co-state vector) in the Hamiltonian are written as:

$$\begin{aligned} \mathbf{F} &= \mathbf{Ax} - \mathbf{Bu} + \mathbf{Bf_e}(x_3) + \begin{bmatrix} \mathbf{0}_{(2n+4n)*1} \\ 1 \end{bmatrix} 1 \\ \boldsymbol{\lambda}^T &= [\boldsymbol{\lambda_{1n}}, \boldsymbol{\lambda_{2n}}, \boldsymbol{\lambda_r}, \lambda_3]^T \end{aligned} \tag{5.31}$$

The vector $\boldsymbol{\lambda_r}$ is a $4n * 1$ vector that corresponds to the radiation state vector. The dynamic equations for the co-states are shown as follows:

$$\begin{aligned} \dot{\boldsymbol{\lambda}} &= -\frac{\partial H}{\partial \mathbf{x}} \\ \dot{\boldsymbol{\lambda}}_{\mathbf{1n}}{}^T &= -\frac{\partial H}{\partial \mathbf{x_1}} = \boldsymbol{\lambda_{2n}}{}^T[\mathbf{M} + \mathbf{M_a}(\infty)]^{-1}\mathbf{K_h} \\ \dot{\boldsymbol{\lambda}}_{\mathbf{2n}}{}^T &= -\frac{\partial H}{\partial \mathbf{x_2}} = -\boldsymbol{\lambda_{1n}}{}^T - \boldsymbol{\lambda_r}{}^T\mathbf{B_r} + \mathbf{u}^T \\ \dot{\boldsymbol{\lambda}}_{\boldsymbol{r}}{}^T &= -\frac{\partial H}{\partial \mathbf{x_r}} = \boldsymbol{\lambda_{2n}}{}^T[\mathbf{M} + \mathbf{M_a}(\infty)]^{-1}\mathbf{C_r} - \boldsymbol{\lambda_r}{}^T\mathbf{A_r} \\ \dot{\lambda_3} &= -\frac{\partial H}{\partial x_3} = -\boldsymbol{\lambda_{2n}}{}^T[\mathbf{M} + \mathbf{M_a}(\infty)]^{-1}\frac{\partial \mathbf{f_e}(x_3)}{\partial x_3} \end{aligned} \tag{5.32}$$

The optimality condition $H_u = 0$ can be evaluated using equation 5.9 and 5.31. Since

H_u is the same as shown in equation 5.15 and is linear to the control $\mathbf{u}$, it yields a singular arc solution. To solve the optimal control problem, the entire WEC array dynamic system needs to be transformed to the Laplace domain by using Laplace-Transformation [24]. Assume that the WEC array has initial condition $\mathbf{x_1}(t_0) = \mathbf{0}$, $\mathbf{x_2}(t_0) = \mathbf{0}$ and $\mathbf{x_r}(t_0) = \mathbf{0}$. The Laplace domain WEC array system is written as:

$$\mathbf{X_1}(s) = \frac{1}{s}\mathbf{X_2} \tag{5.33}$$

$$s\mathbf{X_2}(s) = [\mathbf{M} + \mathbf{M_a}(\infty)]^{-1}[\mathbf{F_e}(s) - \mathbf{K_h}\mathbf{X_1}(s) - \mathbf{C_r}\mathbf{X_r}(s) - \mathbf{U}(s)] \tag{5.34}$$

The radiation sub-system is written as a linear system in equation 5.35, with the WEC array velocity as input.

$$\mathbf{X_r}(s) = [s\mathbf{I} - \mathbf{A_r}]^{-1}\mathbf{B_r}\mathbf{X_2}(s) \tag{5.35}$$

Combining equation 5.33, 5.34 and 5.35, the state $\mathbf{X_2}(s)$ is solved and written as:

$$\mathbf{X_2}(s) = \Big[s^2[\mathbf{M} + \mathbf{M_a}(\infty)] + s[\mathbf{C_r}[s\mathbf{I} - \mathbf{A_r}]^{-1}\mathbf{B_r}] + \mathbf{K_h}\Big]^{-1}\Big[s[\mathbf{F_e}(s) - \mathbf{U}(s)]\Big] \quad (5.36)$$

In equation 5.36, the velocity is solved in Laplace domain with the wave excitation force and the control force as inputs. The displacement and the radiation states can be solved respectively by substituting the solution in equation 5.36 to equation 5.33 and 5.35.

$$\mathbf{X_1}(s) = \Big[s^2[\mathbf{M} + \mathbf{M_a}(\infty)] + s[\mathbf{C_r}[s\mathbf{I} - \mathbf{A_r}]^{-1}\mathbf{B_r}] + \mathbf{K_h}\Big]^{-1}\Big[[\mathbf{F_e}(s) - \mathbf{U}(s)]\Big] \quad (5.37)$$

$$\begin{aligned}\mathbf{X_r}(s) = \Big[[s\mathbf{I} - \mathbf{A_r}]^{-1}\mathbf{B_r}\Big]\Big[s^2[\mathbf{M} + \mathbf{M_a}(\infty)] + s[\mathbf{C_r}[s\mathbf{I} - \mathbf{A_r}]^{-1}\mathbf{B_r}]\ldots \\ \cdots + \mathbf{K_h}\Big]^{-1}\Big[s[\mathbf{F_e}(s) - \mathbf{U}(s)]\Big]\end{aligned} \quad (5.38)$$

The co-states equations are transformed to Laplace domain assuming arbitrary initial conditions $\boldsymbol{\lambda_{1n}}(t_0) = \boldsymbol{\lambda_{10}}$, $\boldsymbol{\lambda_{2n}}(t_0) = \boldsymbol{\lambda_{20}}$, and $\boldsymbol{\lambda_r}(t_0) = \boldsymbol{\lambda_{r0}}$.

$$\boldsymbol{\lambda_{1n}}^T(s) = \frac{1}{s}\Big[\boldsymbol{\lambda_{2n}}^T(s)[\mathbf{M} + \mathbf{M_a}(\infty)]^{-1}\mathbf{K_h} + \boldsymbol{\lambda_{10}}^T\Big] \tag{5.39}$$

$$\boldsymbol{\lambda_{2n}}^T(s) = \frac{1}{s}\Big[\mathbf{U}^T(s) - \boldsymbol{\lambda_{1n}}^T(s) - \boldsymbol{\lambda_r}^T(s)\mathbf{B_r} + \boldsymbol{\lambda_{20}}^T\Big] \tag{5.40}$$

$$\boldsymbol{\lambda_r}^T(s) = \frac{1}{s}\Big[\boldsymbol{\lambda_{2n}}^T(s)[\mathbf{M} + \mathbf{M_a}(\infty)]^{-1}\mathbf{C_r} - \boldsymbol{\lambda_r}^T(s)\mathbf{A_r} + \boldsymbol{\lambda_{r0}}^T\Big] \tag{5.41}$$

Substitute equation 5.39 and 5.41 into equation 5.40, $\boldsymbol{\lambda_{2n}}(s)$ is solved as:

$$\begin{aligned}\boldsymbol{\lambda_{2n}}^T(s) = \Big[s\mathbf{U}^T(s) - \boldsymbol{\lambda_{10}}^T - s\boldsymbol{\lambda_{r0}}^T[s\mathbf{I} + \mathbf{A_r}]^{-1}\mathbf{B_r} + s\boldsymbol{\lambda_{20}}^T\Big]\ldots \\ \ldots\Big[s^2\mathbf{I} + s[\mathbf{M} + \mathbf{M_a}(\infty)]^{-1}\mathbf{C_r}[s\mathbf{I} + \mathbf{A_r}]^{-1}\mathbf{B_r} + [\mathbf{M} + \mathbf{M_a}(\infty)]^{-1}\mathbf{K_h}\Big]^{-1}\end{aligned} \tag{5.42}$$

Evaluating the optimality condition $H_u = 0$ yields:

$$H_u = \frac{\partial H}{\partial \mathbf{u}} = -\mathbf{x_2}^T - \boldsymbol{\lambda_{2n}}^T[\mathbf{M} + \mathbf{M_a}(\infty)]^{-1} = 0 \tag{5.43}$$

Transform equation 5.43 into the Laplace domain, then combine with the co-state solution in equation 5.42.

$$\mathbf{X_2}(s)^T = -\boldsymbol{\lambda_{2n}}^T(s)[\mathbf{M} + \mathbf{M_a}(\infty)]^{-1} \tag{5.44}$$

Let:

$$\begin{aligned}
\mathbf{N_1} &= s\boldsymbol{\lambda_{20}}^T - \boldsymbol{\lambda_{10}}^T - s\boldsymbol{\lambda_{r0}}^T[s\mathbf{I} + \mathbf{A_r}]^{-1}\mathbf{B_r} \\
\mathbf{N_2} &= \left[s^2\mathbf{I} + s[\mathbf{M} + \mathbf{M_a}(\infty)]^{-1}\mathbf{C_r}[s\mathbf{I} + \mathbf{A_r}]^{-1}\mathbf{B_r} + [\mathbf{M} + \mathbf{M_a}(\infty)]^{-1}\mathbf{K_h}\right]^{-1} \\
\mathbf{N_3} &= \left[s^2[\mathbf{M} + \mathbf{M_a}(\infty)] + s[\mathbf{C_r}[s\mathbf{I} - \mathbf{A_r}]^{-1}\mathbf{B_r}] + \mathbf{K_h}\right]^{-1}
\end{aligned} \tag{5.45}$$

Substitute $\mathbf{N_1}$, $\mathbf{N_2}$, and $\mathbf{N_3}$ into equation 5.44 and 5.36.

$$\Big[\mathbf{N_3}\big[s[\mathbf{F_e}(s)-\mathbf{U}(s)]\big]\Big]^T = -s\mathbf{U}^T(s)\mathbf{N_2}[\mathbf{M}+\mathbf{M_a}(\infty)]^{-1}+\mathbf{N_1}\mathbf{N_2}[\mathbf{M}+\mathbf{M_a}(\infty)]^{-1} \tag{5.46}$$

Rearrange equation 5.46 to obtain the WEC array optimal control solution in Laplace domain as:

$$\begin{aligned}
&\mathbf{U}^T(s) = \mathbf{U_1}(s)+\mathbf{U_2}(s)\\
&\mathbf{U_1}(s) = {\mathbf{F_e}}^T(s){\mathbf{N_3}}^T\Big[-\mathbf{N_2}[\mathbf{M}+\mathbf{M_a}(\infty)]^{-1}+{\mathbf{N_3}}^T\Big]^{-1}\\
&\mathbf{U_2}(s) = \frac{1}{s}\Big[\mathbf{N_1}\mathbf{N_2}[\mathbf{M}+\mathbf{M_a}(\infty)]^{-1}\Big]\Big[\mathbf{N_2}[\mathbf{M}+\mathbf{M_a}(\infty)]^{-1}+{\mathbf{N_3}}^T\Big]^{-1}
\end{aligned} \tag{5.47}$$

In solution 5.47, $\mathbf{U_2}(s)$ is independent of wave excitation force, and it relies on the initial values of the co-states from $\mathbf{N_1}$. For the steady-state optimal control solution, the transient term $\mathbf{U_2}(s)$ can be removed from equation 5.47.

The Laplace domain steady-state WEC array optimal control solution with irregular wave input is shown as follows:

$$
\begin{aligned}
\mathbf{U}^T(s) &= \mathbf{F_e}^T(s)\mathbf{N_3}^T\Big[-\mathbf{N_2}[\mathbf{M}+\mathbf{M_a}(\infty)]^{-1}+\mathbf{N_3}^T\Big]^{-1} \\
\mathbf{N_2} &= \Big[s^2\mathbf{I}+s[\mathbf{M}+\mathbf{M_a}(\infty)]^{-1}\mathbf{C_r}[s\mathbf{I}+\mathbf{A_r}]^{-1}\mathbf{B_r}+[\mathbf{M}+\mathbf{M_a}(\infty)]^{-1}\mathbf{K_h}\Big]^{-1} \\
\mathbf{N_3} &= \Big[s^2[\mathbf{M}+\mathbf{M_a}(\infty)]+s[\mathbf{C_r}[s\mathbf{I}-\mathbf{A_r}]^{-1}\mathbf{B_r}]+\mathbf{K_h}\Big]^{-1}
\end{aligned}
\tag{5.48}
$$

The steady state solution expressed as equation 5.48 can be further simplified and expressed as:

$$
\begin{aligned}
\mathbf{U}(s) = &\Big[s[\mathbf{C_r}(s\mathbf{I}+\mathbf{A_r})^{-1}\mathbf{B_r}-\mathbf{C_r}(s\mathbf{I}-\mathbf{A_r})^{-1}\mathbf{B_r}]\Big]^{-1} \\
&\Big[s^2[\mathbf{M}+\mathbf{M_a}(\infty)]+s[\mathbf{C_r}(s\mathbf{I}+\mathbf{A_r})^{-1}\mathbf{B_r}]+\mathbf{K_h}\Big]\mathbf{F_e}(s)
\end{aligned}
\tag{5.49}
$$

From equation 5.49, the optimal control $\mathbf{U}(s)$ depends on the value of excitation force $\mathbf{F_e}(s)$ and the radiation state-space matrices. $\mathbf{F_e}(s)$ requires incoming wave information, and estimating the radiation state-space matrices also requires a certain level of accuracy. In the numerical studies, the two items mentioned above are essential to reach the desired performance of a controlled WEC array. In time domain analysis, the inverse Laplace transformation must be employed to find the control solution. Again, the exponential terms should be dropped considering the steady-state control solution. The remaining harmonic terms are the numerical solution.

Similar to the regular wave optimal control problem, a Bang-Bang saturation is applied along with the singular arc control solution. The control law is the same as equation 5.24.

5.4 Optimal WEC Control with Energy Loss in the Hydraulic PTO Unit

Considering an isolated WEC device with a control force u, the dynamic system is modeled as:

$$m\ddot{z}(t) = f_e(t) - f_r(t) - f_s(t) - u(t) \tag{5.50}$$

With the hydraulic system introduced in figure 2.7, the system can be treated as two sub-systems. One that contains the WEC device and the translator that connects the WEC with the hydraulic piston. The other sub-system is the hydraulic PTO. From the WEC system, the ocean wave energy is captured. Then this energy flows through the hydraulic circuit and is converted to the electric energy. In the hydraulic circuit, energy loss comes from several sources as introduced in chapter 2. The generated energy is related to the capture energy by using the following equation:

$$E_{cap} = E_{gen} + E_{loss} \tag{5.51}$$

Where E_{cap} is the captured energy from ocean waves, E_{gen} is the generated electric energy from the hydraulic motor and E_{loss} is the energy loss in the hydraulic circuit.

The loss energy can be found using the exact dynamics of the hydraulic system such as those presented in [11, 96]. However, the dynamic equation of the hydraulic piston has a non-linear relationship with the translator motion shown in equation 5.52. The piston is also shown in figure 2.7.

$$\dot{p}_1 = \frac{\beta(\dot{z}A_{piston} - Q_1)}{A_{piston}(z_{max} - z)} \tag{5.52}$$

In equation 5.52, β is the bulk modulus of the fluid, A_{piston} is the area of the section surface, Q_1 is the fluid going out of the chamber, and z is the displacement of the translator. It can be seen from equation 5.52 that the relationship between the pressure and the buoy displacement is non-linear. Thus, it is difficult to directly derive the energy loss dynamic equation using the optimal velocity of the buoy. In the literature, a loss coefficient is used to represent the energy loss in the hydraulic circuit. Here we propose an alternative polynomial representation of the energy loss. Since the only input from the WEC translator to the hydraulic system is the control

force u, the loss power can be written as a function of u. The function $f(u,t)$ can be expanded using a polynomial approximation as shown in equation 5.53

$$P_{loss} = f(u,t) \approx a_n u^n + a_{n-1}u^{n-1} + \cdots + a_1 u + a_0 \tag{5.53}$$

Using the second order polynomial approximation, the objective function of the optimal control problem for a single WEC is written as:

$$J = -E_{gen} = -(E_{cap} - E_{loss}) = -\big[\int_0^{t_f} u(t)\dot{z}(t)dt - \int_0^{t_f} (a_2 u^2(t) + a_1 u(t) + a_0)dt\big] \tag{5.54}$$

$$J = -\int_0^{t_f} (u(t)\dot{z}(t) + a_2 u^2(t) + a_1 u(t) + a_0)dt \tag{5.55}$$

Let the state vector to be $\mathbf{x} = [x_1 = z, x_2 = \dot{z}, \mathbf{x_r}, x_3 = t]^T$. With equation 5.55, the Hamiltonian is expressed as:

$$H = -ux_2 - a_2 u^2 - a_1 u - a_0 + \boldsymbol{\lambda}^T F \tag{5.56}$$

The Euler-Lagrange equations are:

$$
\begin{aligned}
\dot{\boldsymbol{\lambda}} &= -\frac{\partial H}{\partial \mathbf{x}} \\
\dot{\lambda}_1 &= -\frac{\partial H}{\partial x_1} = \frac{k_h}{m + m_a(\infty)}\lambda_2 \\
\dot{\lambda}_2 &= -\frac{\partial H}{\partial x_2} = u - \lambda_1 - \boldsymbol{\lambda_r}^T B_r \\
\dot{\boldsymbol{\lambda}}_{\boldsymbol{r}} &= -\frac{\partial H}{\partial \mathbf{x_r}} = \frac{\lambda_2}{m + m_a(\infty)} C_r - \boldsymbol{\lambda_r}^T A_r \\
\dot{\lambda}_3 &= -\frac{\partial H}{\partial x_3} = -\frac{\lambda_2}{m + m_a(\infty)} \frac{\partial f_e}{\partial x_3}
\end{aligned}
\tag{5.57}
$$

Evaluating the optimality condition $H_u = 0$ yields:

$$
H_u = \frac{\partial H}{\partial u} = -x_2 - 2a_2 u - a_1 - \frac{\lambda_2}{m} = 0 \tag{5.58}
$$

Solving equation 5.58 produces the optimal controller with energy loss considered:

$$
u = \frac{x_2 + \frac{\lambda_2}{m} - a_1}{2a_2} \tag{5.59}
$$

The solution of u can be obtained by solving the two-value boundary value problem of the state differential equations. This can be done either numerically or analytically

using the Laplace transformation as in section 5.3.

With the same Laplace transformation method, the state equations can be solved and the states $X_2(s)$ and $\lambda_2(s)$are written as:

$$X_2(s) = \frac{s(F_e(s) - U(s))}{(m + m_a(\infty))s^2 + s[C_r(sI - A_r)^{-1}B_r] + k_h} \tag{5.60}$$

$$\lambda_2(s) = \frac{(m + m_a(\infty))\Big[sU(s) + s\lambda_{20} - \lambda_{10} - s\lambda_{r0}^T(sI + A_r)^{-1}B_r\Big]}{(m + m_a(\infty))s^2 + s[C_r(sI + A_r)^{-1}B_r] + k_h} \tag{5.61}$$

Note that equation 5.60 and 5.61 assume zero initial condition for the states and $\lambda_{10}, \lambda_{20}, \lambda_{r0}$ as initial conditions for the co-states. Substitute equation 5.60 and 5.61 into equation 5.59, the optimal controller is solved in the Laplace domain as:

$$\begin{aligned}
U(s) &= \frac{(m + m_a(\infty))[sC_2F_e(s) - C_1C_2a_1] + C_3C_1}{(m + m_a(\infty))[2C_1C_2a_2 + sC_2 - sC_1]} \\
C_1 &= (m + m_a(\infty))s^2 + s[C_r(sI - A_r)^{-1}B_r] + k_h \\
C_2 &= (m + m_a(\infty))s^2 + s[C_r(sI + A_r)^{-1}B_r] + k_h \\
C_3 &= (m + m_a(\infty))\Big[s\lambda_{20} - \lambda_{10} - s\boldsymbol{\lambda_{r0}}^T(sI + A_r)^{-1}B_r\Big]
\end{aligned} \tag{5.62}$$

As can be seen from equation 5.62, the term C_3 has only the initial conditions for co-states. Since it is independent of the wave excitation force and it is the transient term, C_3 can be dropped from the steady state solution.

5.5 Simulation Result

The controls developed in section 5.2.1, 5.3 and 5.4 are tested on an array of two identical heaving buoys. The array information is shown in table 5.1.

Table 5.1
WEC array of two heaving buoys, and wave profile.

	WEC1	*WEC2*	*Array*
$R\,[m]$	2	2	n/a
$D\,[m]$	3	3	n/a
layout $(x, y)\,[m]$	$[0, 0]$	$[30, 0]$	n/a
regular $\omega\,[rad/s]$	n/a	n/a	1
irregular $\omega\,[rad/s]$	n/a	n/a	$[0.1, 3.5]$

The mesh of the array is generated by using Matlab and open source BEM solver Nemoh. The mesh of each buoys is shown in figure 5.3. Hydrodynamic coefficients $M_a(\omega)$, $B_r(\omega)$, and $F_{ex}(\omega)$ are solved by using Nemoh as solver and using both regular and irregular wave shown in table 5.1 as inputs. The hydrodynamic coefficients are solved for both isolated WEC that locates at the center of the ocean surface and the WEC array of 2 WECs.

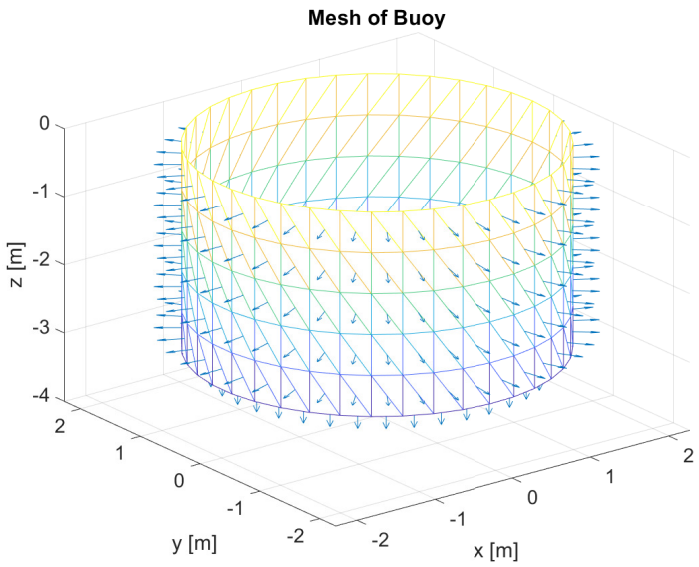

Figure 5.3: Mesh of the first buoy in the array

5.5.1 Simulation Result With Regular Wave Input

The system response is propagated with system dynamic equation shown in equation 5.12, and control shown in equation 5.23 and 5.24. The control force limit is selected to be $\gamma = 1000[kN]$. Impedance matching control is realized by using a PD controller. The equation for this PD control is shown in equation 5.25. The PD impedance matching control is used as a comparison to the singular arc control which has been derived in this thesis.

The control in equation 5.24 is first tested on an isolated WEC with the same information shown in table 5.1. From the system response and control force shown in figure 5.4, 5.5, and 5.6, it is shown that the PD impedance matching control provides

in the same control force and system response when the system at steady state. This finding agrees with the discussion in section 5.2.2.

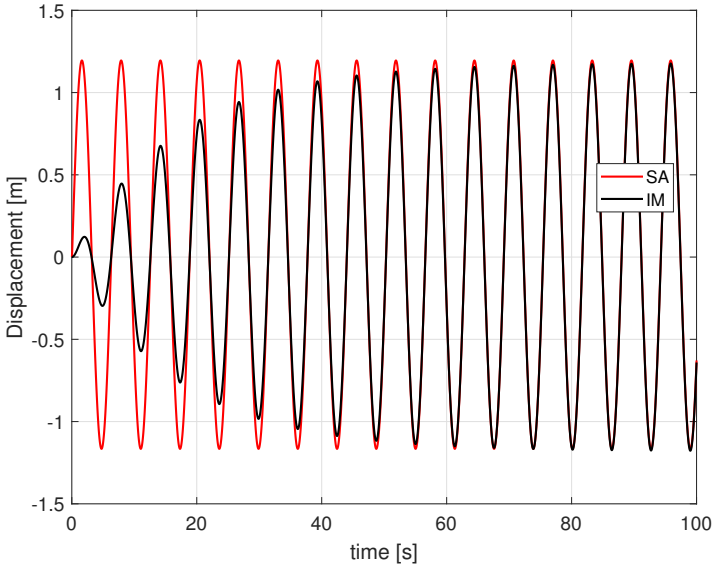

Figure 5.4: Displacement of the isolated WEC with regular wave input at $1\,[rad/s]$. 'IM' represents the result from using impedance matching control. 'SA' represents the result from using singular arc control.

The extracted energy from the WEC using both controls are shown in figure 5.7. It is shown that the BSB control law requires energy to bring the WEC from static to steady state. From figure 5.6, the control force was at the limit of BSB control law for a shot period of time and then the system reached steady state. The impedance matching control requires less energy for the system to reach steady state. However, it takes more time for the impedance matching control to bring the system to steady state. The BSB control law can harvest maximum amount of power faster than the impedance matching control.

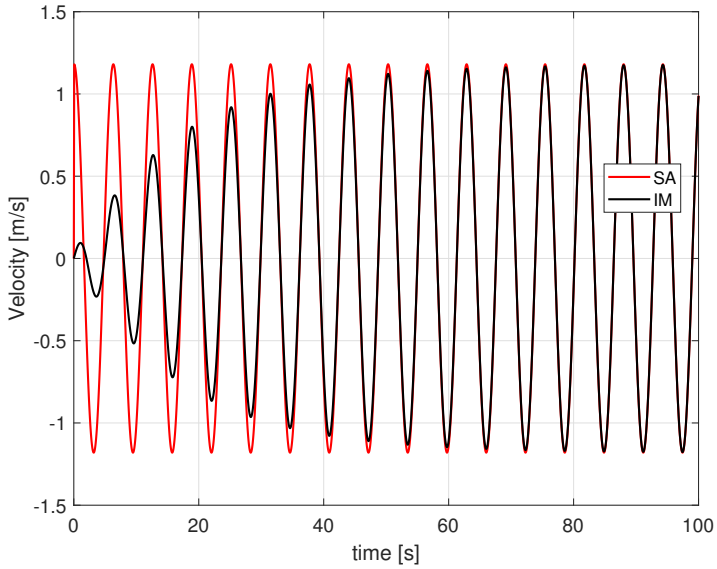

Figure 5.5: Velocity of the isolated WEC with regular wave input at $1\,[rad/s]$. 'IM' represents the result from using impedance matching control. 'SA' represents the result from using singular arc control.

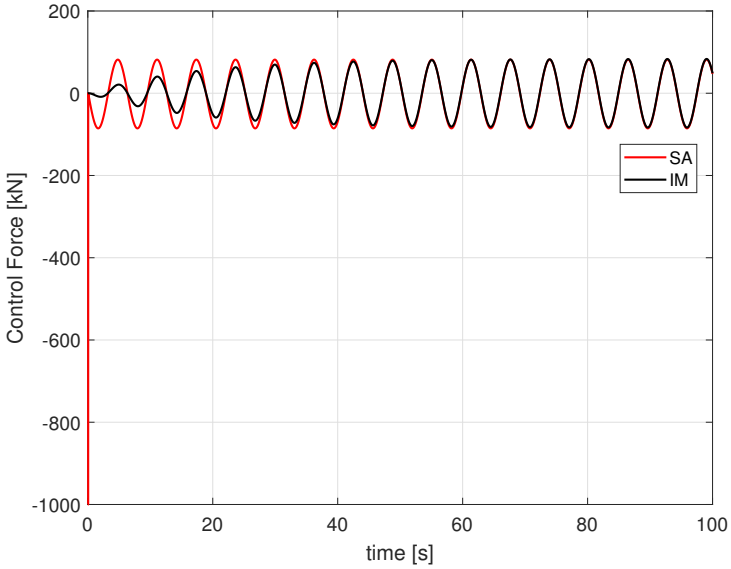

Figure 5.6: Control force of the isolated WEC with regular wave input at $1\,[rad/s]$. 'IM' represents the result from using impedance matching control. 'SA' represents the result from using singular arc control.

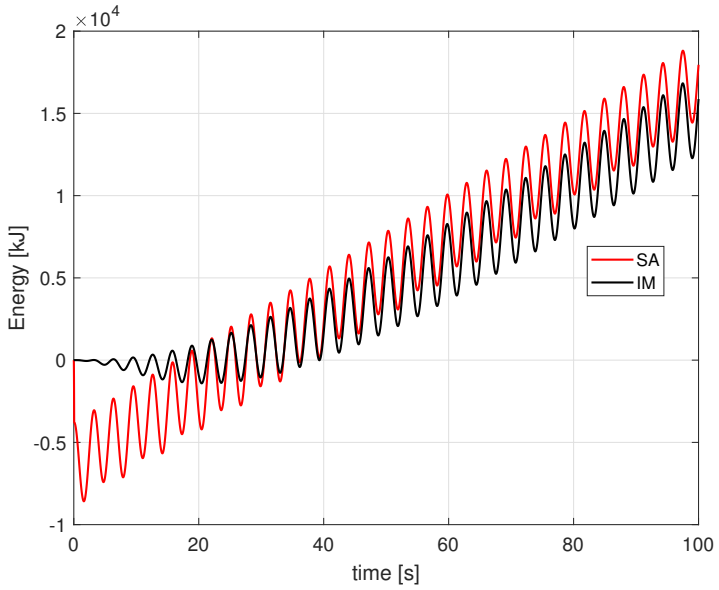

Figure 5.7: Energy absorbed from the isolated WEC with regular wave input at 1 $[rad/s]$. 'IM' represents the result from using impedance matching control. 'SA' represents the result from using singular arc control.

The array of two WECs shown in table 5.1 is simulated using both BSB control law and PD impedance matching. As shown in figure 5.8, the two controls produce the same control force as proved analytically in section 5.2.2.

As can be seen from figure 5.9, the control force acting on WEC1 is smaller than the control force on the isolated WEC, and the control force on WEC2 is out of phase compared with the control force on the isolated WEC.

The performance of each WEC in the array is compared with that of the isolated WEC. The energy extraction for each WEC in the array is shown in figure 5.10. By averaging power simulated using array and isolated WEC, the q-factor is calculated to be 0.82. The q-factor can also be calculated by dividing steady state energy

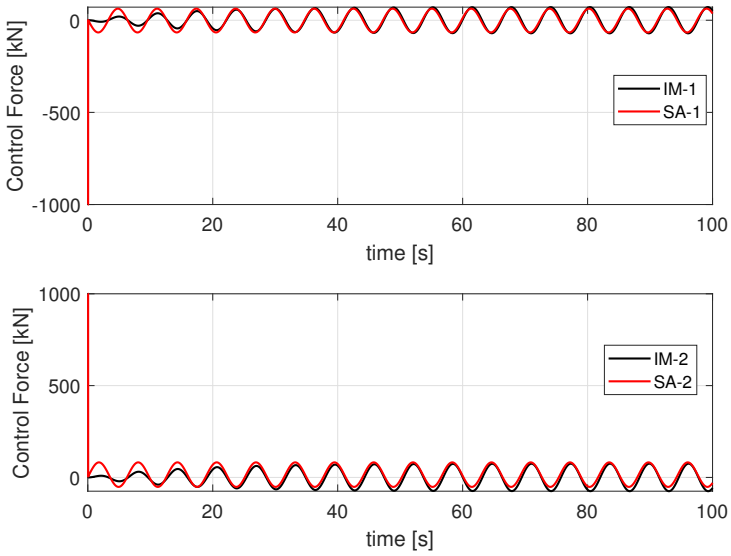

Figure 5.8: Control force for each WEC in the array with regular wave input at $1\,[rad/s]$. The top figure and 1 represents the WEC at $(0, 0)\,[m]$. The bottom figure and 2 represents the WEC at $(30, 0)\,[m]$.

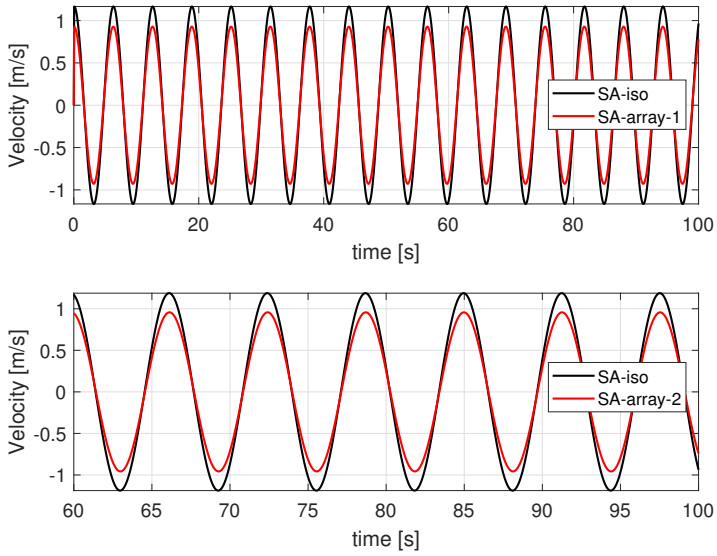

Figure 5.9: Control force for each WEC in the array.

absorption from the array by the energy absorption from the isolated WEC. It can be seen from figure 5.11 that when the array reaches steady state, the q-factor is

approaching the the q-factor value calculated from averaged power.

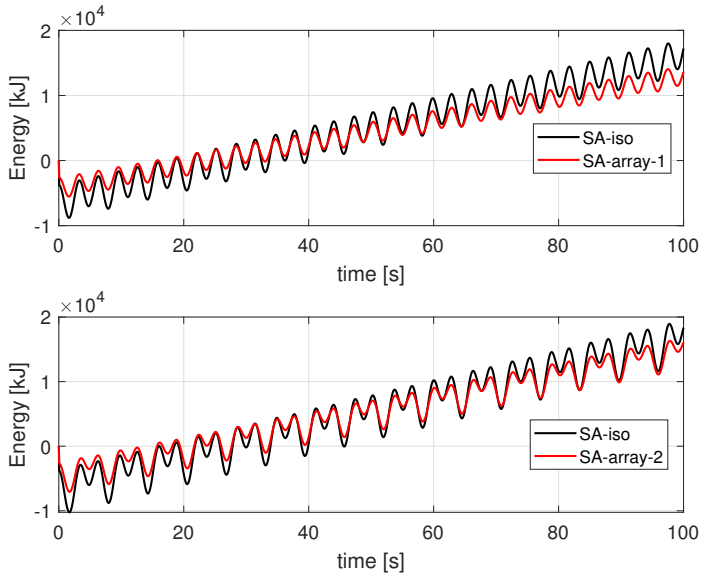

Figure 5.10: Comparison of the energy extracted from each WEC in the array with the energy extracted from the isolated WEC.

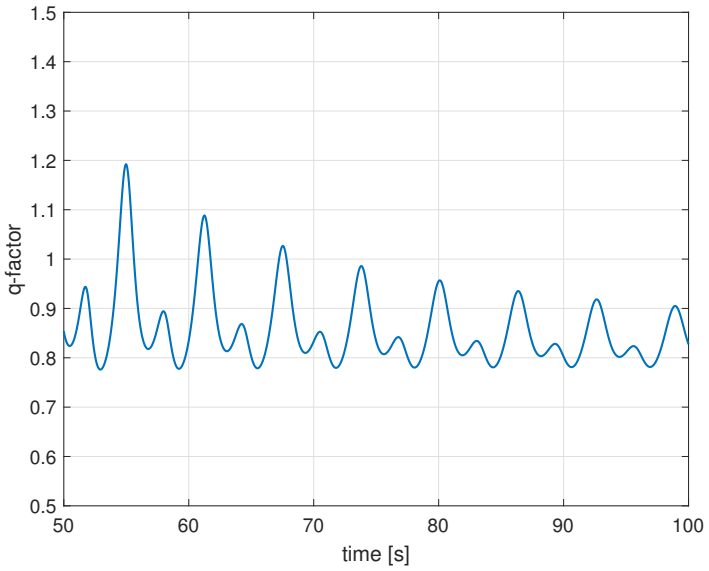

Figure 5.11: q-factor calculated from the steady state energy absorption.

5.5.2 Simulation Result With Irregular Wave Input

The hydrodynamic coefficients for the WEC array are calculated using Nemoh with the information shown in table 5.1. The radiation state space systems are approximated using matrices $M_a(\omega)$ and $B_r(\omega)$ via system identification.

As discussed in section 5.3, the solution shown in equation 5.49 is in Laplace domain. To operate numerical simulations, the solution needs to be converted to time domain and only steady state part of the solution will be kept.

The system shown in equation 5.29 and 5.30 is constructed with a Bretschneider spectra. The significant wave height and the peak period are $1.158\,[m]$ and $8\,[s]$ respectively. While the WEC array dynamics is constructed with irregular wave and radiation states, the input to the array is selected to be a regular wave of $\omega = 0.797\,[rad/s]$. Here the regular wave is selected since it is easier to identify the steady terms in the control force with respect to the excitation frequency.

Similar to section 5.5.1, the control is first solved for an isolated WEC. By solving the inverse Laplace transformation, the steady terms of the control u are find to be:

$$u_{iso_{sa}} = -228.97cos(0.79744t) - 354611.0sin(0.79744t) \tag{5.63}$$

where $u_{iso_{sa}}$ is the singular arc control solution computed for an isolated WEC.

For the sake of comparison, the impedance matching control should also be converted to the Laplace domain, and be converted back to time domain with steady state part kept. The steady state impedance matching control is found to be:

$$u_{iso_{im}} = 15146.0cos(0.79744t) - 362111.0sin(0.79744t) \tag{5.64}$$

where $u_{iso_{im}}$ is the impedance matching control solution computed for an isolated WEC.

As can be seen from equation 5.63 and 5.64, the two controls have similar coefficients for the sine term. Since cosine coefficients are smaller than 5% of the sine coefficients, the sine terms of these two forces are dominant. Thus, the two control forces are approximately the same. This comparison is shown numerically in figure 5.12. The two control forces in figure 5.12 are approximately the same.

As shown in figure 5.13 and 5.14, the singular arc control and PD impedance matching control produce the same WEC response and energy absorption. Both control forces can be defined numerically with the coefficients shown in equation 5.65.

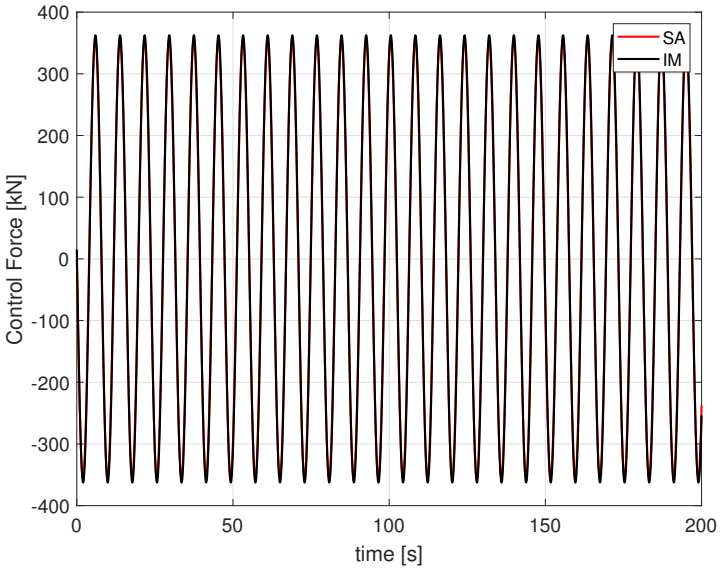

Figure 5.12: Comparison of singular arc solution with PD impedance matching control.

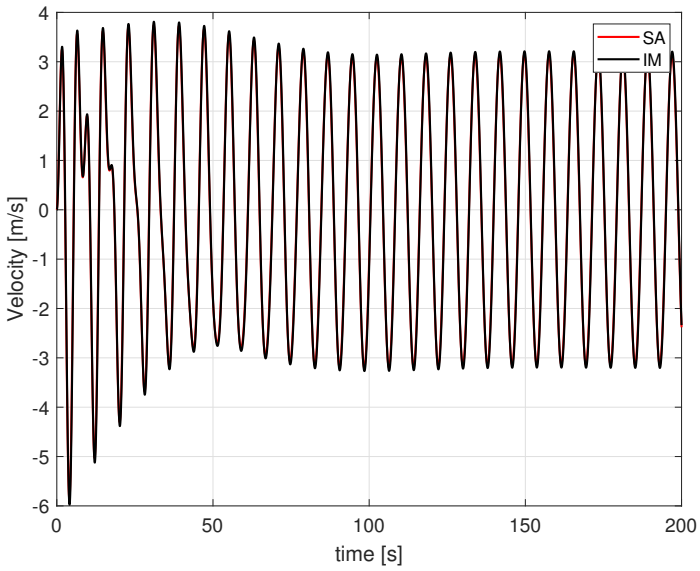

Figure 5.13: Velocity of an isolated WEC using singular arc control and impedance matching control.

$$u_{sa} = a_{sa}cos(\omega t) + b_{sa}sin(\omega t)$$
$$u_{im} = a_{im}cos(\omega t) + b_{im}sin(\omega t) \tag{5.65}$$

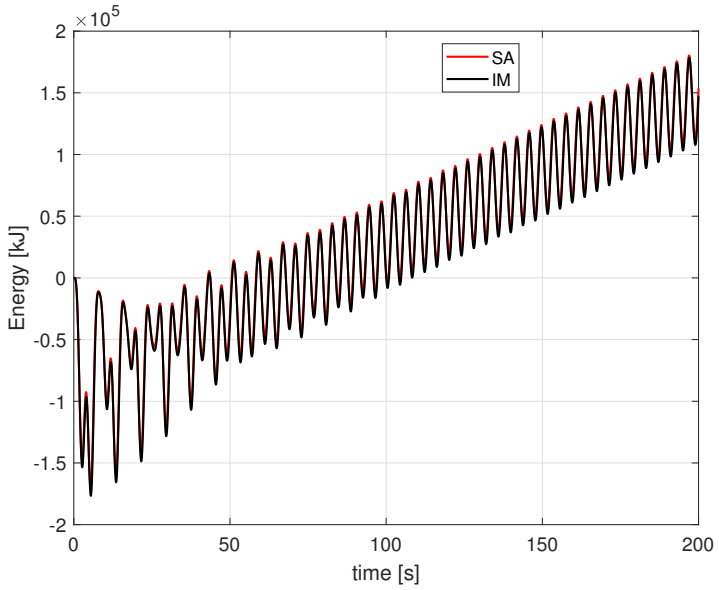

Figure 5.14: Energy absorbed from an isolated WEC using singular arc control and impedance matching control.

The control force is then calculated for the WEC array shown in table 5.1. The coefficients are calculated using both singular arc control and impedance matching control and are shown in table 5.2. Similar to the coefficients calculated from an isolated WEC, the singular arc solution is approximately the same to the impedance matching control for the WEC array.

Table 5.2
Singular arc and impedance matching control solutions. Excitation frequency $\omega = 0.797\, rad/s$

	a_{sa}	b_{sa}	a_{im}	b_{im}
WEC1	82970	399588	105888	423655
WEC2	−350888	198277	−365699	228088

The WEC array is simulated in time domain using the control forces presented in equation 5.65 and table 5.2. In figure 5.15, the control force acting on each WEC in

the array is compared against the control force on the isolated WEC.

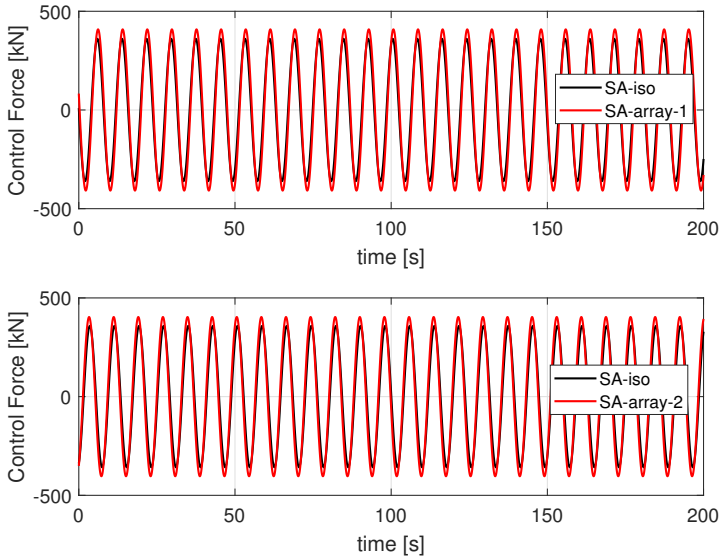

Figure 5.15: Control force for each WEC in the array. The excitation frequency is $0.797\,[rad/s]$. The top figure and 1 represents the WEC at $(0, 0)\,[m]$. The bottom figure and 2 represents the WEC at $(30, 0)\,[m]$.

The velocity and energy absorption of each WEC in the array is shown in figure 5.16 and 5.17

The difference in the magnitude of energy between figure 5.10 and 5.17 comes from the scaling of wave elevation. In section 5.5.1, the wave elevation is assumed to be 0.1 of the significant wave height used in section 5.5.2.

The q-factor calculated from averaged power is 0.56, the q-factor calculated using steady state energy absorption is shown in figure 5.18.

As discussed in section 5.3, the energy absorption of each WEC in the array depends

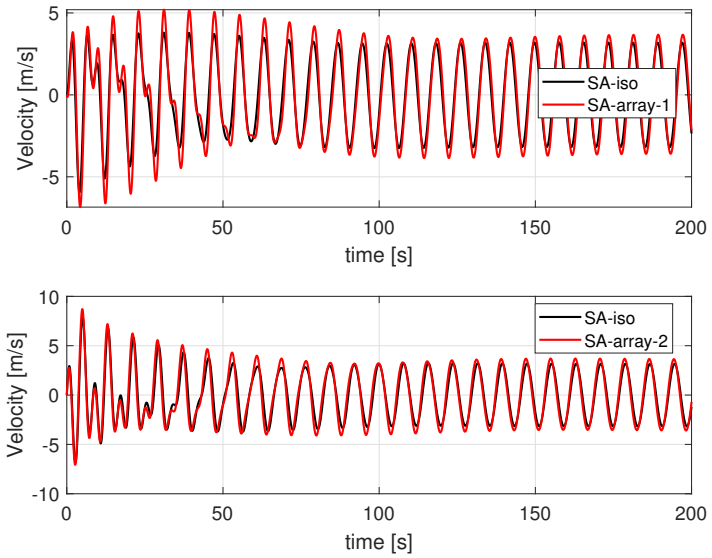

Figure 5.16: Velocity for each WEC in the array. The excitation frequency is $0.797\,[rad/s]$. The top figure and 1 represents the WEC at $(0, 0)\,[m]$. The bottom figure and 2 represents the WEC at $(30, 0)\,[m]$.

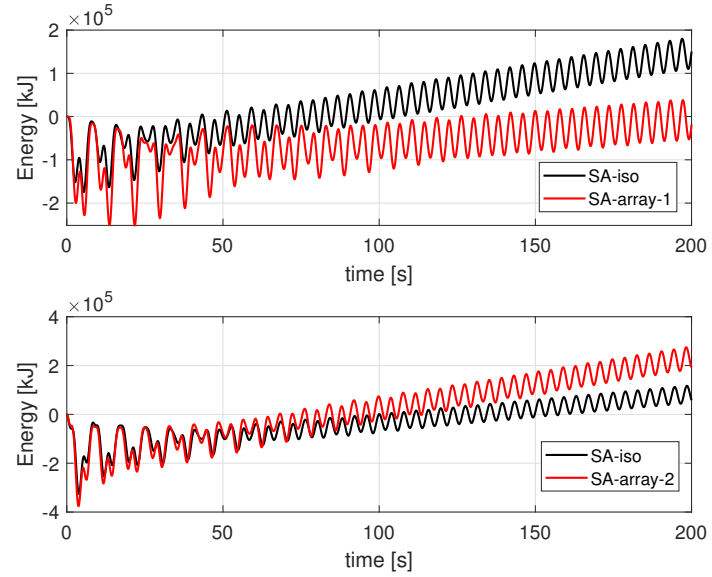

Figure 5.17: Energy absorbed from each WEC in the array. The excitation frequency is $0.797\,[rad/s]$. The top figure and 1 represents the WEC at $(0, 0)\,[m]$. The bottom figure and 2 represents the WEC at $(30, 0)\,[m]$.

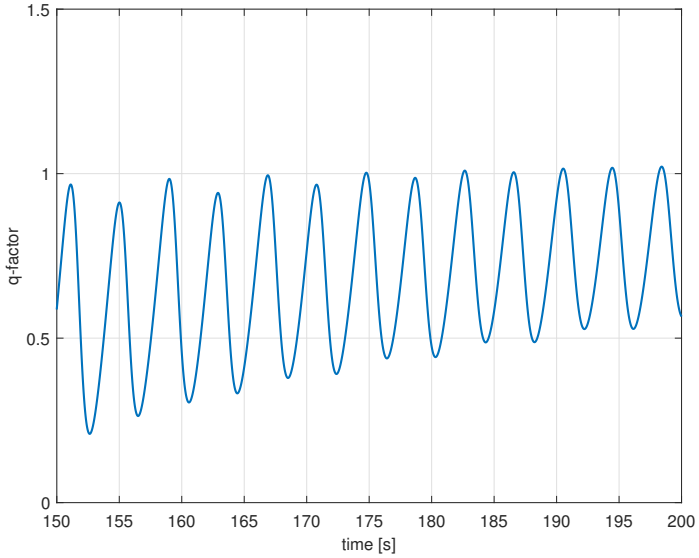

Figure 5.18: q-factor calculated from the steady state energy absorption.

on the accuracy of radiation state space approximation and the accuracy of numerical results from the inverse Laplace transformation.

As can be seen from the calculated q-factors, the optimal controls for both cases produce q-factor smaller than one. The hydrodynamic interaction of WEC array for both cases are destructive. The singular arc control yields optimal energy absorption for a given WEC array using the hydrodynamic interaction information. The "optimal" statement is only valid with respect to the given hydrodynamic interaction. The control does not affect the hydrodynamic interaction of the array, since the hydrodynamic coefficients are characteristics of the WEC array.

Chapter 6

Conclusion

Three objectives are completed in this thesis. The optimization has been done with both array layout and the dimension of each device as design parameters. A novel hybrid array configuration that has both heaving buoys and bottomed hinged OSWCs is proposed and investigated. The optimization of both array layout and device dimensions has been done using the hybrid arrays. The analytical optimal control solution is derived for WEC array using both regular and irregular wave inputs.

6.1 Concluding Remarks

In chapter 3, optimal dimension for each WEC in an array has been studied. BEM solver was used to solve for the exact hydrodynamics which supports the optimization of dimension. Higher q-factors were obtained by optimizing dimension with a given optimal layout. The array produced an average of 39.21% higher q-factor when optimizing with optimal control and 8.87% higher q-factor when optimizing with derivative control.

During the optimization with given optimal layout under regular wave, it is found that control method is a critical factor in designing arrays with optimal dimension. When optimal control is employed, the center buoy of array has most significant impact in array performance, and other buoys on the side have smaller impact. Optimization solution using derivative control implies larger dimension for certain columns in the array (Table. 3.5.) Not only this observation indicates the significance of control algorithm on array design, but also show that, for this type of control, the members in the same column will have similar dimensions. This can be of critical importance when designing the array with a significant wave direction.

Optimization in section 3.3.3 showed that this formulation of problem is able to produce an optimal solution when optimizing both array layout and dimension of

buoys. When optimizing array layout and dimension of buoys under irregular wave with optimal control, the resulting dimension and layout has similar characteristics with optimization solution from regular wave. Computation time for irregular wave optimization increases significantly when compared with regular wave optimization.

This study employed BEM solver which supports the computation of exact hydrodynamics. But computationally, however, it is not efficient. In addition, there are numerical errors when computing radiation impedance for an array contains buoys of different dimensions. A more computationally efficient hydrodynamic model needs to be employed for optimization with irregular waves. Also, with extreme dimension of buoy, like plane plate or tall columns, higher energy may be obtained by using different mode other than heave.

In chapter 4, the hybrid array generates smaller coupled radiation impedance terms at frequencies lower than $1\,rad/s$. This indicates that when the devices are properly designed, the hybrid array has smaller hydrodynamic interaction, compared to a traditional array in the same ocean space.

As shown in table 4.3 in chapter 4, the hybrid configuration achieved a q-factor variance of 0.006, which is four times smaller than that of the traditional configuration. In this work, the average q-factor for the hybrid array is 1.004, and the average q-factor for the traditional array is 1.0166. It implies that the array performance maintains the same level since the q-factor of the the hybrid array is only 1.2% lower

than the traditional one. However, it is worth noting that at some of the separation distances, the q-factors from the hybrid array are significantly lower than those from the traditional array. Similarly, there are also separation distances that hybrid array can produce significantly larger q-factors. Therefore, three more tests, with Gaussian distributed error introduced to the location of each WEC, showed that the hybrid array is more robust against the uncertainty in the array layout.

The average power per unit ocean surface area r_p, is used in this paper to evaluate the performance of both types of arrays. The metric r_p allows more factors, like the cost of an energy storage system and the cost of wires on the sea bed, to be considered during the design process. The more devices placed on the given area, the larger r_p will be. On the other hand, the interaction becomes less consistent when the separation distance changes from large to small.

The optimal layout for an array remains the same no matter including the dimension of each buoy as design variable or not. In section 4.6.2, this statement holds true for both regular and hybrid array optimization. This finding allows the optimization problem to be separated into two problems if necessary. The same desired optimal solution can be obtained by solving both problems. The same optimization algorithm also finds the optimal solution when the array contains buoys of different types such as heave-mode buoys and pitch-mode buoys. The design of a WEC array is more flexible and the optimization can be conducted on more complex ocean environment

which requires different type of buoys to be in the same array.

In chapter 5, the optimal control solution is obtained by using the optimality condition $H_u = 0$ and no state constraints. With both regular and irregular wave excitation, the problem is found to be on a singular arc. Considering the saturation of control force amplitude, a Bang-Singular-Bang control law is proposed and investigated for the WEC array. With PTO energy loss included, the optimal control solution is not on a singular arc. Same saturation of control force amplitude is employed.

When the input to the WEC array is a regular wave, this thesis has proved both analytically and numerically that the singular arc solution yields the same control force as the impedance matching control. It can be concluded from simulation results that the Bang-Singular-Bang control law is able to bring the array to its steady state faster than the PD impedance matching control. Thus, the Bang-Singular-Bang control law extracts maximum power faster than the impedance matching control. However, it requires relatively large control force at the beginning of simulation when the Bang-Bang control is active.

When the input to the WEC array is an irregular wave, the steady state singular arc solution at each frequency again yields the same control force as the steady state impedance matching control. The investigation of WEC array optimal control problem found that the unconstrained singular arc control solutions that have been derived in this thesis produce the same energy absorption as the control calculated

using impedance matching criteria. Both controls can provide the maximum possible energy extraction of a given WEC array. The optimal control force and energy extraction investigated in this study depend only on the hydrodynamics of the array and does not require wave prediction. However, the performance of the singular arc control rely on the accuracy of excitation force estimation, the accuracy of radiation state space approximation and the accuracy of numerical inverse Laplace transformation.

The singular arc control maximizes the energy absorption using given hydrodynamic interaction calculated for a WEC array. The control does not change the hydrodynamic interaction since it is a characteristics of the WEC array.

6.2 Future Works

Regarding the optimization of WEC array, the heaving buoys are assumed to be cylindrical and the radius and height are chosen as design variables. Currently, the shape of WEC has been studied and proved to have significant impact on energy extraction [69]. The next step of WEC array optimization will further expand the type of design variable to include the non-linear shape parameters.

The hybrid array proposed in this thesis only contains two types of devices. In application, the WEC farms are often grouped with wind turbines together in a large

frame of platform. The hybrid array will be investigated along with the wind turbine structure together. Ultimately, the optimization will be employed to determine the optimal mode of motion for each WEC unit.

The optimal control problem can be formulated with the complete dynamics of both the WEC device and PTO unit. Since the relationship between piston pressure p_1, p_2 and WEC displacement z is non-linear, a non-linear optimal control algorithm must be employed.

References

[1] "Ren21. 2019. renewables 2019 global status report." Paris: REN21 Secretariat, 2019. [Online]. Available: http://www.ren21.net/renewables/report

[2] M. M. Moarefdoost, L. V. Snyder, and B. Alnajjab, "Layouts for ocean wave energy farms: Models, properties, and optimization," Omega, vol. 66, pp. 185 – 194, 2017, new Research Frontiers in Sustainability. [Online]. Available: http://www.sciencedirect.com/science/article/pii/S0305048316303127

[3] M. Penalba, I. Touzn, J. Lopez-Mendia, and V. Nava, "A numerical study on the hydrodynamic impact of device slenderness and array size in wave energy farms in realistic wave climates," Ocean Engineering, vol. 142, pp. 224 – 232, 2017. [Online]. Available: http://www.sciencedirect.com/science/article/pii/S0029801817303517

[4] S. Huang, S. Sheng, A. Gerthoffert, Y. Cong, T. Zhang, and Z. Wang,

"Numerical design study of multipoint mooring systems for the floating wave energy converter in deep water with a sloping bottom," Renewable Energy, vol. 136, pp. 558 – 571, 2019. [Online]. Available: http://www.sciencedirect.com/science/article/pii/S0960148119300278

[5] U. A. Korde, J. Lyu, R. D. Robinett, D. G. Wilson, G. Bacelli, and O. O. Abdelkhalik, "Constrained near-optimal control of a wave energy converter in three oscillation modes," Applied Ocean Research, vol. 69, pp. 126 – 137, 2017. [Online]. Available: http://www.sciencedirect.com/science/article/pii/S0141118717303206

[6] J. Lyu, O. Abdelkhalik, and L. Gauchia, "Optimization of dimensions and layout of an array of wave energy converters," Ocean Engineering, vol. 192, p. 106543, 2019. [Online]. Available: http://www.sciencedirect.com/science/article/pii/S0029801819306778

[7] M. K. Hubbert, "Nuclear Energy and the Fossil Fuel," in API-56-007. API: American Petroleum Institute, Jan. 1956, p. 19. [Online]. Available: https://doi.org/

[8] G. Bacelli, "Optimal control of wave energy converters," 2014. [Online]. Available: http://mural.maynoothuniversity.ie/6753/

[9] R. L. Bedard, M. Previsic, G. Hagerman, B. Polagye, W. Musial, J. Klure,

A. von Jouanne, U. Mathur, J. Partin, C. Collar, C. R. Hopper, and S. Amsden, "North american ocean energy status - march 2007," 2007.

[10] M. Mustapa, O. Yaakob, Y. M. Ahmed, C.-K. Rheem, K. Koh, and F. A. Adnan, "Wave energy device and breakwater integration: A review," Renewable and Sustainable Energy Reviews, vol. 77, pp. 43 – 58, 2017. [Online]. Available: http://www.sciencedirect.com/science/article/pii/S1364032117304409

[11] S. Zou, "Optimal control of wave energy converters," 2018. [Online]. Available: https://digitalcommons.mtu.edu/etdr/702

[12] e. Kari Burman, Andy Walker, "Ocean energy technology overview: Federal energy management program (femp)," 07 2009.

[13] D. Evans, "Some theoretical aspects of three-dimensional wave-energy absorbers," First Symposium on Wave Energy Utilization, Gothenburg., 1979.

[14] Budal, "Theory for absorption of wave power by a system of interacting bodies," Journal of Ship Research, vol. 21, no. 4, pp. 248 – 253, 1977. [Online]. Available: http://ingentaconnect.com/content/sname/jsr

[15] J. Falnes, "Radiation impedance matrix and optimum power absorption for interacting oscillators in surface waves," Applied Ocean Research, vol. 2, no. 2, pp. 75 – 80, 1980. [Online]. Available: http://www.sciencedirect.com/science/article/pii/0141118780900322

[16] . Y. D. Kagemoto, H., "Interactions among multiple three-dimensional bodies in water waves: An exact algebraic method," Journal of Fluid Mechanics, vol. 166, pp. 189–209, 1986.

[17] J.-R. Nader, S.-P. Zhu, and P. Cooper, "Hydrodynamic and energetic properties of a finite array of fixed oscillating water column wave energy converters," Ocean Engineering, vol. 88, pp. 131 – 148, 2014. [Online]. Available: http://www.sciencedirect.com/science/article/pii/S0029801814002352

[18] M. Gteman, J. Engstrm, M. Eriksson, J. Isberg, and M. Leijon, "Methods of reducing power fluctuations in wave energy parks," Journal of Renewable and Sustainable Energy, vol. 6, no. 4, p. 043103, 2014. [Online]. Available: https://doi.org/10.1063/1.4889880

[19] J. Falnes, Ocean Waves and Oscillating Systems. Cambridge University Press, 2002.

[20] G. Li and M. R. Belmont, "Model predictive control of sea wave energy converters part i: A convex approach for the case of a single device," Renewable Energy, vol. 69, pp. 453 – 463, 2014. [Online]. Available: http://www.sciencedirect.com/science/article/pii/S0960148114002456

[21] ——, "Model predictive control of sea wave energy converters part ii: The case of an array of devices," Renewable Energy, vol. 68, pp. 540 – 549,

2014. [Online]. Available: http://www.sciencedirect.com/science/article/pii/S0960148114001190

[22] O. Abdelkhalik, S. Zou, R. Robinett, G. Bacelli, D. Wilson, and R. Coe, "Control of Three Degrees-of-Freedom Wave Energy Converters Using Pseudo-Spectral Methods," Journal of Dynamic Systems, Measurement, and Control, vol. 140, no. 7, 01 2018. [Online]. Available: https://doi.org/10.1115/1.4038860

[23] G. Bacelli, P. Balitsky, and J. V. Ringwood, "Coordinated control of arrays of wave energy devices x2014;benefits over independent control," IEEE Transactions on Sustainable Energy, vol. 4, no. 4, pp. 1091–1099, Oct 2013.

[24] S. Zou, O. Abdelkhalik, R. Robinett, G. Bacelli, and D. Wilson, "Optimal control of wave energy converters," Renewable Energy, vol. 103, pp. 217 – 225, 2017. [Online]. Available: http://www.sciencedirect.com/science/article/pii/S0960148116310059

[25] A. Plummer and M. Schlotter, "Investigating the performance of a hydraulic power take-off," 09 2009.

[26] N. J. Baker and M. A. Mueller, "Direct drive wave energy converters," Rev. Energ. Ren. : Power Engineering, vol. 36, pp. 1–7, 01 2001.

[27] S. Astariz and G. Iglesias, "The economics of wave energy: A review," Renewable and Sustainable Energy Reviews, vol. 45, pp. 397 – 408,

2015. [Online]. Available: http://www.sciencedirect.com/science/article/pii/S1364032115000714

[28] M. B. Topper, V. Nava, A. J. Collin, D. Bould, F. Ferri, S. S. Olson, A. R. Dallman, J. D. Roberts, P. Ruiz-Minguela, and H. F. Jeffrey, "Reducing variability in the cost of energy of ocean energy arrays," Renewable and Sustainable Energy Reviews, vol. 112, pp. 263 – 279, 2019. [Online]. Available: http://www.sciencedirect.com/science/article/pii/S1364032119303454

[29] Z. Liu, N. Qu, Z. Han, J. Zhang, S. Zhang, M. Li, and H. Shi, "Study on energy conversion and storage system for a prototype buoys-array wave energy converter," Energy for Sustainable Development, vol. 34, pp. 100 – 110, 2016. [Online]. Available: http://www.sciencedirect.com/science/article/pii/S0973082615300156

[30] Y. Wei, A. Bechlenberg, M. van Rooij, B. Jayawardhana, and A. Vakis, "Modelling of a wave energy converter array with a nonlinear power take-off system in the frequency domain," Applied Ocean Research, vol. 90, p. 101824, 2019. [Online]. Available: http://www.sciencedirect.com/science/article/pii/S0141118718308009

[31] A. Babarit, "Impact of long separating distances on the energy production of two interacting wave energy converters," Ocean Engineering, vol. 37, no. 8, pp.

718 – 729, 2010. [Online]. Available: http://www.sciencedirect.com/science/article/pii/S0029801810000387

[32] T. G. Fitzgerald, C., "A preliminary study on the optimal formation of an array of wave power devices," In:Proceedings of the 7th European Wave and Tidal Energy Conference, 2007.

[33] M. Gteman, "Wave energy parks with point-absorbers of different dimensions," Journal of Fluids and Structures, vol. 74, pp. 142 – 157, 2017. [Online]. Available: http://www.sciencedirect.com/science/article/pii/S0889974617301627

[34] S. Esmaeilzadeh and M.-R. Alam, "Shape optimization of wave energy converters for broadband directional incident waves," Ocean Engineering, vol. 174, pp. 186 – 200, 2019. [Online]. Available: http://www.sciencedirect.com/science/article/pii/S0029801818308564

[35] J. V. Ringwood and U. A. Korde, Hydrodynamic Control of Wave Energy Devices. Cambridge University Press, 2016.

[36] E. Renzi, A. Abdolali, G. Bellotti, and F. Dias, "Wave-power absorption from a finite array of oscillating wave surge converters," Renewable Energy, vol. 63, pp. 55 – 68, 2014. [Online]. Available: http://www.sciencedirect.com/science/article/pii/S096014811300462X

[37] E. Renzi, Y. Wei, and F. Dias, "The pressure impulse of wave slamming on an oscillating wave energy converter," Journal of Fluids and Structures, vol. 82, pp. 258 – 271, 2018. [Online]. Available: http://www.sciencedirect.com/science/article/pii/S0889974618301373

[38] Z. Y. Tay and V. Venugopal, "Hydrodynamic interactions of oscillating wave surge converters in an array under random sea state," Ocean Engineering, vol. 145, pp. 382 – 394, 2017. [Online]. Available: http://www.sciencedirect.com/science/article/pii/S0029801817305310

[39] Q. Zhong and R. W. Yeung, "Model-predictive control strategy for an array of wave-energy converters," Journal of Marine Science and Application, vol. 18, no. 1, pp. 26–37, Mar 2019. [Online]. Available: https://doi.org/10.1007/s11804-019-00081-x

[40] R. Sorensen, Basic Coastal Engineering. Springer US, 1997. [Online]. Available: https://books.google.com/books?id=PafNyKSg4EkC

[41] H.-Y. Cho, H.-M. Kweon, W.-M. Jeong, and W.-M. Jeong, "A study on the optimal equation of the continuous wave spectrum," International Journal of Naval Architecture and Ocean Engineering, vol. 7, no. 6, pp. 1056 – 1063, 2015. [Online]. Available: http://www.sciencedirect.com/science/article/pii/S2092678216300164

[42] W. Garcia-Gabin, "Wave bimodal spectrum based on swell and wind-sea components," IFAC-PapersOnLine, vol. 48, no. 16, pp. 223 – 228, 2015, 10th IFAC Conference on Manoeuvring and Control of Marine Craft MCMC 2015. [Online]. Available: http://www.sciencedirect.com/science/article/pii/S2405896315021758

[43] F. Fusco and J. V. Ringwood, "Short-term wave forecasting for real-time control of wave energy converters," IEEE Transactions on Sustainable Energy, vol. 1, no. 2, pp. 99–106, July 2010.

[44] J. N. Newman, Marine Hydrodynamics. MIT Press, 1935.

[45] J. Falnes and A. Kurniawan, "Fundamental formulae for wave-energy conversion," Royal Society Open Science, vol. 2, pp. 140 305–140 305, 03 2015.

[46] G. Bacelli and J. V. Ringwood, "Nonlinear optimal wave energy converter control with application to a flap-type device," IFAC Proceedings Volumes, vol. 47, no. 3, pp. 7696 – 7701, 2014, 19th IFAC World Congress. [Online]. Available: http://www.sciencedirect.com/science/article/pii/S1474667016428259

[47] J. van 't Hoff, M. Folley, and T. Whittaker, "The design of small seabed-mounted bottom-hinged wave energy converters," 09 2007.

[48] B. Child and V. Venugopal, "Optimal configurations of wave energy device arrays," Ocean Engineering, vol. 37, no. 16, pp. 1402 – 1417,

2010. [Online]. Available: http://www.sciencedirect.com/science/article/pii/S0029801810001447

[49] H. Wolgamot, P. Taylor, and R. E. Taylor, "The interaction factor and directionality in wave energy arrays," Ocean Engineering, vol. 47, pp. 65 – 73, 2012. [Online]. Available: http://www.sciencedirect.com/science/article/pii/S0029801812001138

[50] E. Renzi and F. Dias, "Relations for a periodic array of flap-type wave energy converters," Applied Ocean Research, vol. 39, pp. 31 – 39, 2013. [Online]. Available: http://www.sciencedirect.com/science/article/pii/S0141118712000764

[51] H. E. Krogstad and ivind A. Arntsen, Wave Descriptions and Theory-LINEAR WAVE THEORY. Norwegian University of Science and Technology, 2000.

[52] W. E. Cummins, "The impulse response function and ship motions," 10 1962.

[53] C. M. Chiang, M. Stiassnie, and D. K.-P. Yue, Theory and Applications of Ocean Surface Waves. World Scientific, 2005. [Online]. Available: https://www.worldscientific.com/doi/abs/10.1142/5566

[54] M. Gteman, J. Engstrm, M. Eriksson, and J. Isberg, "Optimizing wave energy parks with over 1000 interacting point-absorbers using an approximate analytical method," International Journal of Marine

Energy, vol. 10, pp. 113 – 126, 2015. [Online]. Available: http://www.sciencedirect.com/science/article/pii/S2214166915000119

[55] M. J. Simon, "Multiple scattering in arrays of axisymmetric wave-energy devices. part 1. a matrix method using a plane-wave approximation," Journal of Fluid Mechanics, vol. 120, p. 125, 1982.

[56] S. Mavrakos and P. McIver, "Comparison of methods for computing hydrodynamic characteristics of arrays of wave power devices," Applied Ocean Research, vol. 19, no. 5, pp. 283 – 291, 1997. [Online]. Available: http://www.sciencedirect.com/science/article/pii/S0141118797000291

[57] A. Babarit, "On the park effect in arrays of oscillating wave energy converters," Renewable Energy, vol. 58, pp. 68 – 78, 2013. [Online]. Available: http://www.sciencedirect.com/science/article/pii/S096014811300164X

[58] A. Babarit and G. Delhommeau, "Theoretical and numerical aspects of the open source bem solver nemoh," 11th European Wave and Tidal Energy Conference (EWTEC2015), 09 2015.

[59] D. Sarkar, E. Contal, N. Vayatis, and F. Dias, "Prediction and optimization of wave energy converter arrays using a machine learning approach," Renewable Energy, vol. 97, pp. 504 – 517, 2016. [Online]. Available: http://www.sciencedirect.com/science/article/pii/S0960148116304931

[60] J.-R. Nader, A. Fleming, G. Macfarlane, I. Penesis, and R. Manasseh, "Novel experimental modelling of the hydrodynamic interactions of arrays of wave energy converters," International Journal of Marine Energy, vol. 20, pp. 109 – 124, 2017. [Online]. Available: http://www.sciencedirect.com/science/article/pii/S2214166917300917

[61] C. Josset, A. Babarit, and A. H. Clment, "A wave-to-wire model of the searev wave energy converter," Proceedings of the Institution of Mechanical Engineers, Part M: Journal of Engineering for the Maritime Environment, vol. 221, no. 2, pp. 81–93, 2007. [Online]. Available: https://doi.org/10.1243/14750902JEME48

[62] N. Tomey-Bozo, A. Babarit, J. Murphy, V. Stratigaki, P. Troch, T. Lewis, and G. Thomas, "Wake effect assessment of a flap type wave energy converter farm under realistic environmental conditions by using a numerical coupling methodology," Coastal Engineering, 2018. [Online]. Available: http://www.sciencedirect.com/science/article/pii/S0378383917305549

[63] R. Henderson, "Design, simulation, and testing of a novel hydraulic power take-off system for the pelamis wave energy converter," Renewable Energy, vol. 31, no. 2, pp. 271 – 283, 2006, marine Energy. [Online]. Available: http://www.sciencedirect.com/science/article/pii/S0960148105002259

[64] J. Wu, Y. Yao, L. Zhou, N. Chen, H. Yu, W. Li, and M. Gteman,

"Performance analysis of solo duck wave energy converter arrays under motion constraints," Energy, vol. 139, pp. 155 – 169, 2017. [Online]. Available: http://www.sciencedirect.com/science/article/pii/S0360544217313361

[65] A. Babarit, "A database of capture width ratio of wave energy converters," Renewable Energy, vol. 80, pp. 610 – 628, 2015. [Online]. Available: http://www.sciencedirect.com/science/article/pii/S0960148115001652

[66] M. Penalba, G. Giorgi, and J. V. Ringwood, "Mathematical modelling of wave energy converters: A review of nonlinear approaches," Renewable and Sustainable Energy Reviews, vol. 78, pp. 1188 – 1207, 2017. [Online]. Available: http://www.sciencedirect.com/science/article/pii/S1364032116308784

[67] H. A. Wolgamot and C. J. Fitzgerald, "Nonlinear hydrodynamic and real fluid effects on wave energy converters," Proceedings of the Institution of Mechanical Engineers, Part A: Journal of Power and Energy, vol. 229, no. 7, pp. 772–794, 2015. [Online]. Available: https://doi.org/10.1177/0957650915570351

[68] H. Wolgamot, R. E. Taylor, and P. Taylor, "Effects of second-order hydrodynamics on the efficiency of a wave energy array," International Journal of Marine Energy, vol. 15, pp. 85 – 99, 2016, selected Papers from the European Wave and Tidal Energy Conference 2015, Nante, France. [Online]. Available: http://www.sciencedirect.com/science/article/pii/S2214166916300170

[69] M. Penalba, A. Mérigaud, J.-C. Gilloteaux, and J. V. Ringwood, "Influence of nonlinear froude–krylov forces on the performance of two wave energy points absorbers," Journal of Ocean Engineering and Marine Energy, vol. 3, no. 3, pp. 209–220, Aug 2017. [Online]. Available: https://doi.org/10.1007/s40722-017-0082-x

[70] G. Giorgi and J. V. Ringwood, "Computationally efficient nonlinear froudekrylov force calculations for heaving axisymmetric wave energy point absorbers," Journal of Ocean Engineering and Marine Energy, vol. 3, pp. 21–33, 2017.

[71] C. Greenwood, D. Christie, V. Venugopal, J. Morrison, and A. Vogler, "Modelling performance of a small array of wave energy converters: Comparison of spectral and boussinesq models," Energy, vol. 113, pp. 258 – 266, 2016. [Online]. Available: http://www.sciencedirect.com/science/article/pii/S036054421630915X

[72] J. C. McNatt, V. Venugopal, and D. Forehand, "A novel method for deriving the diffraction transfer matrix and its application to multi-body interactions in water waves," Ocean Engineering, vol. 94, pp. 173 – 185, 2015. [Online]. Available: http://www.sciencedirect.com/science/article/pii/S0029801814004417

[73] F. F. Flavi, A. Babarit, and A. Clment, "On the numerical modeling

and optimization of a bottom-referenced heave-buoy array of wave energy converters," International Journal of Marine Energy, vol. 19, pp. 1 – 15, 2017. [Online]. Available: http://www.sciencedirect.com/science/article/pii/S2214166917300486

[74] H. Bailey, B. Robertson, and B. Buckham, "Variability and stochastic simulation of power from wave energy converter arrays," Renewable Energy, vol. 115, pp. 721 – 733, 2018. [Online]. Available: http://www.sciencedirect.com/science/article/pii/S0960148117308108

[75] C. Cecioni and G. Bellotti, "Boundary conditions for modeling scattered wave field around floating bodies in elliptic wave models," Applied Ocean Research, vol. 59, pp. 492 – 497, 2016. [Online]. Available: http://www.sciencedirect.com/science/article/pii/S0141118716301377

[76] J. Singh and A. Babarit, "A fast approach coupling boundary element method and plane wave approximation for wave interaction analysis in sparse arrays of wave energy converters," Ocean Engineering, vol. 85, pp. 12 – 20, 2014. [Online]. Available: http://www.sciencedirect.com/science/article/pii/S0029801814001589

[77] S. D. Ossama Abdelkhalik, Shangyan Zou, "On the modelling of arrays of wave energy converters," The Asian Wave and Tidal Energy Conference 2018, 09 2018.

[78] I. Noad and R. Porter, "Modelling an articulated raft wave energy converter," Renewable Energy, vol. 114, pp. 1146 – 1159, 2017. [Online]. Available: http://www.sciencedirect.com/science/article/pii/S096014811730705X

[79] H. Zhang, D. Xu, C. Liu, and Y. Wu, "Wave energy absorption of a wave farm with an array of buoys and flexible runway," Energy, vol. 109, pp. 211 – 223, 2016. [Online]. Available: http://www.sciencedirect.com/science/article/pii/S0360544216305205

[80] E. Luczko, B. Robertson, H. Bailey, C. Hiles, and B. Buckham, "Representing non-linear wave energy converters in coastal wave models," Renewable Energy, vol. 118, pp. 376 – 385, 2018. [Online]. Available: http://www.sciencedirect.com/science/article/pii/S0960148117311412

[81] J. Isberg, J. Engstrm, M. Eriksson, and M. Gteman, "Control of rapid phase oscillations in the modelling of large wave energy arrays," International Journal of Marine Energy, vol. 11, pp. 1 – 8, 2015. [Online]. Available: http://www.sciencedirect.com/science/article/pii/S2214166915000156

[82] K. BUDAR and J. FALNES, "A resonant point absorber of ocean-wave power," Nature, vol. 256, no. 5517, pp. 478–479, Aug. 1975. [Online]. Available: https://doi.org/10.1038/256478a0

[83] J. Song, O. Abdelkhalik, R. Robinett, G. Bacelli, D. Wilson, and U. Korde, "Multi-resonant feedback control of heave wave energy converters,"

Ocean Engineering, vol. 127, pp. 269 – 278, 2016. [Online]. Available: http://www.sciencedirect.com/science/article/pii/S0029801816304346

[84] U. A. Korde, "Wave energy conversion under constrained wave-by-wave impedance matching with amplitude and phase-match limits," Applied Ocean Research, vol. 90, p. 101858, 2019. [Online]. Available: http://www.sciencedirect.com/science/article/pii/S0141118718309039

[85] M. Folley and T. Whittaker, "The effect of sub-optimal control and the spectral wave climate on the performance of wave energy converter arrays," Applied Ocean Research, vol. 31, no. 4, pp. 260 – 266, 2009, renewable Energy: Leveraging Ocean and Waterways. [Online]. Available: http://www.sciencedirect.com/science/article/pii/S0141118709000947

[86] G. Li, G. Weiss, M. Mueller, S. Townley, and M. R. Belmont, "Wave energy converter control by wave prediction and dynamic programming," Renewable Energy, vol. 48, pp. 392 – 403, 2012. [Online]. Available: http://www.sciencedirect.com/science/article/pii/S0960148112003163

[87] O. Abdelkhalik and S. Zou, "Control of wave energy converters using a simple dynamic model," IEEE Transactions on Sustainable Energy, vol. 10, no. 2, pp. 579–585, April 2019.

[88] J. Hals, J. Falnes, and T. Moan, "Constrained Optimal Control of a Heaving Buoy Wave-Energy Converter," Journal of Offshore Mechanics and

Arctic Engineering, vol. 133, no. 1, 11 2010, 011401. [Online]. Available: https://doi.org/10.1115/1.4001431

[89] J. Cretel, G. Lightbody, G. Thomas, and A. Lewis, "Maximisation of energy capture by a wave-energy point absorber using model predictive control," IFAC Proceedings Volumes, vol. 44, no. 1, pp. 3714 – 3721, 2011, 18th IFAC World Congress. [Online]. Available: http://www.sciencedirect.com/science/article/pii/S1474667016441893

[90] S. R. Nielsen, Q. Zhou, B. Basu, M. T. Sichani, and M. M. Kramer, "Optimal control of an array of non-linear wave energy point converters," Ocean Engineering, vol. 88, pp. 242 – 254, 2014. [Online]. Available: http://www.sciencedirect.com/science/article/pii/S0029801814002406

[91] O. Abdelkhalik, R. Robinett, S. Zou, G. Bacelli, R. Coe, D. Bull, D. Wilson, and U. Korde, "On the control design of wave energy converters with wave prediction," Journal of Ocean Engineering and Marine Energy, vol. 2, no. 4, pp. 473–483, Nov 2016. [Online]. Available: https://doi.org/10.1007/s40722-016-0048-4

[92] G. Bacelli and J. Ringwood, "Constrained control of arrays of wave energy devices," International Journal of Marine Energy, vol. 3-4, pp. e53 – e69, 2013, special Issue Selected Papers - EWTEC2013. [Online]. Available: http://www.sciencedirect.com/science/article/pii/S2214166913000374

[93] M. Starrett, R. So, T. K. A. Brekken, and A. McCall, "Increasing power capture from multibody wave energy conversion systems using model predictive control," in 2015 IEEE Conference on Technologies for Sustainability (SusTech), July 2015, pp. 20–26.

[94] Y. Hong, R. Waters, C. Bostrm, M. Eriksson, J. Engstrm, and M. Leijon, "Review on electrical control strategies for wave energy converting systems," Renewable and Sustainable Energy Reviews, vol. 31, pp. 329 – 342, 2014. [Online]. Available: http://www.sciencedirect.com/science/article/pii/S1364032113008022

[95] L. Wang, J. Isberg, and E. Tedeschi, "Review of control strategies for wave energy conversion systems and their validation: the wave-to-wire approach," Renewable and Sustainable Energy Reviews, vol. 81, pp. 366 – 379, 2018. [Online]. Available: http://www.sciencedirect.com/science/article/pii/S136403211731016X

[96] C. Cargo, "Design and control of hydraulic power take-offs for wave energy converters," 2012.

[97] P. Ricci, J. Lopez Mendia, M. Santos-Mugica, P. Ruiz Minguela, J. L. Villate, F. Salcedo, and A. Falcao, "Control strategies for a wave energy converter connected to a hydraulic power take-off," Renewable Power Generation, IET, vol. 5, pp. 234 – 244, 06 2011.

[98] A. F. de O. Falco, "Modelling and control of oscillating-body wave energy converters with hydraulic power take-off and gas accumulator," Ocean Engineering, vol. 34, no. 14, pp. 2021 – 2032, 2007. [Online]. Available: http://www.sciencedirect.com/science/article/pii/S0029801807001011

[99] H. Eidsmoen, "Simulation of a slack-moored heaving-buoy waveenergy converter with phase control.tech," Tech. Rep., 1996.

[100] D. McCandlish and R. E. Dorey, "The mathematical modelling of hydrostatic pumps and motors," Proceedings of the Institution of Mechanical Engineers, Part B: Management and engineering manufacture, vol. 198, no. 3, pp. 165–174, 1984. [Online]. Available: https://doi.org/10.1243/PIME_PROC_1984_198_062_02

[101] F. Wu, P. Ju, X. Zhang, C. Qin, G. J. Peng, H. Huang, and J. Fang, "Modeling, control strategy, and power conditioning for direct-drive wave energy conversion to operate with power grid," Proceedings of the IEEE, vol. 101, no. 4, pp. 925–941, April 2013.

[102] M. A. Mueller, "Electrical generators for direct drive wave energy converters," IEE Proceedings - Generation, Transmission and Distribution, vol. 149, no. 4, pp. 446–456, July 2002.

[103] A. Z. Annuar, D. E. Macpherson, D. I. M. Forehand, and M. A. Mueller, "Optimum power control for arrays of direct drive wave energy converters," in 6th IET

International Conference on Power Electronics, Machines and Drives (PEMD 2012), March 2012, pp. 1–6.

[104] H. Mendonca and S. Martinez, "A resistance emulation approach to optimize the wave energy harvesting for a direct drive point absorber," IEEE Transactions on Sustainable Energy, vol. 7, no. 1, pp. 3–11, Jan 2016.

[105] B. Li, D. E. Macpherson, and J. K. H. Shek, "Direct drive wave energy converter control in irregular waves," in IET Conference on Renewable Power Generation (RPG 2011), Sep. 2011, pp. 1–6.

[106] E. Enferad, D. Nazarpour, S. Golshannavaz, and F. Aminifar, "Direct drive surge wave energy converter with grid integration functionality," International Transactions on Electrical Energy Systems, vol. 26, no. 5, pp. 1066–1084, 2016. [Online]. Available: https://onlinelibrary.wiley.com/doi/abs/10.1002/etep.2125

[107] Z. Nie, X. Xiao, R. McMahon, P. Clifton, Y. Wu, and S. Shao, "Emulation and control methods for direct drive linear wave energy converters," IEEE Transactions on Industrial Informatics, vol. 9, no. 2, pp. 790–798, May 2013.

[108] X. Xiao, L. Xiao, and T. Peng, "Comparative study on power capture performance of oscillating-body wave energy converters with three novel power take-off systems," Renewable Energy, vol. 103, pp. 94 – 105, 2017. [Online]. Available: http://www.sciencedirect.com/science/article/pii/S0960148116309934

[109] I. Temiz, J. Leijon, B. Ekergrd, and C. Bostrm, "Economic aspects of latching control for a wave energy converter with a direct drive linear generator power take-off," Renewable Energy, vol. 128, pp. 57 – 67, 2018. [Online]. Available: http://www.sciencedirect.com/science/article/pii/S0960148118305627

[110] P. S. Sangha, T. Sawata, J. Yon, and P. H. Mellor, "Assessment of fluid drag loss in a flooded rotor electro-hydrostatic actuator motor," in 2015 IEEE International Electric Machines Drives Conference (IEMDC), May 2015, pp. 139–142.

[111] T. Kovaltchouk, B. Multon, H. Ben Ahmed, J. Aubry, F. Rongre, and A. Glumineau, "Influence of control strategy on the global efficiency of a direct wave energy converter with electric power take-off," in 2013 Eighth International Conference and Exhibition on Ecological Vehicles and Renewable Energies (EVER), March 2013, pp. 1–10.

[112] M. Giassi and M. Gteman, "Layout design of wave energy parks by a genetic algorithm," Ocean Engineering, vol. 154, pp. 252 – 261, 2018. [Online]. Available: http://www.sciencedirect.com/science/article/pii/S0029801818301045

[113] W. Chen, F. Gao, X. Meng, and J. Fu, "Design of the wave energy converter array to achieve constructive effects," Ocean Engineering, vol. 124, pp. 13 –

20, 2016. [Online]. Available: http://www.sciencedirect.com/science/article/pii/S0029801816302906

[114] X. Garnaud and C. C. Mei, "Comparison of wave power extraction by a compact array of small buoys and by a large buoy," IET Renewable Power Generation, vol. 4, no. 6, pp. 519–530, November 2010.

[115] A. de Andrs, R. Guanche, L. Meneses, C. Vidal, and I. Losada, "Factors that influence array layout on wave energy farms," Ocean Engineering, vol. 82, pp. 32 – 41, 2014. [Online]. Available: http://www.sciencedirect.com/science/article/pii/S0029801814000651

[116] Y.-C. Chow, Y.-C. Chang, D.-W. Chen, C.-C. Lin, and S.-Y. Tzang, "Parametric design methodology for maximizing energy capture of a bottom-hinged flap-type wec with medium wave resources," Renewable Energy, vol. 126, pp. 605 – 616, 2018. [Online]. Available: http://www.sciencedirect.com/science/article/pii/S0960148118303707

[117] Y.-C. Chow, Y.-C. Chang, C.-C. Lin, J.-H. Chen, and S.-Y. Tzang, "Experimental investigations on wave energy capture of two bottom-hinged-flap wecs operating in tandem," Ocean Engineering, vol. 164, pp. 322 – 331, 2018. [Online]. Available: http://www.sciencedirect.com/science/article/pii/S0029801818310126

[118] J. P. McGuinness and G. Thomas, "The constrained optimisation of small linear arrays of heaving point absorbers. part i: The influence of spacing," International Journal of Marine Energy, vol. 20, pp. 33 – 44, 2017. [Online]. Available: http://www.sciencedirect.com/science/article/pii/S2214166917300607

[119] S. Bozzi, M. Giassi, A. M. Miquel, A. Antonini, F. Bizzozero, G. Gruosso, R. Archetti, and G. Passoni, "Wave energy farm design in real wave climates: the italian offshore," Energy, vol. 122, pp. 378 – 389, 2017. [Online]. Available: http://www.sciencedirect.com/science/article/pii/S0360544217301019

[120] C. Sharp and B. DuPont, "Wave energy converter array optimization: A genetic algorithm approach and minimum separation distance study," Ocean Engineering, vol. 163, pp. 148 – 156, 2018. [Online]. Available: http://www.sciencedirect.com/science/article/pii/S0029801818309521

[121] A. Bryson, Applied Optimal Control: Optimization, Estimation and Control. CRC Press, 2018. [Online]. Available: https://books.google.com/books?id=KUxaDwAAQBAJ

[122] B. Borgarino, A. Babarit, and P. Ferrant, "Impact of wave interactions effects on energy absorption in large arrays of wave energy converters," Ocean Engineering, vol. 41, pp. 79 – 88, 2012. [Online]. Available: http://www.sciencedirect.com/science/article/pii/S0029801812000054

[123] L. Myers and A. Bahaj, "An experimental investigation simulating flow effects in first generation marine current energy converter arrays," Renewable Energy, vol. 37, no. 1, pp. 28 – 36, 2012. [Online]. Available: http://www.sciencedirect.com/science/article/pii/S0960148111001716

[124] A. Bahaj and L. Myers, "Shaping array design of marine current energy converters through scaled experimental analysis," Energy, vol. 59, pp. 83 – 94, 2013. [Online]. Available: http://www.sciencedirect.com/science/article/pii/S0360544213006105

[125] I. Noad and R. Porter, "Optimisation of arrays of flap-type oscillating wave surge converters," Applied Ocean Research, vol. 50, pp. 237 – 253, 2015. [Online]. Available: http://www.sciencedirect.com/science/article/pii/S0141118715000218

[126] F. C. da Fonseca, R. Gomes, J. Henriques, L. Gato, and A. Falco, "Model testing of an oscillating water column spar-buoy wave energy converter isolated and in array: Motions and mooring forces," Energy, vol. 112, pp. 1207 – 1218, 2016. [Online]. Available: http://www.sciencedirect.com/science/article/pii/S0360544216309288

[127] A. Sinha, D. Karmakar, and C. G. Soares, "Performance of optimally tuned arrays of heaving point absorbers," Renewable Energy, vol. 92, pp. 517 –

531, 2016. [Online]. Available: http://www.sciencedirect.com/science/article/pii/S0960148116301446

[128] F. F. Flavi, C. McNatt, F. Rongre, A. Babarit, and A. Clment, "A numerical tool for the frequency domain simulation of large arrays of identical floating bodies in waves," Ocean Engineering, vol. 148, pp. 299 – 311, 2018. [Online]. Available: http://www.sciencedirect.com/science/article/pii/S0029801817306935

[129] F. J. Mendez, P. Camus, R. Medina, and A. Cofino, "Analyzing the multidimensional wave climate with self organizing maps," in OCEANS 2009-EUROPE, May 2009, pp. 1–9.

[130] M. C. Sousounis, L. K. Gan, A. E. Kiprakis, and J. K. H. Shek, "Direct drive wave energy array with offshore energy storage supplying off-grid residential load," IET Renewable Power Generation, vol. 11, no. 9, pp. 1081–1088, 2017.

[131] P. T. Jacobson, G. Hagerman, and G. Scott, "Mapping and assessment of the united states ocean wave energy resource," 12 2011.

[132] G. P. Thomas and D. V. Evans, "Arrays of three-dimensional wave-energy absorbers," Journal of Fluid Mechanics, vol. 108, p. 6788, 1981.

[133] B. Borgarino, A. Babarit, and P. Ferrant, "Impact of wave interactions effects on energy absorption in large arrays of wave energy converters,"

Ocean Engineering, vol. 41, pp. 79 – 88, 2012. [Online]. Available: http://www.sciencedirect.com/science/article/pii/S0029801812000054

[134] I. Chatjigeorgiou and V. Katsardi, "Hydrodynamics and near trapping effects in arrays of multiple elliptical cylinders in waves," Ocean Engineering, vol. 157, pp. 121 – 139, 2018. [Online]. Available: http://www.sciencedirect.com/science/article/pii/S002980181830310X

[135] D. Khojasteh, S. M. Mousavi, W. Glamore, and G. Iglesias, "Wave energy status in asia," Ocean Engineering, vol. 169, pp. 344 – 358, 2018. [Online]. Available: http://www.sciencedirect.com/science/article/pii/S0029801818304323

[136] C. V. Weiss, R. Guanche, B. Ondiviela, O. F. Castellanos, and J. Juanes, "Marine renewable energy potential: A global perspective for offshore wind and wave exploitation," Energy Conversion and Management, vol. 177, pp. 43 – 54, 2018. [Online]. Available: http://www.sciencedirect.com/science/article/pii/S0196890418310628

[137] WorldEnergyCouncil, "World energy resources, marine energy 2016," 2016. [Online]. Available: https://www.worldenergy.org/wp-content/uploads/2017/03/WEResources_Marine_2016.pdf

[138] P. B. Garcia-Rosa, G. Bacelli, and J. V. Ringwood, "Control-informed optimal array layout for wave farms," IEEE Transactions on Sustainable Energy, vol. 6, no. 2, pp. 575–582, April 2015.

[139] P. Balitsky, "Modelling controlled arrays of wave energy converters," June 2013. [Online]. Available: http://eprints.maynoothuniversity.ie/4487/

[140] Z. Liu, N. Qu, Z. Han, J. Zhang, S. Zhang, M. Li, and H. Shi, "Study on energy conversion and storage system for a prototype buoys-array wave energy converter," Energy for Sustainable Development, vol. 34, pp. 100 – 110, 2016. [Online]. Available: http://www.sciencedirect.com/science/article/pii/S0973082615300156

[141] J. Falnes, "Radiation impedance matrix and optimum power absorption for interacting oscillators in surface waves," Applied Ocean Research, vol. 2, no. 2, pp. 75 – 80, 1980. [Online]. Available: http://www.sciencedirect.com/science/article/pii/0141118780900322

[142] M. Penalba, I. Touzn, J. Lopez-Mendia, and V. Nava, "A numerical study on the hydrodynamic impact of device slenderness and array size in wave energy farms in realistic wave climates," Ocean Engineering, vol. 142, pp. 224 – 232, 2017. [Online]. Available: http://www.sciencedirect.com/science/article/pii/S0029801817303517

[143] A. Henry, M. Folley, and T. Whittaker, "A conceptual model of the hydrodynamics of an oscillating wave surge converter," Renewable Energy, vol. 118, pp. 965 – 972, 2018. [Online]. Available: http://www.sciencedirect.com/science/article/pii/S0960148117310510

[144] Y. Cheng, G. Li, C. Ji, G. Zhai, and G. Oleg, "Current effects on nonlinear wave slamming by an oscillating wave surge converter," Engineering Analysis with Boundary Elements, vol. 96, pp. 150 – 168, 2018. [Online]. Available: http://www.sciencedirect.com/science/article/pii/S0955799718301693

[145] L. Wilkinson, T. Whittaker, P. Thies, S. Day, and D. Ingram, "The power-capture of a nearshore, modular, flap-type wave energy converter in regular waves," Ocean Engineering, vol. 137, pp. 394 – 403, 2017. [Online]. Available: http://www.sciencedirect.com/science/article/pii/S0029801817302019

[146] D. Sarkar, E. Renzi, and F. Dias, "Effect of a straight coast on the hydrodynamics and performance of the oscillating wave surge converter," Ocean Engineering, vol. 105, pp. 25 – 32, 2015. [Online]. Available: http://www.sciencedirect.com/science/article/pii/S0029801815002097

[147] H.-F. Yu, Y.-L. Zhang, and S.-M. Zheng, "Numerical study on the performance of a wave energy converter with three hinged bodies," Renewable Energy, vol. 99, pp. 1276 – 1286, 2016. [Online]. Available: http://www.sciencedirect.com/science/article/pii/S0960148116307248

[148] H. Joe, H. Roh, H. Cho, and S.-C. Yu, "Development of a flap-type mooring-less wave energy harvesting system for sensor buoy," Energy, vol. 133, pp. 851 – 863, 2017. [Online]. Available: http://www.sciencedirect.com/science/article/pii/S0360544217309015

[149] R. Gomes, M. Lopes, J. Henriques, L. Gato, and A. Falco, "The dynamics and power extraction of bottom-hinged plate wave energy converters in regular and irregular waves," Ocean Engineering, vol. 96, pp. 86 – 99, 2015. [Online]. Available: http://www.sciencedirect.com/science/article/pii/S0029801814004818

[150] P. Schmitt, H. Asmuth, and B. Elser, "Optimising power take-off of an oscillating wave surge converter using high fidelity numerical simulations," International Journal of Marine Energy, vol. 16, pp. 196 – 208, 2016. [Online]. Available: http://www.sciencedirect.com/science/article/pii/S2214166916300510

[151] W. Hu, L. Zhou, Y. Tian, Z. Jiao, Y. Shang, Z. Song, and L. Yan, "Analysis for the power loss of electro hydrostatic actuator and hydraulic actuator," in 2015 IEEE International Conference on Advanced Intelligent Mechatronics (AIM), July 2015, pp. 613–616.

[152] M. Zucca, P. E. Roccato, O. Bottauscio, and C. Beatrice, "Analysis of losses in a magnetostrictive device under dynamic supply conditions," IEEE Transactions on Magnetics, vol. 46, no. 2, pp. 183–186, Feb 2010.

[153] A. Wahyudie, T. B. Susilo, M. Jama, B. F. Mon, and H. Shaaref, "Design of a double-sided permanent magnet linear generator for laboratory scale ocean wave energy converter," in OCEANS 2017 - Anchorage, Sep. 2017, pp. 1–5.

[154] S. Yang, H. He, H. Chen, Y. Wang, H. Li, and S. Zheng, "Experimental study on the performance of a floating array-point-raft wave energy converter under random wave conditions," Renewable Energy, vol. 139, pp. 538 – 550, 2019. [Online]. Available: http://www.sciencedirect.com/science/article/pii/S0960148119302472

[155] S. P. McDonald, N. J. Baker, M. Espinoza, and V. Pickert, "Power-take-off topology comparison for a wave energy converter," The Journal of Engineering, vol. 2019, no. 18, pp. 5012–5017, 2019.

[156] E. Palomares, A. Nieto, A. Morales, J. Chicharro, and P. Pintado, "Dynamic behaviour of pneumatic linear actuators," Mechatronics, vol. 45, pp. 37 – 48, 2017. [Online]. Available: http://www.sciencedirect.com/science/article/pii/S0957415817300673

[157] K. Rhinefrank, A. Schacher, J. Prudell, T. K. A. Brekken, C. Stillinger, J. Z. Yen, S. G. Ernst, A. von Jouanne, E. Amon, R. Paasch, A. Brown, and A. Yokochi, "Comparison of direct-drive power takeoff systems for ocean wave energy applications," IEEE Journal of Oceanic Engineering, vol. 37, no. 1, pp. 35–44, Jan 2012.

[158] M. Livingston and A. Plummer, "The design, simulation and control of a wave energy converter power take off," 3 2010, 7th International Fluid Power Conference (IFK) ; Conference date: 22-03-2010 Through 24-03-2010.

[159] M. Eriksson, J. Isberg, and M. Leijon, "Hydrodynamic modelling of a direct drive wave energy converter," International Journal of Engineering Science, vol. 43, no. 17, pp. 1377 – 1387, 2005. [Online]. Available: http://www.sciencedirect.com/science/article/pii/S0020722505001394

[160] C. Qin, Y. Liu, P. Ju, W. Guan, F. Wu, and Y. Jin, "Equivalent modeling of direct-drive wave array in frequency domain," in 2018 International Conference on Power System Technology (POWERCON), Nov 2018, pp. 2198–2203.

[161] L. Huang, B. Hu, M. Hu, C. Liu, and H. Zhu, "Research on primary excitation fully superconducting linear generators for wave energy conversion," IEEE Transactions on Applied Superconductivity, vol. 29, no. 5, pp. 1–5, Aug 2019.

[162] P. R. M. Brooking and M. A. Mueller, "Power conditioning of the output from a linear vernier hybrid permanent magnet generator for use in direct drive wave energy converters," IEE Proceedings - Generation, Transmission and Distribution, vol. 152, no. 5, pp. 673–681, Sep. 2005.

[163] J. C. McNatt, V. Venugopal, and D. Forehand, "A novel method for deriving the diffraction transfer matrix and its application to multi-body interactions in water waves," Ocean Engineering, vol. 94, pp. 173 – 185, 2015. [Online]. Available: http://www.sciencedirect.com/science/article/pii/S0029801814004417

[164] G. Li and M. R. Belmont, "Model predictive control of a sea wave energy converter: a convex approach," IFAC Proceedings Volumes, vol. 47, no. 3, pp. 11 987 – 11 992, 2014, 19th IFAC World Congress. [Online]. Available: http://www.sciencedirect.com/science/article/pii/S1474667016435238